Diesel Reforming Medium and Long Run Tests

DIPLOMARBEIT

zur Erlangung des akademischen Grades

Diplom-Ingenieur

im Rahmen des Studiums

Physikalische Energie und Messtechnik

Eingereicht an der Technischen Univeristät Wien

von

Giuseppe Somare
Matrikelnummer 1428018

Betreuung
Univ.Prof. Dipl.-Ing. Dr.techn. Ernst Bauer
Univ.Prof. Dipl.-Ing. Dr.techn. Linert Wolfgang
Dr. Martin Hauth

Februar 2017

Abstract

The steam pre-reforming is one the most viable solutions for solid oxide fuel cell (SOFC) system as well as for several other industrial applications. It allows electrical efficiencies in SOFC systems of the order of 60 % (compared to catalytic partial oxidation achieving 40 %).

In particular high density energy and diesel easy storage possibility make diesel steam reforming one of the most promising fuel conversion technologies. However, one of the major problems in diesel steam reforming is carbon formation at the catalyst.

In the view of understanding this phenomenon better, steam reforming tests were performed in a pre-reforming catalyst system at TU Graz. It was aimed to carry out long term tests (between 50 and 100 hours) based on operating parameters, which were already available from a previous master thesis.

Test results were compared with theoretical equilibrium values and the agreement was satisfactory.

Table of Contents

Acronyms

APU	auxiliary power unit
AFC	alkaline fuel cell
DIR	direct internal reforming
DMFC	direct methanol fuel cell
GHSV	gas hourly space velocity
HHV	high heating value
IID	indirect internal reforming
LHV	low heating value
MCFC	molten carbonate fuel cell
MET	methanation reaction
OC	oxygen to carbon ratio
OSR	oxidative steam reforming
PAFC	phosphoric acid fuel cell
PEMFC	polymer electrolyte membrane fuel cell
POX	partial oxidation
SC	steam to carbon ratio
SOFC	solid oxide fuel cell
SR	steam reforming
SV	space velocity
WGS	water gas shift reaction

1. Introduction

Since the year 2000 more attention has been attracted to hydrogen and its relation with distributed energy generation. This connection is closely related to stationary fuel cell applications particularly for the possibility to combine heat and power generation. Today the power market is characterized by large scale centralized power generation. Even though with high voltage operation electrical transfer losses over short and medium distance are still acceptable, over long distances these are excessive and not cost efficient. On the other hand, the heat generation market, supply of hot water, heating for buildings and steam for industrial applications, is mostly not centralized and heat can be carried over long distances at high costs. Renewable energy resources encounter several difficulties with the present organization of the market. In remote areas the renewable energy plants develop slowly, power transfer over long distance is difficult and big energy storages are required to deal with fluctuations in energy demand. Currently, distributed energy generation seems to be the most viable way for renewable energy resources. In this perspective, a holistic consideration of heat and electricity production should be taken into account. This opens the possibility for fuel cell stationary systems [1].

Hydrogen has been traditionally important in the chemical industry such as in ammonia and methanol syntheses, oil refining and several petrochemical technologies. Hydrogen is not an alternative fuel, but rather an energy carrier. It means that hydrogen must be produced from primary energy. Despite of several applications involving hydrogens as primary fuel, the hydrogen economy for several reasons has developed very slowly: difficulty of on board storage of hydrogen, safety issues, public acceptance and the lack of specific legislation [2].

The purpose of fuel processing in fuel cells is to convert a commonly available fuel, such as gasoline, diesel, or natural gas, into a gas stream containing the compounds required by the cell. In other words, fuel processing is the conversion of the raw fuel into the fuel gas required by the fuel cell stack [3]. Each type of fuel cell stack has specific fuel requirements. Generally, the lower is the operating temperature of the stack, the stricter are the fuel requirements.

At present, diesel reforming together with other non-gaseous fuels reforming process is one of the most promising technologies for auxiliary power unit (APU) because of ease of storage and already existing refueling infrastructure [4].

The scope of the present work is to test medium and long run catalytic steam reforming with diesel. The focus of the work is the stability of the process in relation with some parameters and particularly with carbon formation, which represents one of the major undesirable effects for a SOFC. The reforming tests were carried out with a pre-reforming catalyst.

The probability of carbon formation in the reformer or fuel cell catalyst strongly depends on the presence of higher hydrocarbons. Through pre-reforming the presence of higher hydrocarbons can be strongly reduced or eliminated in the feed of the reformer. In the same way sulfur, which can be present in the feedstock, can be eliminated before it enters the main reformer or fuel cell. The lower operating temperatures of the pre-reformer facilitates the deposition of sulfur on the pre-reforming catalyst. Hence, there would not be any need of a desulfurization unit in the downstream of a reformer. Also, the lifetime of the reformer is extended due to the complete sulfur removal in the pre-reformer [5]. The focus of the present work was mainly placed on carbon formation and not on sulfur deposition.

The pre-reforming process is generally used in industry to convert high hydrocarbons into a mixture of H_2, CO_2, CO and CH_4, through a steam reforming reaction at relatively low temperature (400 -550 °C) [5]. Additionally, the pre-reforming is responsible also for the partial conversion of methane into hydrogen [6].

Several liquid fuels such as diesel, jet fuels and NATO F17 have been used in a pre-reforming reactor but also gases such as natural gas, butane and propane can be pre-reformed before direct fuel cell applications [5]. In these gaseous fuels higher hydrocarbons are converted to methane and carbon oxides with reduced risk of carbon formation at SOFC anode.

2. Principles of fuel cells

2.1. Background

Even though the experimental work conducted in this thesis was exclusively focused on diesel and partially methane pre-reforming, the purpose of the medium and long rung tests performed will be of key importance for the stationary SOFCs at AVL. In fact, they can be considered pre-reforming tests for SOFC systems. For this reason, a general description of fuel cells functioning mechanisms and technologies has been added in the present work.

In a fuel cell the chemical energy is transformed directly in electrical energy by a process involving an electrode/electrolyte system [6]. Contrary to an electrolytic cell, where the free Gibbs energy change of the reaction, $\Delta_R G$, is positive and the reaction takes place when the electrical energy is applied, in a fuel cell the reaction runs spontaneously since $\Delta_R G$ is negative. The functioning of a fuel cell is analogous to the one of a battery, where also a chemical reaction runs spontaneously. However, while the battery operation is discontinuous and is depending on the energy stored inside, a fuel cell is externally refueled and its operation is continuous.

The simplest model of fuel cell consists in two porous electrodes separated by an electrolyte. The electrochemical reaction in a fuel cell is the result of two different spatially separated half-reactions, occurring respectively at the anode at the cathode of the cell. The anodic reaction is a fuel oxidation and releases electrons, which are transported through an external circuit and reach the cathode. At the cathode the reduction half-reaction takes place. The circuit is then completed by the transport of ions through electrolyte from one electrode to the other. Although there are several types of fuel cells with different transport mechanisms, for explanation purpose, two mechanisms, representing the predominant models are discussed [6].

In **acid electrolyte fuel cell**, the hydrogen gas ionizes, releasing electrons and creating H^+ ions according to the half reaction:

$$2H_2 \rightarrow 4H^+ + 4e^- \quad (1)$$

At the cathode the oxygen reacts with the electrons coming from the anode trough the external circuit and ions H^+ form the electrolyte to form water.

$$O_2 + 4e^- + 4H^+ \rightarrow 2H_2O \quad (2)$$

The overall chemical reaction taking place in the fuel cell is the following:

$$H_2 + \frac{1}{2} O_2 \rightarrow H_2O \quad (3)$$

Fig. 1 depicts the functioning schema of an acid electrolyte fuel cell.

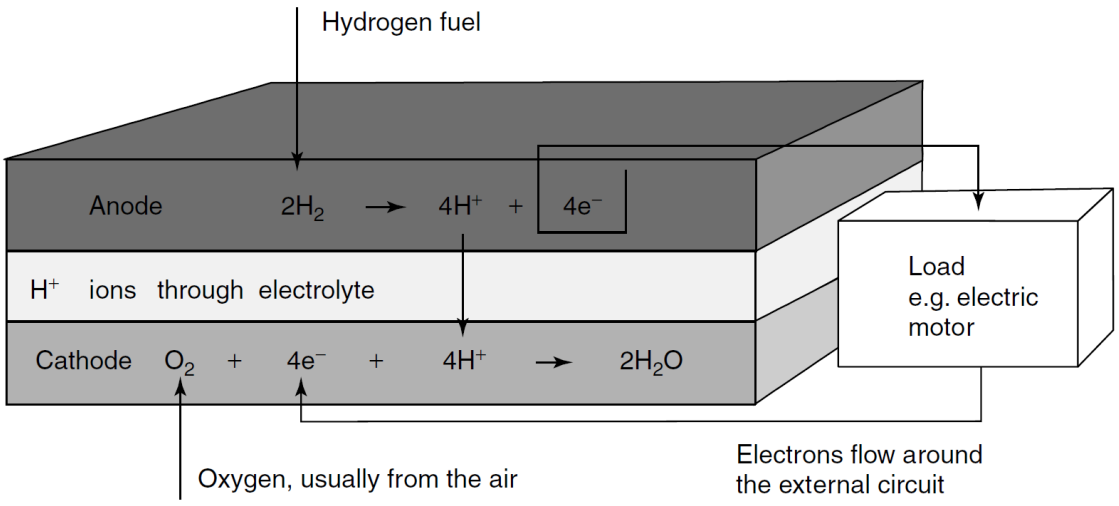

Figure 1 Schema of electrode reactions and charge flow in an acid electrolyte fuel cell [6]

In the **alkaline electrolyte fuel cell,** the overall reaction is exactly the same but, due to the fact the mobile ions in electrolyte are OH^- anions, the two half reactions occurring at the electrodes are different. At the anode the ions OH^- react with H_2, releasing electrons according to the reaction:

$$2H_2 + 4OH^- \rightarrow 4H_2O + 4e^- \quad (4)$$

At the cathodes, oxygen reacts with electrons taken from the external circuit and the water in the electrolyte forming new OH^- ions:

$$O_2 + 2H_2O + 4e^- \rightarrow 4OH^- \quad (5)$$

In both cases, acid electrolyte and alkaline electrolyte, the ions, H^+ or OH^- are migrating through the electrolyte while the electrons through the external circuits as in Figs. 1 and 2.

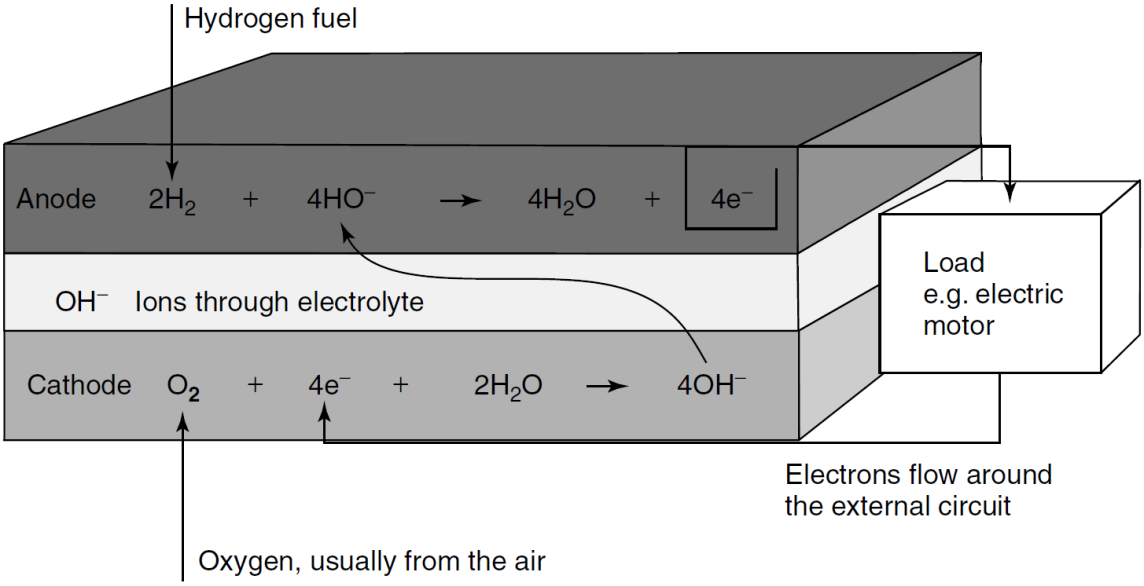

Figure 2 Schema of electrode reactions and charge flow in an alkaline electrolyte fuel cell [6].

Because the voltage produced by a single layer is very small, about 0.7 V, it is necessary, for practical applications, to connect many cells in series to reach a useful voltage. In general, the method used to collect and deliver electrons to electrode is the “bipolar plate”. The method consists of connecting the cell over the entire electrode surfaces to plates made of good conductor material, and, at the same time, supplying hydrogen to the anode and oxygen to

the cathode. These plates have gas channels where gases flow. The connection in series of several cells is depicted in Fig. 3.

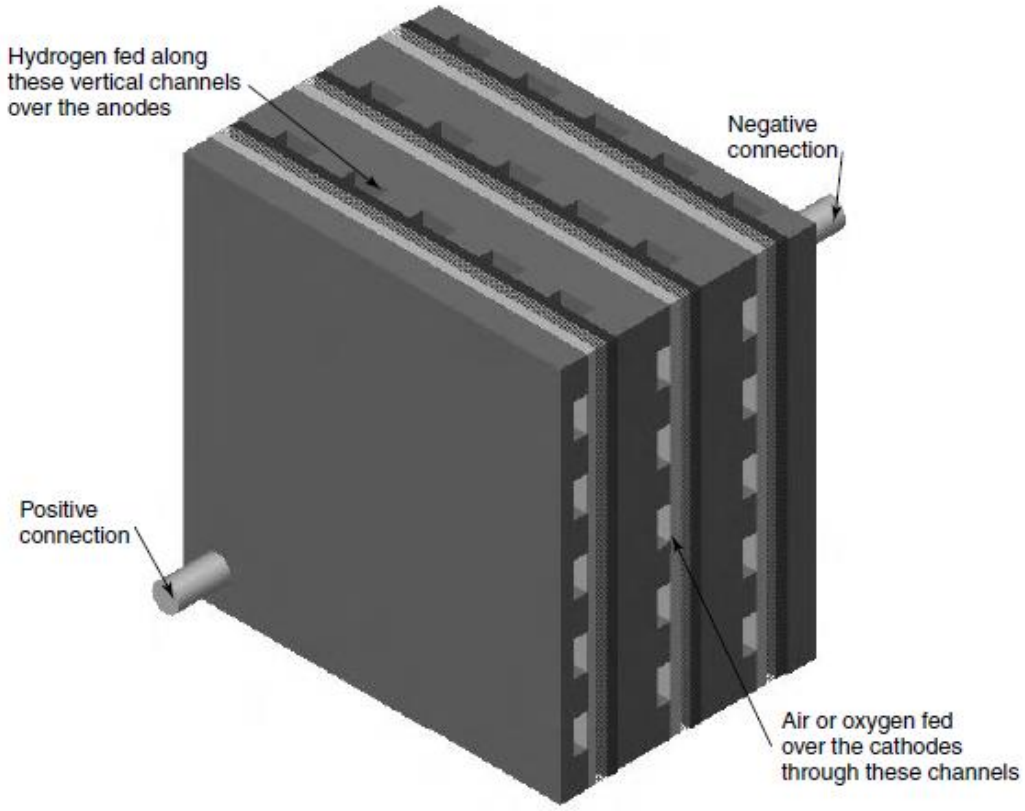

Figure 3 A three cell stacks of bipolar plates with anodic and cathodic connections [6].

2.2. Electrochemical principles

The theoretical value of an open circuit voltage (OCV) that can be produced during an electrochemical reaction is given by:

$$E = -\Delta_R G / vF \tag{6}$$

Where $\Delta_R G$ is the free Gibbs energy variation of the overall reaction, F (96485.3365 C/mol), is the Faraday constant and v is the number of charge carriers in the considered reaction [7].

In an electrochemical cell where the overall reaction follows the chemical Eqn. (3), v is equal 2 and at standard conditions, where the temperature 298.15 K and the pressure is 1 bar, the

free Gibs energy variation of the reaction, $\Delta_R G^0$, is -478.8 KJ/mol. The OCV in this case would be c.a. 1.23V. Due to irreversible mechanisms and deviation from standard conditions, the OCV is an ideal value which is never obtained in a real H_2-fuel cell. The OCV according to Eqn. (3) represents also the highest possible value compared to the OCV values of fuel cells with different overall reactions.

When the electric circuit is closed and starts providing electric power, a number of irreversible processes should be considered. Moreover, due to standard conditions deviations, also an open circuit exhibits a different value of voltage from the theoretical value of OCV. The different value of a real measured voltage in comparison with the OCV can be ascribed to the following reasons or contributions [6]:

- Nernst losses, ΔU_N, due to the deviation from standard pressure and temperature;
- activation polarization losses, ΔU_{act}, due to the electrodes kinetics;
- ohmic losses, ΔU_{ohm}, due to the internal resistivity in a fuel cell: ions in electrolyte and electrons in the electrically conductive part of the cell. It determines a linear drop in voltage;
- Concentration losses, ΔU_{conc}, due to lower concentration of the reactants at the electrodes when the cell is in operation;

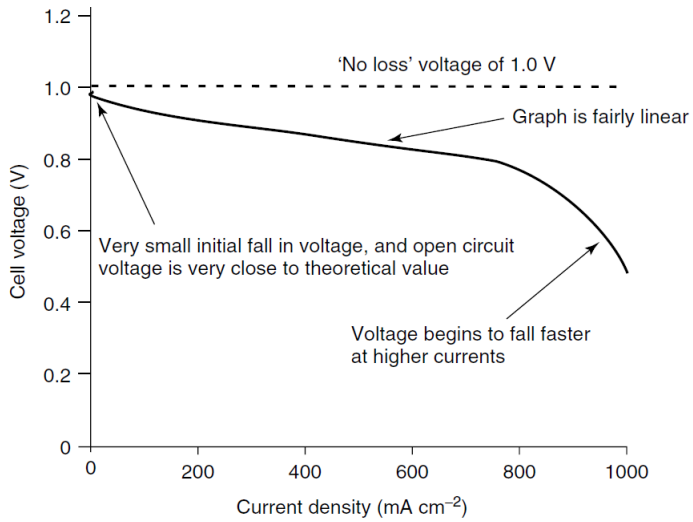

Figure 4 The current-voltage characteristic in a low temperature, air pressure, fuel cell [6].

Fig. 4 shows the dependence of the cell voltage from current density for low temperature and air pressure fuel cell. The different irreversibility processes determine a voltage drop at different regimes: ΔU_{act} is characteristic for low current density, ΔU_{ohm} for intermediate and ΔU_{conc} for higher.

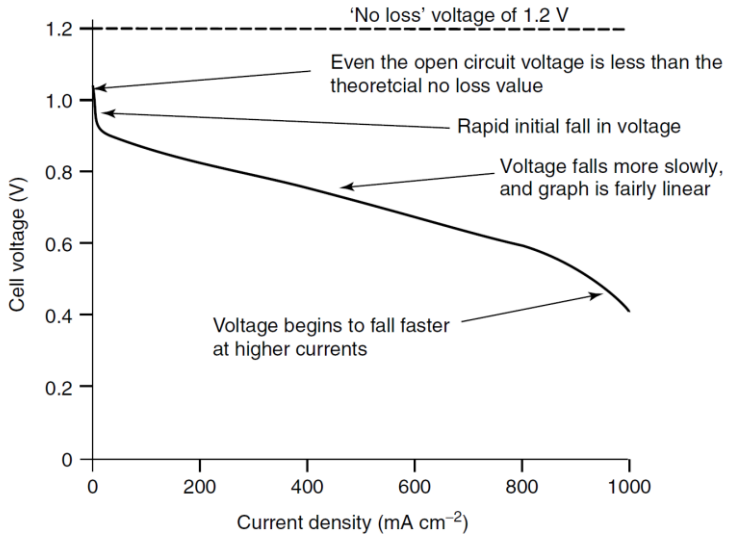

Figure 5 The current-voltage characteristic in a high temperature (800 °C), air *pressure, fuel cell [6].*

For a high temperature and air pressure fuel cell the situation is slightly different. The voltage value at lower current density is very close to the OCV and ΔU_{act} determines a smaller drop in the voltage as depicted in Fig. 5.

2.3. Fuel cell efficiency

In any system involving energy conversion, the efficiency is defined as the ratio between useful energy output and energy input [8]. In a fuel cell the energy output corresponds to the electrical energy, while the energy input is the enthalpy of hydrogen. Assumed that the Gibbs energy is completely converted into electrical energy, it is possible to define the theoretical efficiency as

$$\eta_{th} \stackrel{\text{def}}{=} \frac{-\Delta_R G}{-\Delta_R H} = 1 - \frac{T\Delta_R S}{-\Delta_R H} \tag{7}$$

where $\Delta_R H$ and $\Delta_R S$ are, respectively, the reaction enthalpy and the reaction entropy of the overall cell reaction [7]. In case of a H_2-fuel cell, the dependence of η_{th} versus temperature compared with the dependence of the Carnot efficiency versus temperature is outlined in Fig. 6. In this case the overall reaction is expressed by the chemical Eqn. (3) and, as enthalpy variation, it is considered the high heating value[1] (HHV). This means that H_2O considered in the reaction (3) is water and not steam.

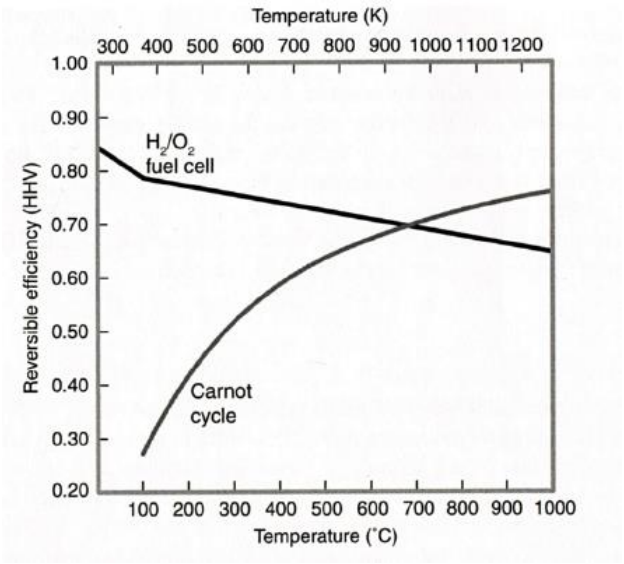

Figure 6 Comparison of theoretic reversible HHV H_2-fuel cell efficiency and Carnot efficiency [7].

Fuel cells have a significant thermodynamic reversible efficiency advantage at low temperature, but they lose this advantage at high temperatures. However, as already seen in previous sections, the cell voltage is strongly affected by polarizations that determine voltage losses. The voltage losses are generally less significant at higher temperature.

[1] *"The higher heating value (also known gross calorific value or gross energy) of a fuel is defined as the amount of heat released by a specified quantity (initially at 25°C) once it is combusted and the products have returned to a temperature of 25°C, which takes into account the latent heat of vaporization of water in the combustion products."* Source: http://hydrogen.pnl.gov/tools/lower-and-higher-heating-values-fuels .

2.4. Different types of fuel cells

2.4.1. General Remarks

Even though the pre-reforming process tests carried out in this work are aimed at general improvement in the SOFC fueling, it will be briefly presented an overview over different type of fuel cells, since the reforming process constitutes a fundamental solution for their fuel processing.

2.4.2. Polymer electrolyte membrane fuel cell (PEMFC)

One of the most remarkable characteristics of a PEMFC is the high density, which makes it particularly suitable for mobile and portable applications. The cell operates at low temperatures 60-80 °C and the electrolyte consists of a polymer [7]. PEMFC are particularly suitable for operation with pure hydrogen. Fuel processors have been developed for utilization also with other feedstocks. The only implementation, which allows a direct utilization of a fuel different than hydrogen is the direct methanol fuel cell (DMFC) [9].

The polymer is an ion conductor electrolyte and the two porous electrodes, which are basically carbon supports with platinum catalyst particles. One of the major problems of PEM fuel cells, in contrast to the high temperature fuel cells, is that they are particularly prone to CO poisoning. While carbon monoxide in some of the high temperature fuel cell can be used as a fuel, in cell with electrodes containing platinum as catalyst, even a very small quantity of carbon monoxide has detrimental effects. The carbon monoxide has to be converted to carbon dioxide trough the water shift reaction.

$$CO + H_2O \rightleftharpoons CO_2 + H_2 \quad (8)$$

2.4.3. Phosphoric acid fuel cells (PAFC)

The electrolyte in PAFC fuel cell is phosphoric acid at 150-220 °C. At lower temperature phosphoric acid is not a good ions conductor and also the risk of anodic CO poisoning becomes relevant. Electrodes are in porous carbon with a surface layer of black carbon. The efficiency ranges between 37-42% [9].

2.4.4. Alkaline fuel cells (AFC)

The AFC is one of the first modern fuel cells with practical application [9]. The cell reactions at the electrodes are expressed by chemical Eqns. (4) and (5). The electrolyte in this case is an alkaline solution, sodium hydroxide and potassium hydroxide solution, which are relatively low corrosive and have low costs. Other variables such as pressure, temperature, and electrode structure depends on cell designs. For example, the Apollo fuel cell operates at 260 °C [6], while the temperature of the Orbiter alkaline fuel cell was about 90 °C [6]. As for the PEMFC also for AFC the presence of CO represents a poison for the cell. In the AFC an efficiency of 70% is reachable.

2.4.5. Molten carbonate fuel cells (MCFC)

In MCFC the electrolyte is a mix of different molten carbonates such as $LiCO_3$ and $KiCO_3$ on a ceramic matrix, generally $LiAlO_3$ [9]. The operative temperature is 600-700 °C. The mobile ions are $CO_3^=$. At this temperature the molten carbonates are good conductors for the $CO_3^=$ ions.

Due to the high temperature it is possible just to use metal electrodes Ni at the anode and NiO at the cathode. An efficiency of 60% can be reached. The MCFC are flexible regarding the type of used feedstock. A mix of CO, CO_2 and CH_4 can be used.

2.4.6. Solid oxide fuel cell (SOFC)

The SOFC uses as electrolyte a solid oxide as Z_rO_2 stabilized with Y_2 [9]. The electrodes are ceramic materials such as Co-ZrO_2 or Ni-ZrO_2 for the anode and $LaMnO_3$ for the cathode. The mobile ions are $O^=$.

The operative temperature varies between 600-1000 °C. Different feedstocks can be used. One of the standard feedstocks is CH_4, which can be internally reformed trough a steam reforming reaction followed by water shift reaction. For higher hydrocarbons an external reformer can be used.

In Fig. 7 the systems of fuel cells are schematically depicted and summarized.

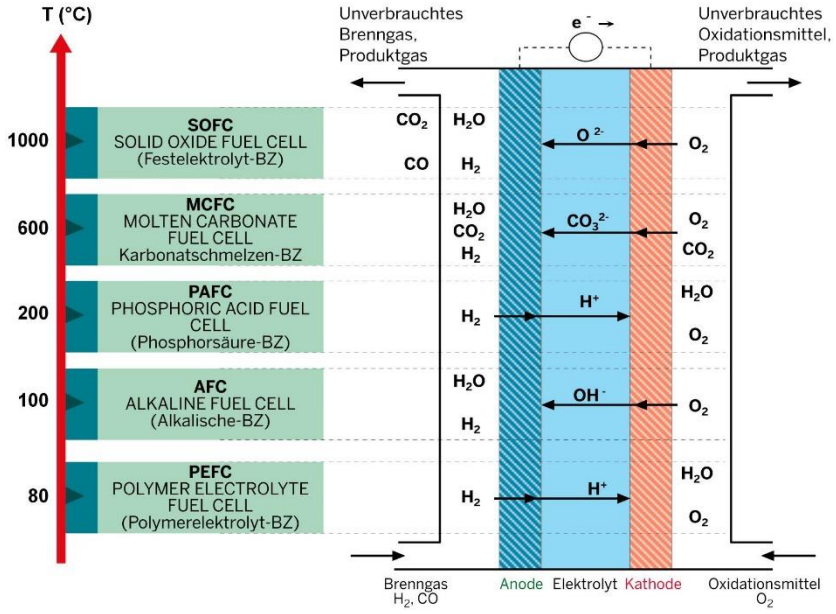

Figure 7 Scheme of different fuel cells systems [10].

2.5. Reforming configuration in fuel cell systems

Reforming is an essential process to obtain hydrogen from methane or higher hydrocarbons. External reforming is generally needed for low and medium temperature fuel cells. For high temperature fuel cells, such as SOFC and MCFC, an internal reforming system can be used. Here methane conversion takes place inside of the cell system [6]. For both high temperature fuel cell systems there are two viable ways of internal reforming:

- Direct internal reforming (DIR)
- Indirect internal reforming (IIR)

In the direct internal reforming methane is converted directly on the anode. This process offers optimal efficiency to loss of energy ratio. The energy required for the reforming reaction

is provided directly by the fuel cell system. For the internal reforming the anode should be able to act also as reforming catalyst [11]. While DIR is commonly used in SOFC, in MCFC stack DIR can be carried out if a supported metal catalyst is incorporated [6]. Even though Ni at very high temperature is a good steam reforming catalyst, the low surface area of the porous nickel anode has insufficient catalytic activity to support the steam reforming reaction at 650 °C . In addition, a general problem for Ni catalysis is the tendency to promote the formation of carbon, so the internal reforming is generally possible just with methane, with high steam to carbon ratios but not with higher hydrocarbons [11].

IIR involves conversion of methane by reformers in thermal contact with the stack. It receives heat just form the adjacent cell and the steam has to be produced separately. Indirect reforming is generally less efficient than direct reforming, but provides a more stable cell efficiency with no risk of carbon formation at the anode.

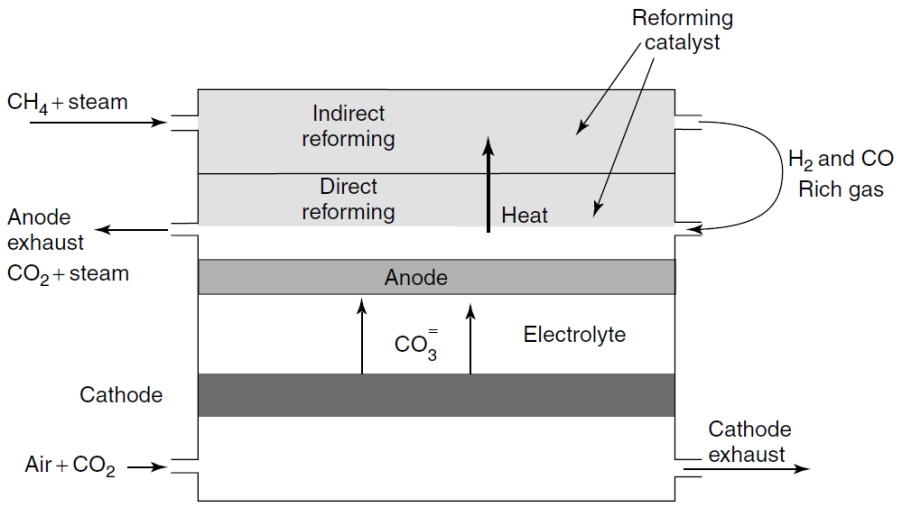

Figure 8 Direct and indirect internal reforming architecture [6].

In Fig. 8 are schematized the two different technologies of internal reforming for a MCFC.

Since one of the major problems with higher hydrocarbons is the elevated risk of carbon formation, one method to prevent or reduce this undesirable effect is to covert higher hydrocarbons already at relatively low temperature (400-550 °C) through a process of pre-reforming.

3. Reforming technologies

3.1. General Remarks

This chapter analyses different reforming technologies. We concentrate mostly on the catalytic steam reforming technology, which was the focal point of the present experimental work.

3.2. Catalytic Steam reforming

The process of steam reforming (SR) with generic hydrocarbon can be expressed by the following three chemical reactions [12]:

$$C_nH_m + nH_2O \rightarrow nCO + \left(n + \frac{1}{2}\,m\right)H_2 \qquad \Delta_R H^0 > 0 \qquad (9)$$

$$CO + H_2O \rightleftharpoons CO_2 + H_2 \qquad \Delta_R H^0 = -41 KJ/mol \qquad (10)$$

$$CO + 3H_2 \rightleftharpoons CH_4 + H_2O \qquad \Delta_R H^0 = -206\ KJ/mol \qquad (11)$$

The reaction (9) is the steam reforming reaction, the reaction (10) is the water-gas shift reaction (WGS) and the reaction (11) is the methanation reaction (MET). The reaction (9) is irreversible for all the higher hydrocarbons with n bigger than 1, there is no formation of intermediate products and, with a sufficient activity of the catalyst, complete conversion is expected. Considerations over the thermodynamics of the reactions can help to understand the process. While the stream reforming reaction is very endothermic, reaction (10) and (11) are exothermic. In the case of $C_{14}H_{28}$ the standard reaction enthalpy of (9), $\Delta_R H^0$, is 2045 KJ/mol, for CH_4 it will be instead 206 KJ/mol. The overall reaction heat can be negative, positive or zero.

Any given feedstock will require a specific operating window of parameters such as temperature and stream to carbon ratio. Whereas on industrial scale natural gas is generally

easily reformed, reforming of heavy fuels such as naphtha, kerosene or diesel is more problematic.

The most common material for the catalyst is nickel. Nickel is not expensive while it is very active in SR. The kinetics of the catalyst depend strongly on the kind of feedstock and surface reactions [12].

For methane steam reforming the process could be summarized with the following reactions [13]:

$$CH_4 + * \rightarrow CH_x* + \frac{1}{2}(4-x)H_2 \quad (12)$$

$$CH_x + OH* \rightarrow CO + \frac{1}{2}(x+1)H_2 + 2* \quad (13)$$

$$H_2O + * \rightleftharpoons OH + \frac{1}{2}H_2 \quad (14)$$

where the symbol * represents a surface site of nickel. The equations (12) and (13) express a two-step mechanism comprising respectively the CH_4 activation and the CO desorption.

For all higher hydrocarbons, the process takes place by irreversible absorption on the nickel surface and only compounds containing single carbon atom leave the surface [14]. The following chemical reactions with the catalyst surface are involved [13]:

$$C_nH_m + * \rightarrow C_nH_{m-y}* \rightarrow C_{(n-1)}H_z* + CH_x* \quad (15)$$

$$C_{(n-1)}H_z* \rightarrow C_{(n-2)}H_z* + CH_x* \quad (16)$$

Together with reactions (9), (10), (11) the following side reactions take place [15]:

$$CH_4 \rightleftharpoons C + 2H_2 \qquad \Delta_R H^0 = 75KJ/mol \quad (17)$$

$$2CO \rightleftharpoons C + CO_2 \qquad \Delta_R H^0 = -173KJ/mol \quad (18)$$

$$C_nH_m \rightarrow nC + \frac{1}{2}mH_2 \qquad \Delta_R H^0 > 0 \quad (19)$$

These reactions represent respectively the dissociation of methane, of carbon monoxide (Boudouard reaction) and of hydrocarbons. All of them tend to promote the carbon formation.

Fig. 9 depicts the typical temperature profile along the reactor axis in a pre-reforming reaction. The different lines represent the catalysis deactivation process.

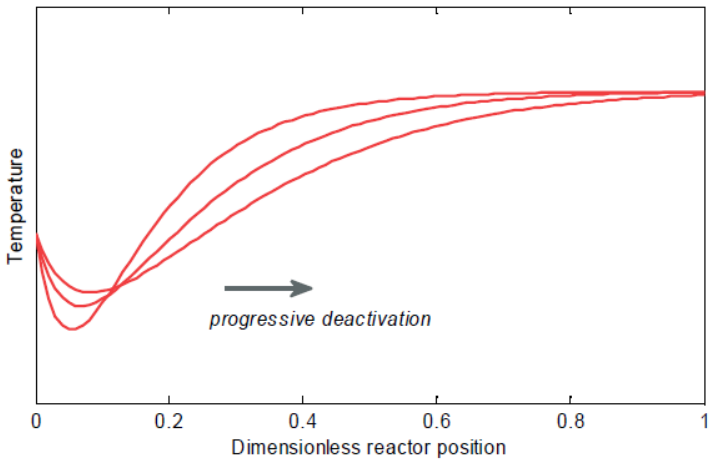

Figure 9 Typical temperature profile along the reactor [12] .

A short description of the three typical ways of the catalyst degradation, which can occur in the steam reforming process, is provided in the following three sub-sections.

3.2.1. Carbon formation

Carbon formation is mostly related with heavy feedstock like diesel and it will be the major problem in our tests. The processes of carbon formation can generally be characterized in three different ways [13]:

- wiskers carbon;
- gum formation;
- pyrolytic coke;

Wiskers are carbon filaments which tend to grow on catalyst particles typically over a certain temperature T_C [12] (Fig. 10). T_C depends strongly on the type of feedstock, but, generally, the

formation of wiskers occurs between 350 °C and 600 °C. These filaments could be strong and may cause breakdown of the catalyst pellets and blockage of catalyst pores [13].

The explanation of wiskers formation can be viewed either thermodynamically or kinetically. The thermodynamics of carbon formation via equations (14) and (15) is normally evaluated by the so-called principle of equilibrated gas: *"Carbon formation is to be expected on a nickel catalyst if the gas composition corresponds to one with a thermodynamic driving force for carbon after the establishment of the methane reforming and the shift equilibrium"* [13]. Basically, carbon is formed if the gas, after the equilibrium of reaction (9) and (10) has been established, shows affinity to carbon formation [15]. Thermodynamics can determine possible risks of carbon formation, but it cannot warrant a carbon free operation.

Kinetics also can play a decisive role in explaining the formation mechanisms of wiskers. The carbon formation can be kinetically considered a competition between carbon the reactions leading to carbon formation and the gasification reaction [15]. A valid empirical relation is the following:

$$\left(\frac{P_{H_2O}}{P_{C_nH_m}}\right) = -\frac{a}{T} + b \qquad (20)$$

According to Eqn. (20) carbon formation is expected below a certain critical steam to hydrocarbon ratio. Constants a and b depend on the type of hydrocarbon and the catalyst. Parameters for feedstock such as Naphta, LPG and natural gas are already available in literature [15].

Together with the wiskers formation higher hydrocarbons are responsible also for the formation of gum and pyrolytic coke. Gum consists of condensed polymers that are generally formed at temperature T_P below 350 °C. The polymers molecules can grow very fast in dimensions with continuous reactions till polymers products can eventually encapsulate the nickel particles. Generally, after the beginning of gum formation, the deactivation process of catalysis proceeds very fast [12]. Gum formation is heavily dependent on the kinetics of two different competing mechanisms, hydrocraking and adsorption. At T_P these two mechanisms

proceed at comparable rate, which prevent any gum formation. However, below T_P the adsorbtion rate, which causes gum formation, predominates over the one of hydrocraking.

It is generally possible to identify for different hydrocarbons an operative window of temperature where free carbon formation conditions are present. Fig. 11 depicts the operative window between T_p and T_c. Heavy hydrocarbons tend to be particularly prone to carbon formation and their operative temperature window tends to be narrower [16].

Pyrolytic coke occurs at high temperature and it is a result of thermal cracking of higher hydrocarbons [13]. Generally, it occurs at temperatures over 600 °C [12]. Coke formation is enhanced by the sulfur poisoning or due to the poor activity of the catalyst [17]. However, since the pre-reforming process is generally performed at lower temperatures, pyrolytic carbon formation does not pose a serious problem in the present study.

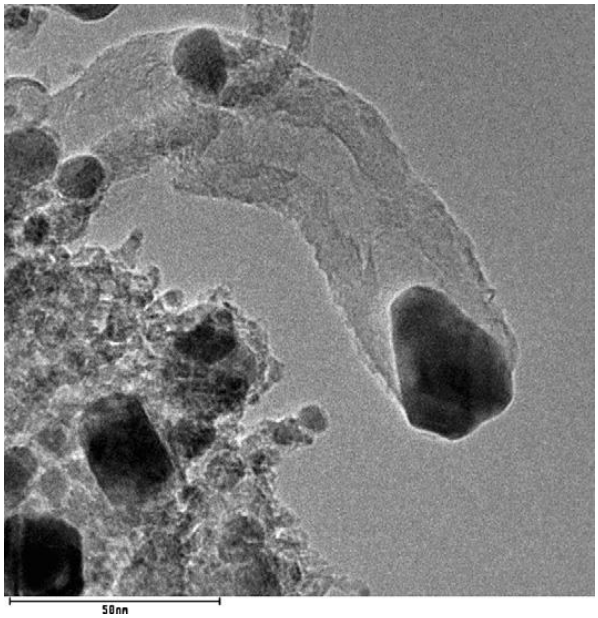

Figure 10 Wisker on the Ni catalysis surface [13].

In order to minimize the carbon deposition, it is always useful to refers to the steam to carbon ratio (SC) and to oxygen to carbon ratio (OC). To a first approximation, the carbon formation is always proportional to the inverse of these two parameters. The reduced carbon formation at high SC ratios is to be attributed to high rates of steam carbon gasification [18].

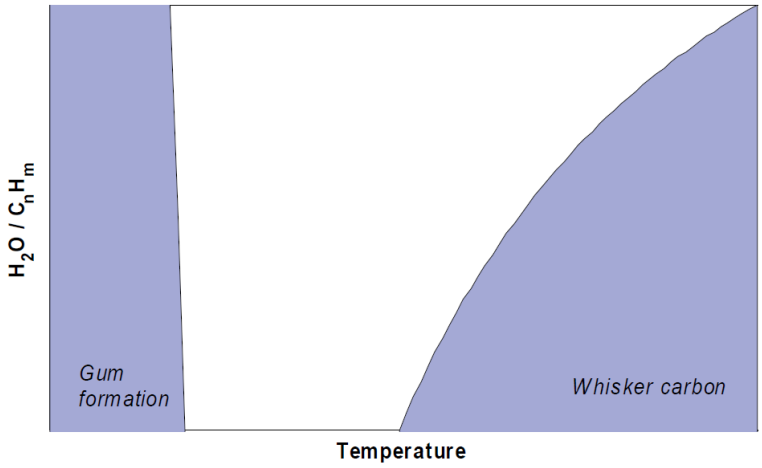

Figure 11 Temperature operative window $T_p<T< T_c$ [12].

There are several methods to regenerate the catalyst from deactivation due to carbon formation. Products of polymerization can be removed by either oxidative or reductive regeneration processes [18]. Regeneration with steam has been explained and conducted at 500 °C in [19]. In our tests the temperature was raised to 580 °C to enhance carbon gasification process during the carbon removal procedure with steam and forming gas. Higher temperatures could have been detrimental for the piping system.

3.2.2. Sulfur poisoning

In the present work the focus was on the carbon formation. However, together with carbon formation also sulfur poisoning poses serious problem to the catalyst. The usual concentration of sulfur in natural gas ranges from 5 to 20 ppm, while in liquid hydrocarbons it can reach 500 ppm [15].

Sulfur compounds like hydrogen sulfide can be reversibly, but strongly chemisorbed at the nickel surface according to the reaction:

$$Ni + H_2S \rightleftharpoons Ni - S + H_2 \tag{21}$$

Pre-reforming nickel catalyst is particularly prone to sulfur poisoning and the catalyst activity decreases with the increase of sulfur coverage, θ. At the equilibrium conditions, the dependence of the sulfur coverage of the nickel surface on temperature and on ratio of H_2S to H_2 can be estimated by the following relation:

$$\theta = 1.45 - 9.53 \cdot 10^{-5} \cdot T + 4.17 \cdot 10^{-5} \cdot T \ln\left(\frac{pH_2\,S}{pH_2}\right) \tag{22}$$

Thermodynamically, sulfur tolerance depends also on the temperature. Fig. 12 shows the free Gibbs energy variation, ΔG, for sulfide formation for three different metals. The dependence of ΔG versus temperature shows that the sulfide tends to form at lower temperature.

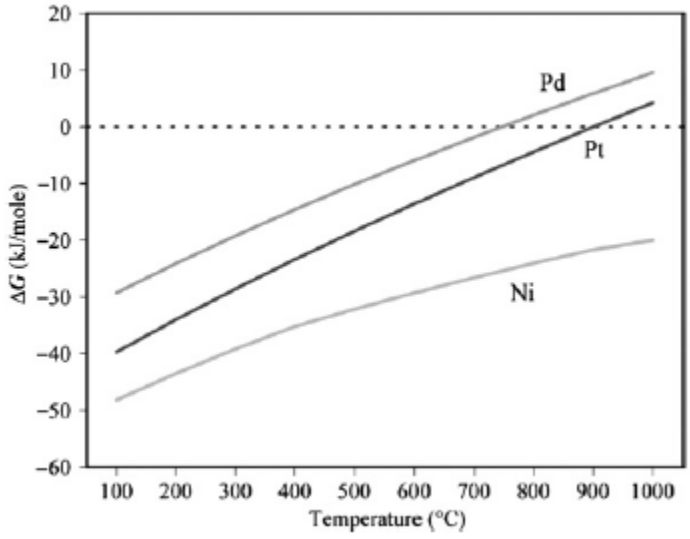

Figure 12 ΔG of sulfide formation for Ni, Pt and Pd [18].

Precious metals are generally less prone to sulfur poisoning than nickel. Due to the low operative temperature, the sulfide formation in a pre-reformer can be considerably high [12].

Regeneration can be performed by heating in flowing hydrogen to obtain the reverse reaction that forms the metal sulfide. However, this method is unpractical because adsorption of sulfur is reversible only at elevated temperatures at which sintering is likely to occur. Additionally, regeneration rates with H_2 are slow even at high temperatures [20].

Catalyst may also be regenerated in oxygen rich atmosphere. This oxidation process seems to regenerate the active metal sites and to remove the sulfur in the form of SO_2. The nickel in oxidized form needs then to be reduced before it is again active for reforming [20]. A third possibility is the regeneration though steam. The process occurs at approximately 700 °C and the presence of H_2S and SO_2 suggests that the following reactions take place:

$$Ni - S + H_2O \rightarrow NiO + H_2S \quad (23)$$

$$H_2S + H_2O \rightarrow SO_2 + 3H_2 \quad (24)$$

3.2.3. Sintering

Another process that can lead to catalyst degradation over the time is sintering of nickel. This process is characterized by augment of nickel particles and reduction of nickel surface area and activity. The Tammann temperature is commonly used as a parameter for sintering. It is approximately half of the meting temperature. At the Tammann temperature the mobility and reactivity of the molecules in a solid becomes significant. The Tammann temperature of Nickel is 591 °C. However, sintering can already start at temperatures below the Tammann temperature. Other parameters such as chemical atmosphere, composition and structure of the catalyst, can contribute to sintering [13].

3.3. Non-catalytic Steam reforming

Non-catalytic steam reforming requires higher temperatures. The cracking of methane into radicals occurs at temperatures about 1000 °C. This process conducts to formation of acetylene, ethylene and coke, which tend to react with steam radicals. However, to have a significant conversion temperatures over 1500 °C should be reached [13]. One approach is to promote the process by using plasma technology [5].

3.4. Partial Oxidation (POX)

Essentially, partial oxidation is a combustion, but with a less-than-stoichiometric amount of oxygen, λ smaller than 1. The products are carbon monoxide and hydrogen.
With CH_4 the main reaction can be expressed as [6]:

$$CH_4 + \frac{1}{2}O_2 \rightarrow CO + 2H_2 \qquad \Delta_R H^0 = -247\ KJ/mol \tag{25}$$

The reaction is exothermic and, unlike the SR reactions, no water is fed in the process. Similar to steam reforming, the reformate gas must go through shift reaction to produce more hydrogen and also to preferential oxidation to reduce the CO content to an acceptable level [8].

The reaction can occur with or without catalyst. The non-catalytic process can be performed typically between 1000 °C and 1200 °C. High-temperature POX can also work with higher hydrocarbons than those in catalytic processes and therefore it is suitable for diesel processing [6].

In case of catalytic POX, the typical operating conditions are the temperature range between 700 °C and 1000 °C, atmospheric pressure and OC 1.2.

For heavier hydrocarbons the reaction is:

$$C_nH_m + \frac{n}{2}O_2 \rightarrow nCO + \frac{m}{2}H_2 \qquad \Delta_R H^0 < 0 \tag{26}$$

The reactions (25) and (26) produce less hydrogen than in the case of SR (9). This means that POX is usually less efficient than steam reforming.

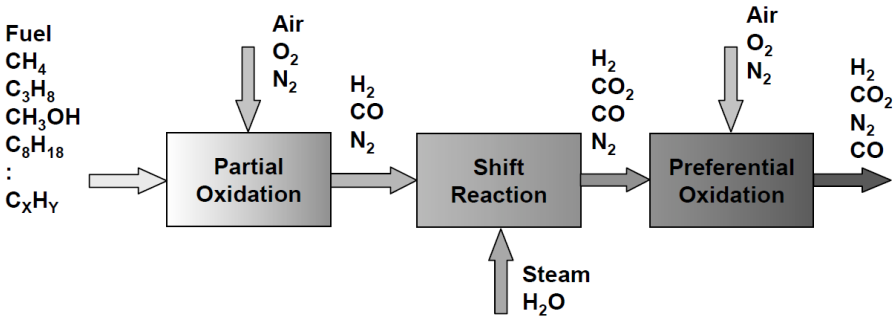

Figure 13 Representation of the partial oxidation process [8].

3.5. Autothermal Reforming

POX can be combined with the endothermic steam reforming process. This type of reforming is called oxidative steam reforming (OSR) [21]. If the exothermic oxidation balances exactly the endothermic steam reforming and makes the total reaction thermoneutral, the whole process is named autothermal reforming and it is a special case of the OSR.

In an autothermal reformer, instead of external combustion and heat transfer to the steam reforming reactor, heat is generated internally by POX and is then carried by the reacting gases and POX products (H_2 and CO) to the steam reforming zone. OSR is an already well established technology for the production of H_2 in petrochemical productions. However, a plant to separate N_2 from air is required which makes the process quite expensive.

The production requirements of H_2 for fuel cells are in general less stringent than the ones in petrochemical industry [21]. In this case OSR has some advantages over SR and POX.

Compared with SR, OSR requires less thermal integration, which makes the reactor lighter and less fuel is consumed at the start-up.

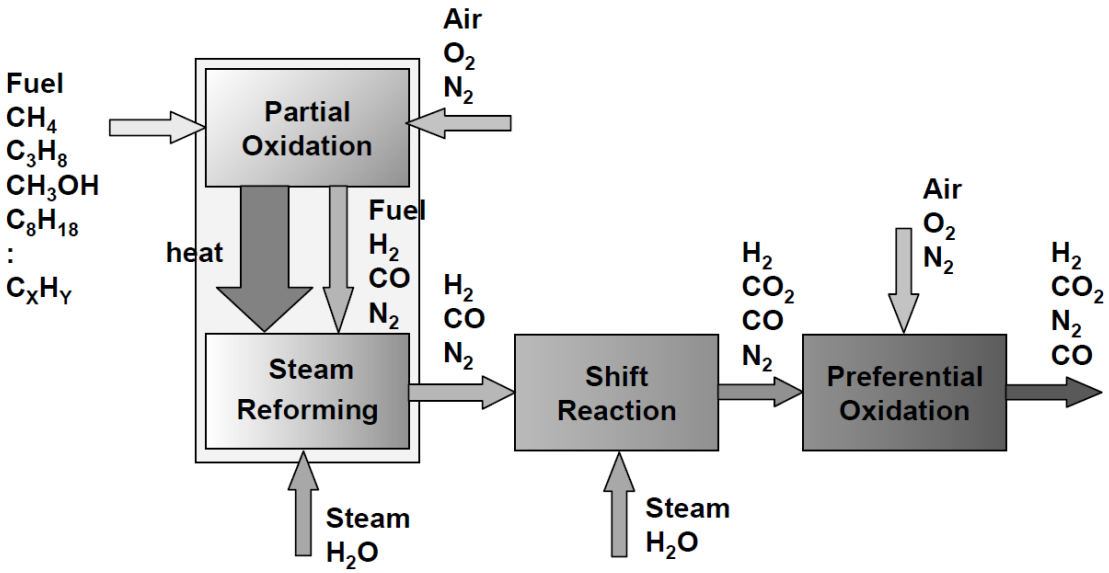

Figure 14 Representation of the autothermal reforming process [8].

3.6. Steam reforming parameters

Several parameters are generally used for the characterization of a SR process. They permit understanding catalyst performance. In addition to the temperature, it is crucial to know the velocity of the reactants flow with respect to the catalyst bed and the proportion of feedstocks such as CH_4, diesel or other hydrocarbons to the steam involved in the reforming reactions [22].

Space time (τ)

τ can be expressed as the ratio of volume of the reactor and the volumetric flow rate at reactor inlet conditions:

$$\tau[h] = \frac{V_{reactor}[m^3]}{\dot{V}_{reactants}\left[\frac{m^3}{h}\right]} \quad (27)$$

Space velocity (SV)

The SV is defined as the reciprocal of the space time and can be expressed as:

$$SV[h^{-1}] = \frac{\dot{V}_{reactants}\left[\frac{m^3}{h}\right]}{V_{reactor}[m^3]} \quad (28)$$

Gas hourly space velocity (GHSV)

The GHSV is defined as the quotient of the incoming volumetric to flow rate at normal temperature and pressure of reactants divided by the reactor volume:

$$GHSV[h^{-1}] = \frac{\dot{V}_{reactants}\left[\frac{Nm^3}{h}\right]}{V_{reactor}[m^3]} \quad (29)$$

Steam to carbon ratio (SC ratio)

Another useful parameter to determine free carbon formation conditions is the SC ratio, which can be expressed as:

$$\frac{S}{C}[\,] = \frac{Moles\ of\ steam\ fed\ to\ the\ reactor\ \left[\frac{mol}{s}\right]}{n \times Moles\ of\ hydrocarbon\ fed\ to\ the\ reactor\ \left[\frac{mol}{s}\right]} \quad (30)$$

where n is the number of carbon atoms in the hydrocarbon formula [22]. As already mentioned, the SC ratio plays an important role in determining carbon formation conditions. SC ratio and GHSV were the two parameters used during the tests of the present work, where the catalyst bulk volume was taken as volume of the reactor.

Generally, with a higher SC ratio the conversion rate is higher. However, for industrial application a lower SC ratio would reduce the mass flow though the plant, which helps to minimize the dimensions of the equipment and reduce the overall energy consumption [17] [23].

4. Experimental setup and software applications

4.1. Description

Since the test rig was located at TU Graz and reforming system was previously used a AVL several changes to the system had to be done to make the reforming apparatus independent from the control system in use at AVL. First, it was necessary to add an electrical cabinet to the reformer (Fig. 15). The electrical cabinet contained 5 EMKO PID manual heating controllers and a National Instruments CrIO-9067 chassis with 5 modules (Fig 16).

The EMKO process controller is a programmable switch that gives the possibility to determine automatically the PID (proportional integral derivative) parameters of the heating ramp.

The CrIO-9067 chassis was used for the data acquisition system of temperatures and pressures and for the control of the two 8626 Bürkert mass flow controllers and the diesel pump P326 Thomas Predos green Piston.

An electrical manual water pump, Stepdos 03 RC, and a manual steam evaporator, aDrop aThmos, were used to generate and introduce the necessary quantity of steam into the reformer. The electrical steam evaporator could not process more than 30 ml/minute of water, however the flow rate of steam in the present work was much lower.

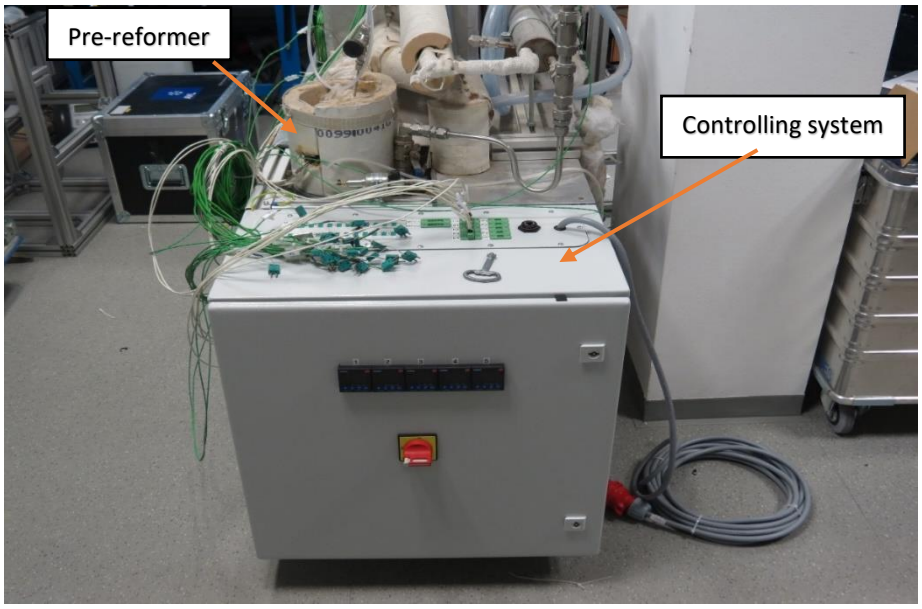

Figure 15 Reforming system with the electrical cabinet

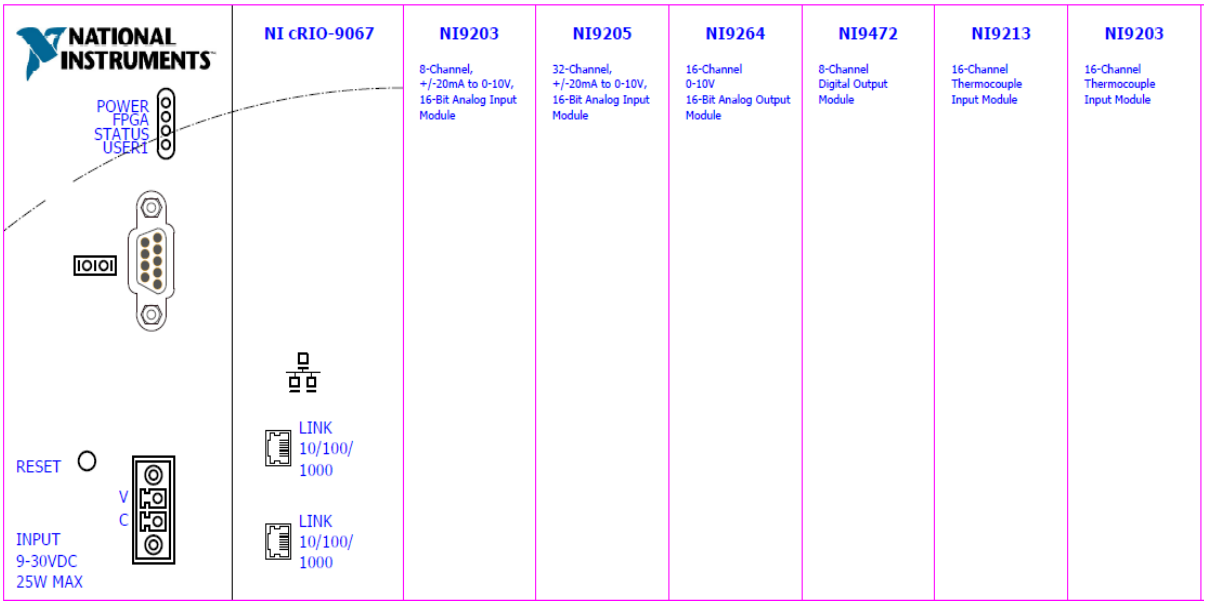

Figure 16 Schema of disposition of different modules in Crio chassies

The flow chart of the system is depicted in Fig. 17. The setup comprised 21 thermocouples, 5 heating cables, Horst HSQ, and 3 pressure sensors, type AVL APT100. The heating cables HB1 and HB2 were placed after the water evaporator and were controlled trough the thermocouples THB1 and THB2 respectively.

In Figs. 18 and 19 are depicted the positions of the thermocouples inside the diesel evaporator. The thermocouple T8 was located before the inlet of the diesel evaporator. In the

diesel evaporator the thermocouples were placed as may be seen from Fig. 18. The thermocouple T1, which was also controlling the heating cable HB3, was located at the top of the evaporator. The thermocouples T2-T7 were located progressively below T1.

Due to its composition diesel presents a wide range of high evaporation points and it is generally difficult to vaporize [4]. Typically, the highest evaporations points lie over 350 °C. Moreover, in our set-up there was no pre-heating system before the diesel was entering the evaporator. Therefore, it was decided to set the temperature at the thermocouple T1 to 500 °C to vaporize the diesel instantly when it was entering the evaporator. The thermocouples T2-T7 were used to measure the distribution of temperature inside the diesel evaporator. By methane SR the relative high temperature in the diesel evaporator was not important.

The thermocouple T9 (Fig. 21) and the pressure sensor P0 (0-600 mbar) were located just downstream the diesel evaporator, to measure the temperature and pressure in the pipe between the diesel evaporator and the reactor. This pipe needed to be constantly kept at a temperature higher than 400 °C to avoid any possible diesel condensation and consequent tar formation inside it. The heating cable HB4 was used to heat the pipe from the outlet of the diesel evaporator to the inlet of the reactor. T12 controlled the heating cable HB4 through a PID controller. The pressure sensor P1 (0-300 mbar) was located before the inlet of the reforming reactor.

T13-T20 were situated inside the reforming reactor (Fig. 20). The heating cable inside the reforming area was controlled by the thermocouple T19 trough a PID controller. The last thermocouple in the reactor was T20. The pressure sensor P2 (0-300 mbar) was located just downstream the reforming reactor. The two pressure sensors P1 and P2 were used to estimate the pressure drop between the inlet and the outlet of the reforming reactor. The difference between the pressure P1 and P2 was used to determine possible carbon formation phenomena inside the reactor.

The temperature of the outlet gas was measured at the thermocouple T21, just after the cooling system (Fig. 22). It was important that the temperature at T21 was close to the room temperature to avoid water condensation at gas analyzer. Part of the reforming gas was analyzed and part was going to an aspiration system. The condensed byproducts were collected in a container.

The use EMKO controllers allowed to reduce substantially the LabView coding. However, there were some limitations: it was not possible to log automatically the values of the temperatures at T1, T12 and T19. Once the system reached the operative temperatures, these values were read and inserted manually in the Labview application.

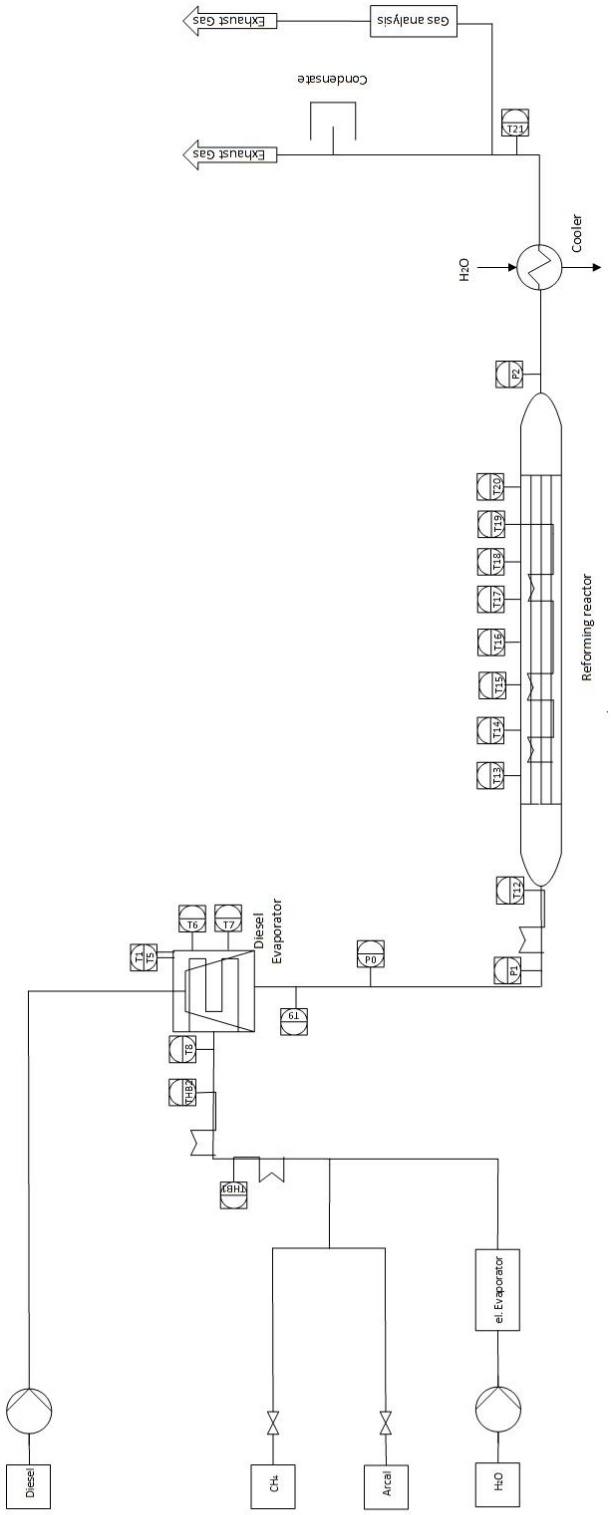

Figure 17 Flow chart of the system.

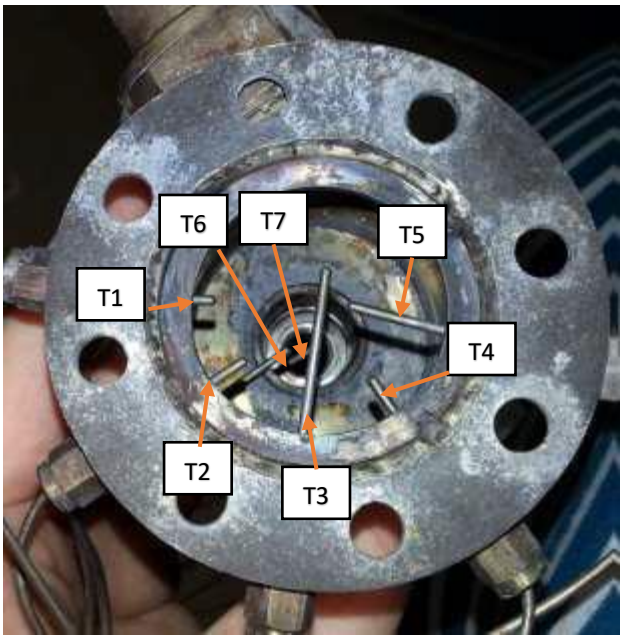

Figure 18 Diesel evaporator viewed from inside [24].

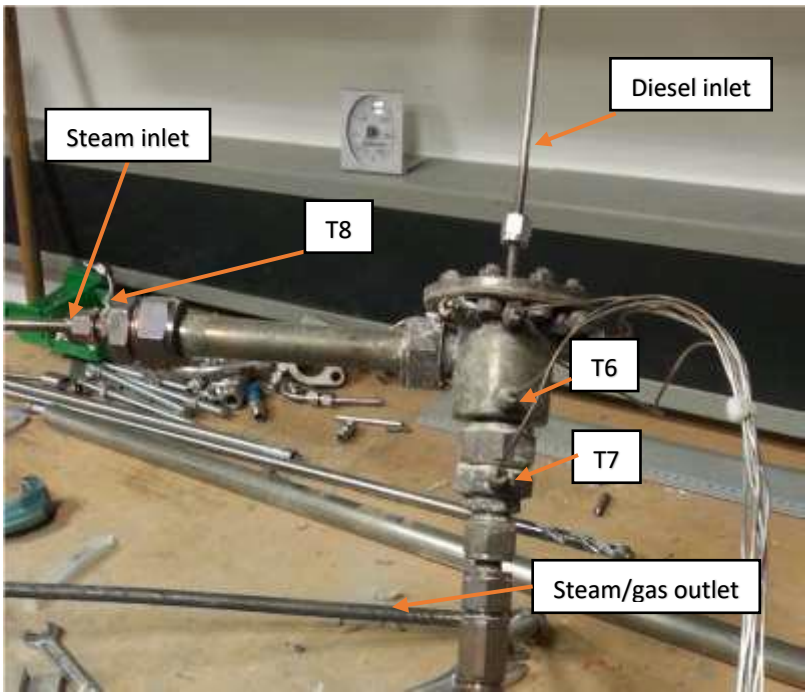

Figure 19 Diesel evaporator viewed from outside [24].

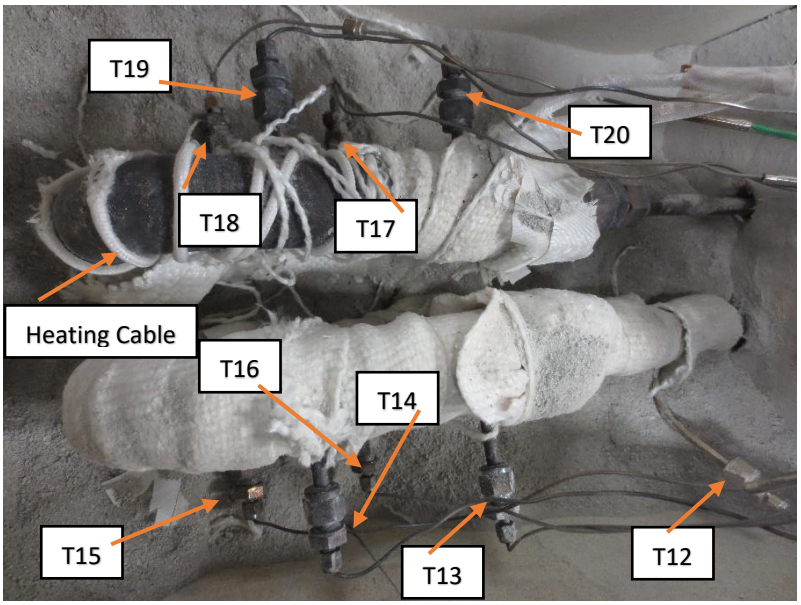

Figure 20 Picture of the reforming part with thermo-elements.

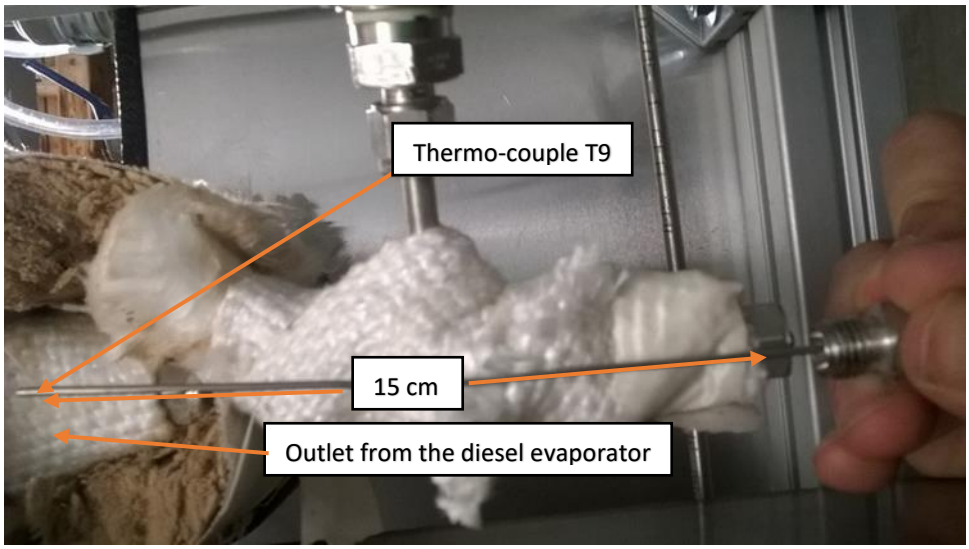

Figure 21 Position of the thermocouple T9 viewed from below.

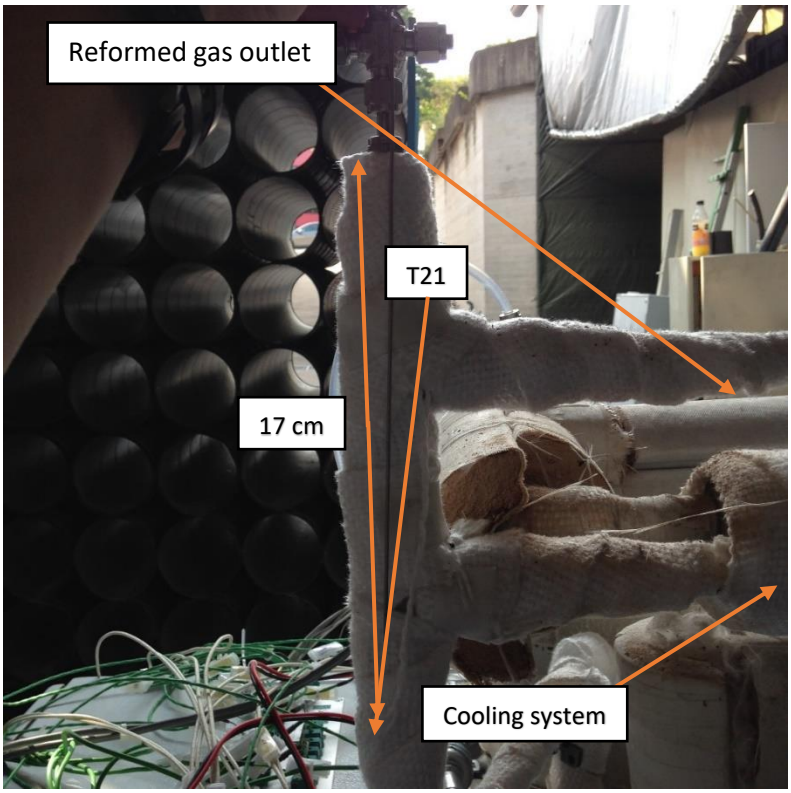

Figure 22 Position of the thermocouple T21

Since at the beginning of the testing the heating cables were winded up directly on the pipes, quite often, when the isolation of the heating cable was falling apart due to the frequent temperature excursions, the contact between the pipe and the metallic resistance of the heating cable was causing short circuits. Therefore, the pipes were first winded up with a material for electrical isolation and then with the heating cables, as illustrated in Fig. 23.

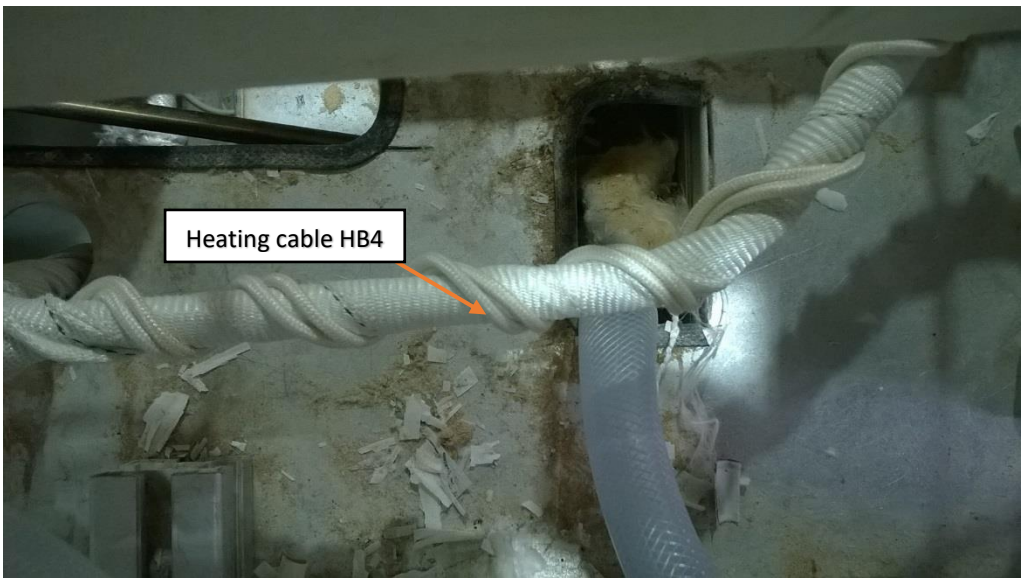

Figure 23 Isolation layer between the heating cable HB4 and the pipe

The structure moved to TU Graz together with the reforming gas bundle is depicted in Fig 24.

Figure 24 Reformer under the aspiration system and forming gas bundle

The gas analyzer used to sample the outlet gas was the ABB model AO2000 with 6 different modules for CO_2, CO, CH_4, O_2 and H_2 (Fig. 25). Data was collected every 5 seconds and logged on an excel file. The gas analyzer did not have an integrated pump to aspire air from the exhaust of the reforming system. It was necessary to adapt an external pump, otherwise the outlet gas could not have reached the gas analyzer. In several occasions steam condensed inside the internal filters of the gas analyzer and water needed to be promptly removed.

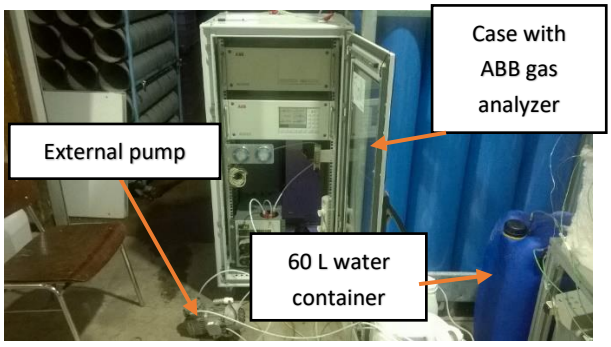

Figure 25 Case containing the ABB gas analyzer and external pump

The gases used for the tests were free sulfur methane and forming gas. The forming gas, Arcal F5, consisted on a 95% N_2 and 5% H_2 mixture. It has been used as a reducing agent by heating

and cooling and for partial activation of the catalyst. The forming gas was delivered directly to TU Graz in bundles. The methane was used mostly for the complete activation of the catalyst and for the first preparatory tests.

Sulfur free diesel has been used. Diesel is a mixture of different hydrocarbons ranging from $C_{12}H_{20}$ to $C_{16.2}H_{30.6}$ [25]. Since in the previous work [24] was used the formula $C_{16}H_{34}$ (hexadecane) to calculate the necessary normal flow rate from SC ratio and GHSV during the tests, the same approximation has been adopted in the present work. This approximation was in satisfactory accordance with the equilibrium, at least for concentrations of CH_4 and H_2 in the outlet gas.

4.2. Labview control application

A Labview application has been implemented for data acquisition and control of the diesel pump and two MFCs. The application consisted mostly in two parts

One program was installed directly on the National Instrument Controller CrIO-9067. The program includes an FPGA routine for the control of the digital signal to the diesel pump. The digital signal for the diesel pump should have a pulse width (time on) of 25ms. In Fig. 26 are summarized the main functionalities of the program installed on the controller: reading instructions from the host, sending signals to MFCs and diesel pump, acquiring data from thermocouples, pressure sensors and MFCs and sending data to the host. The clock of the sampling loop was 1KHz and with a period of 200ms.

Figure 26 Main functionalities of the program installed on the NI controller

The second part of the application was a program installed on the host (laptop). The application was mainly a console application able to send instructions to NI controller and log data every second (Fig. 27).

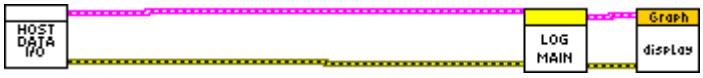

Figure 27 Main functionalities of the program running on the host

In the Labview application it has been implemented also an alarm system to block the methane mass flow controller, the diesel and the water pump and activate automatically the forming gas mass flow controller, in case a set limit of temperature and pressure was exceeded. The first version of the alarm was just deactivating the pumps and the mass flow controller of methane when the limit was exceeded. However, once the values of pressure and temperature were again below the limits, the pumps and mass flow controller were reactivated. As explained in the test of 06-09, this alarm system was wrongly designed. In fact, when one of the alarm limits was exceeded, it would have been necessary to block permanently the two pumps and MFC of methane and at the same time to activate the MFC of the forming gas.

After these changes, the alarm was too reactive and the reforming reaction could not run longer than few hours: when a single pressure peak was exceeding the alarm limit, the reaction was promptly interrupted (tests on 22-09-2016 and 23-09-2016). Therefore, it has been decided to average the signals of pressure over the last 3 second. With this solution, it was possible to perform longer tests.

4.3. Catalyst

The catalyst was changed inside the reactor before starting with measurements. The catalyst material consisted on a mixture of nickel monoxide, aluminum oxide, aluminum silicate and magnesium oxides tablets of the sized of 4.7x4.7 mm. The volume of the catalyst inside the reactor was simply determined by weighting the empty and the full reactor, considering the difference and dividing it by the bulk density, which in our case was 1.2 Kg/dm^3. Since the main purpose of the present work was to verify the performance of the catalyst after several hours of operation, the risk to damage it was elevated. The ruined catalyst was changed two times. During our set of measurements two different catalysis volumes were used: 0.683 dm^3 and 0.6725 dm^3. In Fig. 28 are reported the two ruined catalysts during the change.

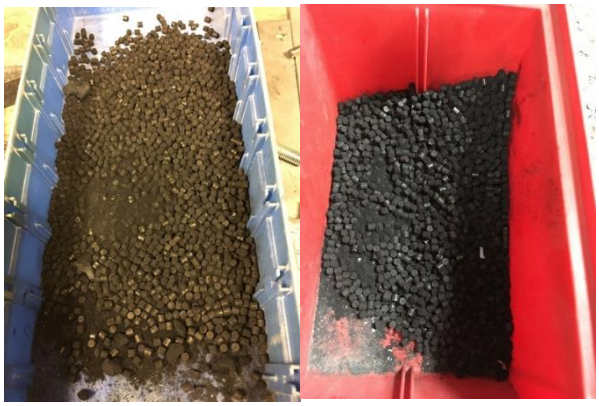

Figure 28 Ruined Ni-catalysts during the change (left: first catalyst, right second catalyst).

The catalyst had to be activated before being fully operative. In the present work, the catalyst was first partially reduced with forming gas and then completely activated though methane reforming process.

4.4. Equilibrium determination

For every SC ratio used in our diesel test the equilibrium has been calculated using a virtual reforming reactor written in Matlab/Simulink. It was sufficient to insert the respective quantity of water and diesel in Nl/h to have an appropriate outlet composition. The calculation has been performed with the diesel formula $C_{12}H_{26}$. Since the distribution of temperatures in the reactor during the reforming process ranges typically form 430 °C to 560 °C, it was not feasible to make a direct comparison between the values obtained from the computed equilibrium and those obtained from the real reforming process. However, an evaluation of the theoretical equilibrium suggested a possible window of temperatures, at which the actual reforming process took place. The results are summarized in chapter 6.

5. Measurements

5.1. Introductory Remarks

The measurements performed at TU Graz were principally aimed at determining stability conditions of diesel SR at relatively low temperature (400-600 °C). In contrast with the previous work [24], medium and long time stress tests with diesel reforming were performed. Typically, the duration of tests ranged from several hours to several days.

The major problem was to control the carbon formation process when the system was not directly overseen. As previously explained, the carbon formation could occur during the SR process. However, it may happen also during accidents unrelated to the reforming process. For example, in case of interruption of SR process when diesel pump is not promptly deactivated the direct contact with vaporized diesel and the catalyst has detrimental effects. During tests performed in the present work, a failure of the water pump occurred 3 times with the consequence that pure diesel without steam was supplied to the catalyst. In all cases the pressure at the inlet of the catalyst, after an initial drop, increased steeply.

5.2. Calibrations

The two mass flow controllers, one for forming gas and the other for methane worked both with 10 V I/O signals. They were controlled by the I/O modules NI9205 and NI9264.

The calibration of the two mass flow controllers was performed with a so-called Gilibrator-2[2]. The working principle of Gilibrator-2 is to measure the time that soap bubbles generated at the bottom of a plastic cylindrical column take to reach the top of it. The time gives the value of the volume flow rate. The calibration was performed by sending to the MFC an input signal ranging from 0 V to 3.5 V for the forming gas MFC and to 5 V for the methane MFC at intervals of 0.5 V. For every input signal to MFC, the measurement of the volume flow rate was

[2] *Gilibrator-2 System provides an automated way to check almost any commercially available air sampling pump for proper air flow function before deployment. Source: http://www.sensidyne.com/air-sampling-equipment/calibration-equipment/gilibrator-2/*

repeated 5 times with Gilibrator and, at the same time, the values of the signal output form the MFC were acquired. The values of the volume flow rate and the signal output were averaged. The volumetric flow rate has been converted to normal flow rate and plotted versus the signal output as depicted in Fig. 30. The normal flow rate is simply the volumetric flow rate at 0 °C temperature and at 1.01325 bar pressure. A linear interpolation has been obtained and used as calibration parameter in the Labview application.

Figure 29 Picture of Gilibrator 2 (source: http://www.sensidyne.com/air-sampling-equipment/calibration-equipment/gilibrator-2/)

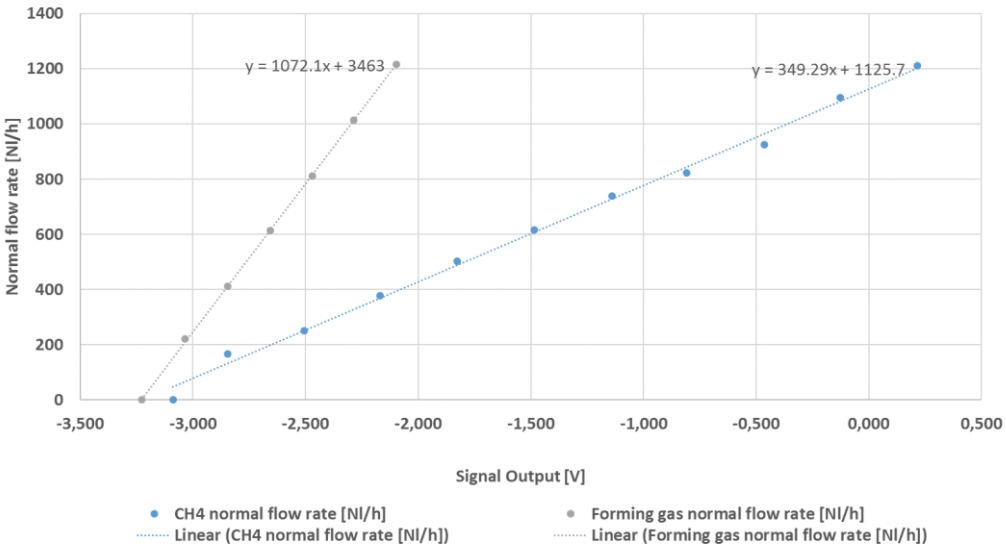

Figure 30 Calibration results for the methane and forming gas MFCS

The settings of the manual water pump allows user to calibrate directly the pump according to actual flow measured. The water pump was calibrated at the beginning of the measurements, on the 04-10-2016 and on 20-10-2016.

The diesel pump was initially calibrated by measuring the weight of diesel after 5 minutes by sending a 10 Hz frequency signal. The calibration has been performed by converting the frequency signal in Hz to the mass flow rate in gr/h. In the piping system of the diesel pump the accumulation of air was one of the major problem. Sometimes, during the tests, air had to be eliminated with a syringe from the piping system. Before starting each test the diesel pump was recalibrated.

The three pressure sensors have been calibrated using GE's Druck DPI 611 Pressure Calibrator. The calibration consisted in converting the current signal in mA to the measured pressure values in mbar.

5.3. Test matrix

The carbon free parameter results presented in the previous AVL thesis on diesel reforming [24] were considered for the test matrix. For our tests relatively small GHSV were chosen to avoid big mass flow rate of water and diesel when the apparatus was not overseen: GHSV=600 h^{-1} and GHSV=1200 h^{-1}.

The temperatures of T12 and T19 were always set at 545°C for several reasons. Namely, in literature diesel pre-reforming tests are often performed at 550°C. Since it was necessary to compare results under similar conditions, temperatures at T12 and T19 during different tests were kept constant.

Table 1 Test matrix.

Reactor Controlling temperature T12=545°C, T19=545°C						
GHSV[h-1]	SC					
600	4	3	2.5	2	1.9	1.8
1200	4	3	2.5	2	1.9	1.8

After several tests, it was decided that the most suitable GHSV was 1200 h^{-1}. In fact, it was expected that the diesel pump was working better with a higher diesel mass flow.

By using $C_{12}H_{26}$ formula in the equilibrium, carbon formation was not predicted in the range of pre-reforming temperature, 400-600 °C, with SC ratio 1.9 and 1.8. Therefore, also these two references were included in the test matrix. However, a rise in pressure difference was found on 13-10 with SC ratio 2. Thus, it was preferred to continue with SC ratios not lower than 2.2.

5.4. First catalyst measurements

The reactor was filled with the catalyst on 04-08-2016 and its volume was 0.683 dm^3.

5.4.1. Test of 02-09-2016 / Catalyst 1

It was an overnight test with methane at GHSV 600 h^{-1} and SC ratio 2. The actual values for SC and GHSV, obtained reading the signal output from MFC, were 2.1 and 591 h^{-1}. The test was aimed at assessing the stability of the system operating for 12 hours without direct supervision of the operator and at activating the catalyst with methane reforming (Fig. 31).

The reactor had been previously heated up to reach 500 °C and kept at this condition for approximately 6 hours. During this operation 400 Nl/h of forming gas has been supplied to the system for partial reduction of the catalyst. The complete reduction has been achieved by reforming with CH_4.

During the overnight test the values of the inlet and outlet pressures, temperatures inside the reforming reactor and outlet gas composition were stable.

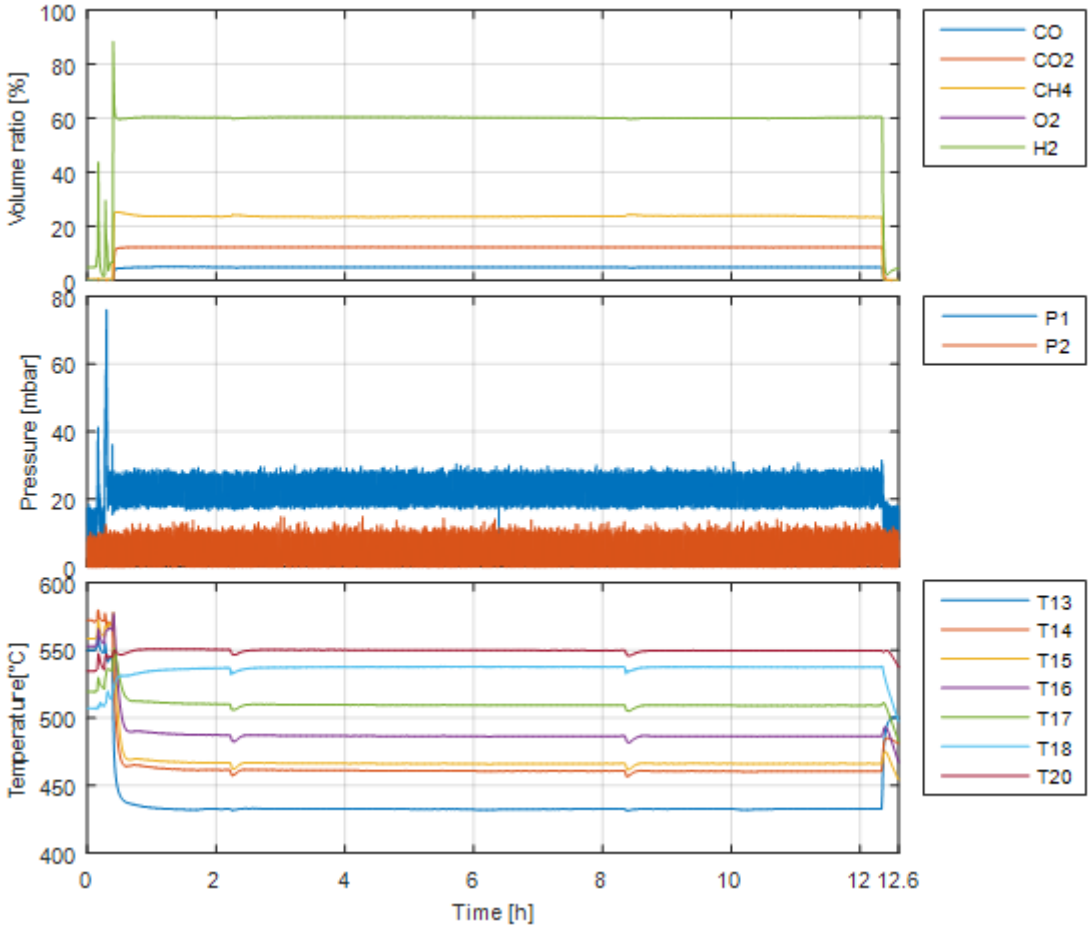

Figure 31 Overnight methane steam reforming test with SC ratio 2.1 and GHSV 591 h^{-1}. Temperature T12 and T19 were both at 545 °C.

The PID controllers regulating the temperature at T12 and T19 were both set to 545 °C. T20, the thermocouple close to the outlet of the reactor registered the highest temperature. The lowest temperature was registered at T13. In general, low temperatures were measured in the first section of the reactor. The actual temperatures at T12 and T19 could not be displayed because T12 and T19 thermo-couples were connected to the PID controller and as such their values could not be logged. Pressure and temperature values were quite stable during the whole duration of the test.

5.4.2. Test of 06-09-2016 / Catalyst 1

On 06-09-2016 the first test with diesel was performed. Two preparatory tests at SC=2, GHSV=600 h^{-1} and 1000 h^{-1} were carried out before the overnight test (Fig. 32).

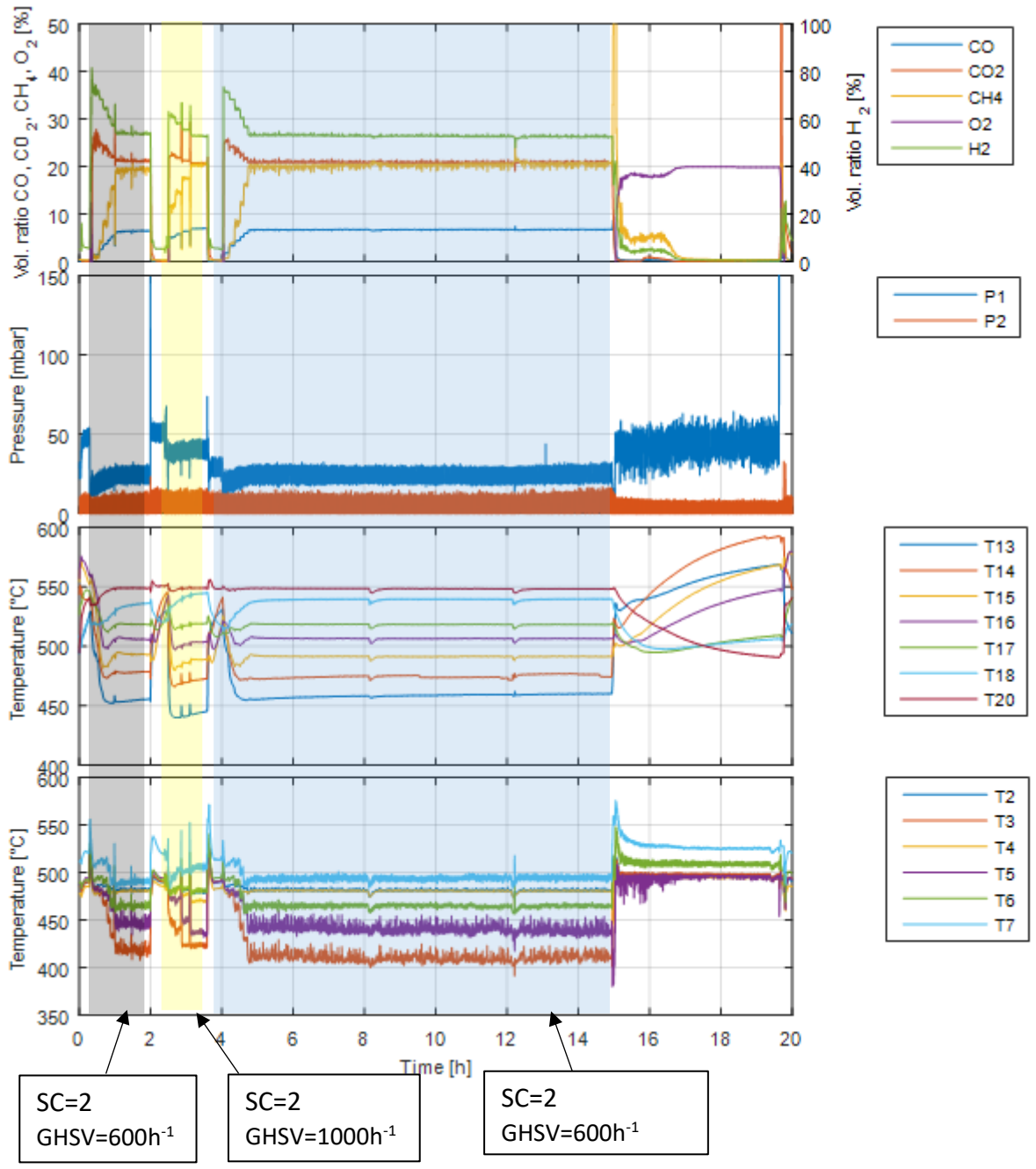

Figure 32 Volume ratio of the outlet gas, pressure at the inlet and outlet of the reactor, temperature distribution in the reactor and temperature distribution in the diesel evaporator on 06-09-2016 (T12=545 °C, T19=545 °C and T1=500 °C).

In the equilibrium simulation it was noticed that carbon formation was predicted within the temperature range of 400-600 °C already at SC ratio 1.7. To avoid starting with a too low SC ratio, the water pump was first set to values required for selected parameters of SC ratio and GHSV. Then the mass flow rate of diesel was gradually increased. This is visible from the stepped shape curves of the outlet gas concentration diagram (Fig. 32).

The overnight test started at approximately 16:20 and it was interrupted due to a problem with the water pump, which stopped working at 03:37 on 07-09-2016. This happened possibly because there was no hole on the top of the water container. Presumably, the pump was not operating due to the low pressure inside the container.

The pressure P1, which was stable with a value of 20 mbar, decreased abruptly and then increased just after a few minutes. The alarms, set at 40 mbar, temporary blocked the diesel pump. However, the alarm system was not properly designed: every time the pressure was under the 40 mbar alarm limit, the diesel pump was reactivated. Therefore, the catalyst remained in contact with the vaporized diesel for several hours.

Moreover, forming gas was not supplied to the system, when the pumps were deactivated. Most probably this caused also the oxidation of catalyst. In Fig. 32 it is possible to see, that after 15 hours, a decrease of pressure was followed by a sudden increase of it, the increase of the methane concentration and the presence of 20% vol. oxygen in the outlet gas. The presence of oxygen is attributable to the presence of air which was expelled later by manually activated forming gas flow.

In the morning on 07-09-2016 the water pump and the forming gas mass flow controller were activated to clean the catalyst from the carbon depositions. A concentration of CO_2 was present in the outlet gas for some hours and the pressure difference, P1- P2, compared with the same quantity of forming gas was several times higher.

The system was washed with 400 Nl/h of forming gas and steam ranging from 373 Nl/h to 746 Nl/h (Fig. 33). After approximately 5 hours the steam flow was set permanently to 373

Nl/h. However, the pressure difference P1-P2 remained quite high throughout the washing operation. Approximately after 3 hours the concentration of CO_2 was zero. Instead, the ones of CO and CH_4 remained stable during the washing process. The concentration values of CO and CH_4 were not negligible for all the carbon removal/washing procedure. In the other carbon removal procedures with the second catalyst these values were considerably lower or even close to zero.

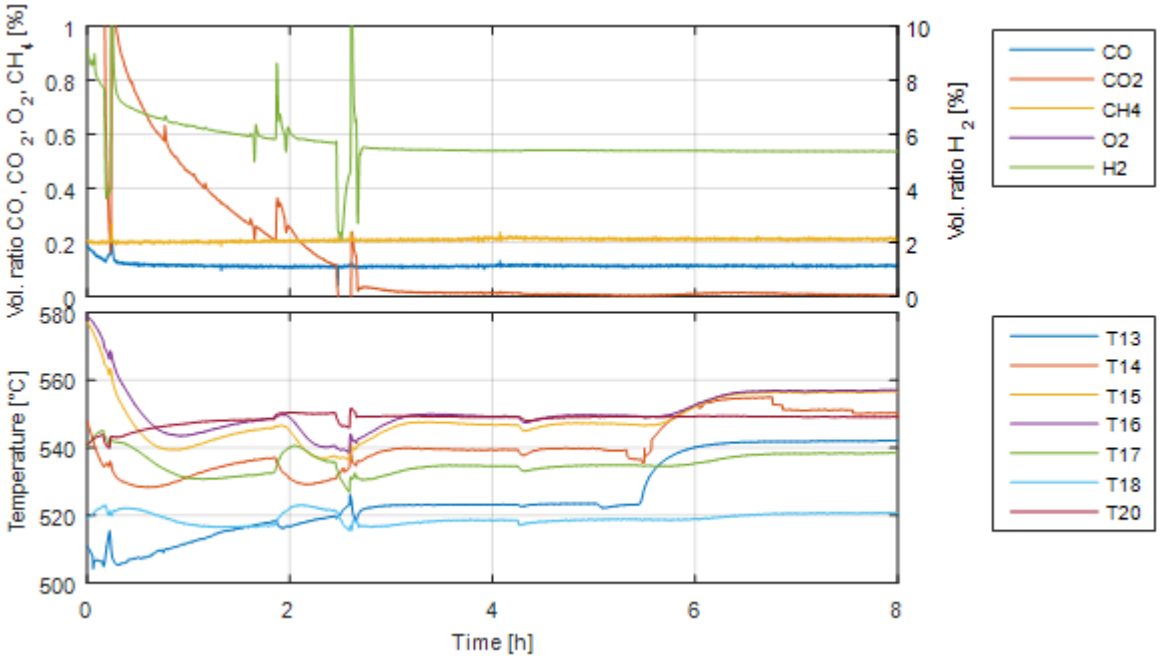

Figure 33 Washing after carbon formation on 07-09-2016. The temperatures T12 and T19 were kept at 545 °C. The steam flow rate was ranging often between 373 Nl/h and 746 Nl/h.

5.4.3. Test of 13-09-2016 / Catalyst 1

Between the 07-09-2016 and 13-09-2016 further tests were conducted with an SC ratio higher than 2. Since improvements could not be identified and the values of outlet gas composition were deteriorated due to the heavy carbon formation at the catalyst on 06-09-2016, the results of these tests are not discussed.

The test on the 13-09-2016, reported in Fig. 34, was the last of this series. If compared with the test of 06-09-2016 the activity of the catalyst was drastically changed: the concentration of H_2 decreased from approximately 52% to 40%, while the one of CH_4 increased from 20% to

35%. The initial pressure drop between the two tests was also very consistent. On 06-09-2016 ΔP was around 20 mbar, while on 13-09-2016 it increased to 147 mbar.

Moreover, after approximately 4 hours also the activity of the catalyst changed and the concentration of CH_4 exceeded the one of H_2. The ΔP reached 190 mbar.

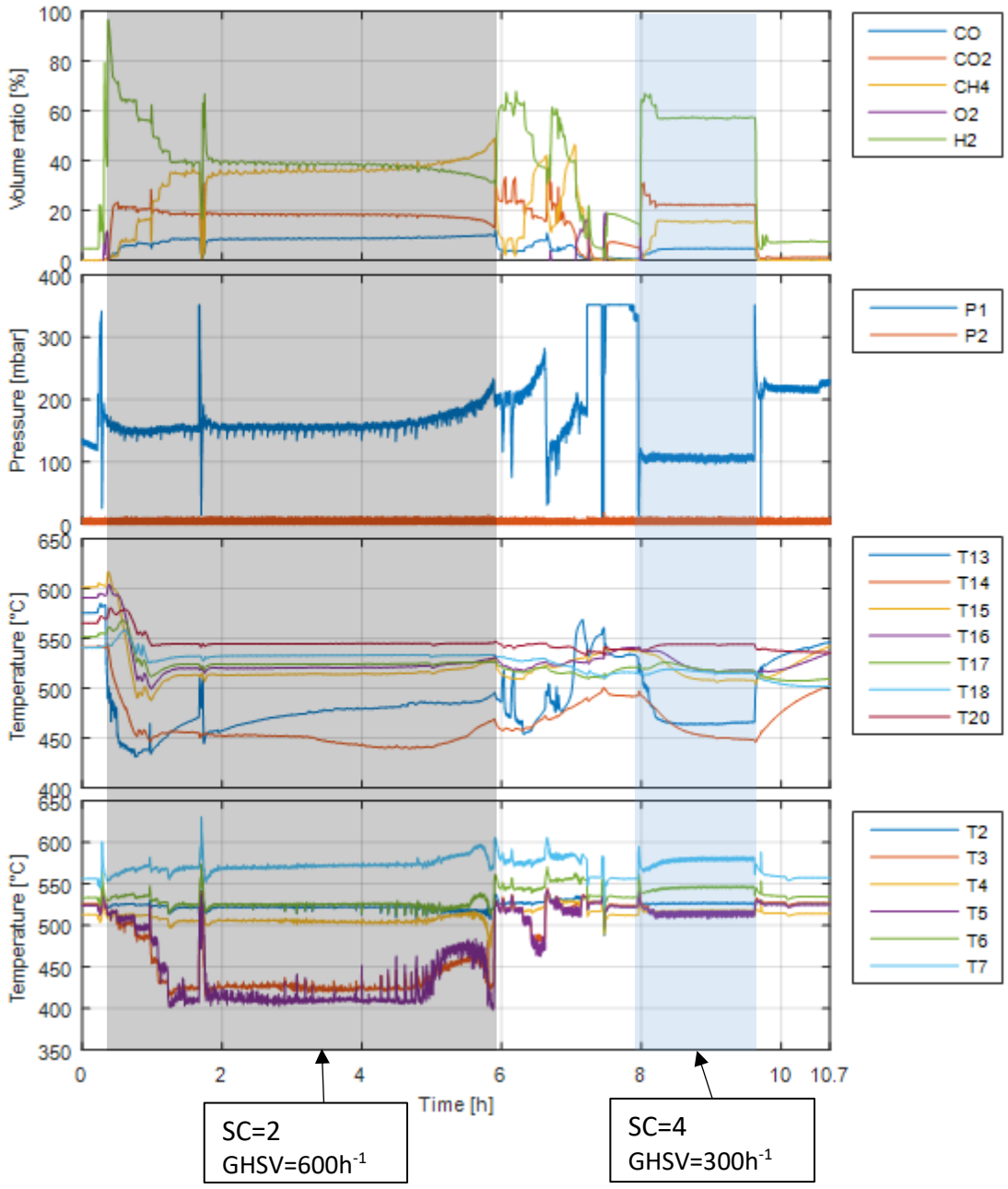

Figure 34 Volume ratio of the outlet gas, pressure at the inlet and outlet of the reactor, temperature distribution in the reactor and temperature distribution in the diesel evaporator on 13-09-2016 (T12=545 °C, T19=545 °C and T1=500 °C).

Another test with SC ratio 4 and GHSV 300h^{-1} was performed for approximately 1.7 hour which seemed to be more stable. However, it was decided to replace the catalyst since it was strongly deteriorated.

The alarm system was also modified to ensure that every time when a registered value of temperature or pressure exceeded the alarm limit value, the pumps would have been completely deactivated till the test would have been restarted. At the same time the mass flow controller of forming gas would have been automatically activated to avoid a possible oxidation of the catalyst.

5.5. Second catalyst measurements

On 14-09-2016 the first catalyst was changed and replaced with a new one, whose volume was 0.06725 dm^3.

5.5.1. Test of 16-09-2016 / Catalyst 2

Before starting with the diesel test it was necessary to reactivate the new catalyst.

First the catalyst was partially reduced in forming gas atmosphere. Since the manual suggests that for a complete activation of the catalyst a N_2 and H_2 mixture should be used with at least 10% H_2, the activation has been completed by steam reforming with CH_4. The activation process with CH_4 is depicted in Fig. 35.

It was decided to perform a test which lasted several hours to see also if the problem with pumps or any other issue could occur again. Initially, the SC ratio was 2 and then it was changed to 2.8 (values calculated from the signal output of MFC). Due to connection problems during the first 5 hours the data of outlet gas composition were not logged.

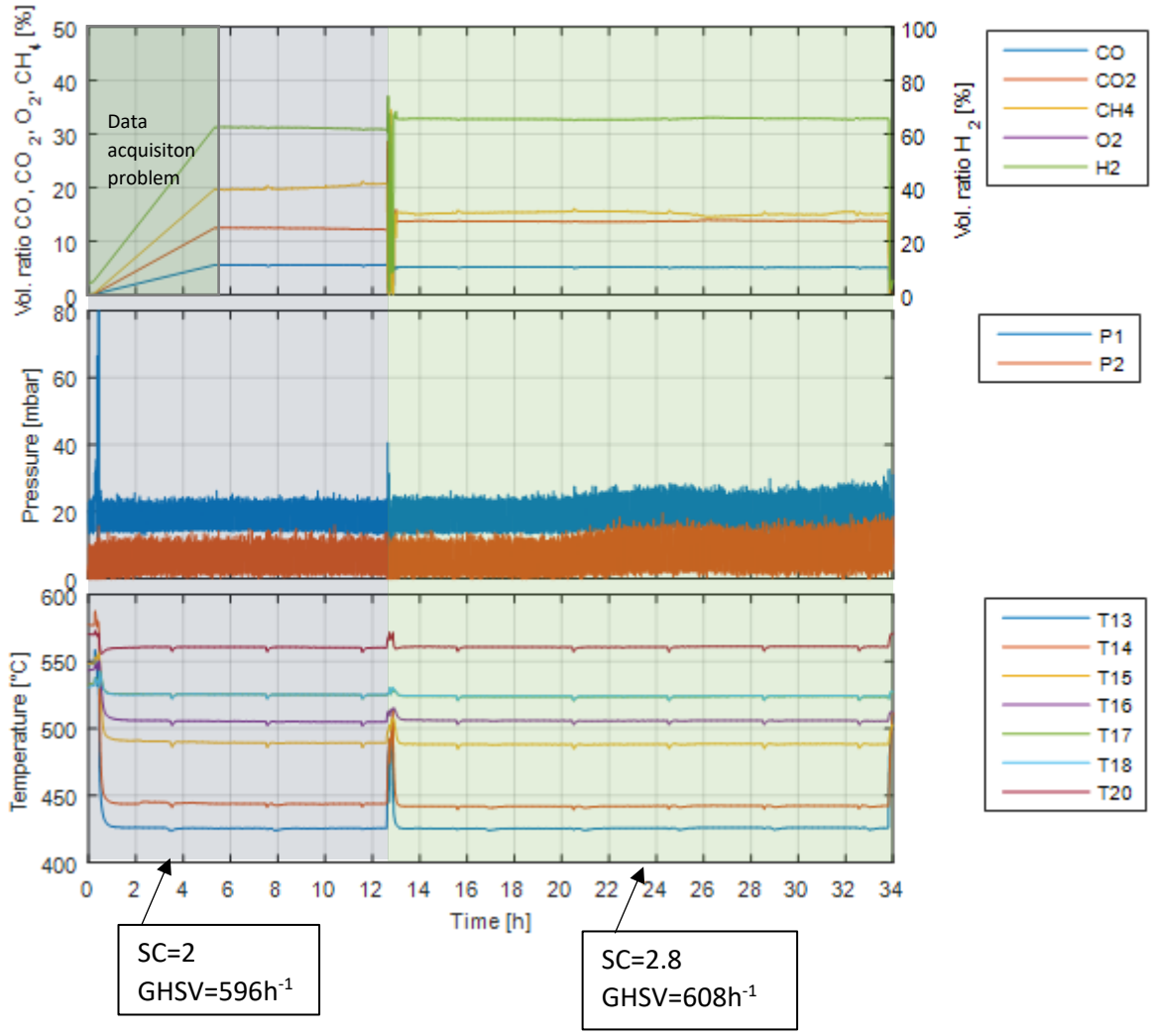

Figure 35 Volume ratio of the outlet gas, pressure at the inlet and outlet of the reactor and temperature distribution in the reactor on 16-09-2016 (T12=545 °C, T19=545 °C).

Increases in the pressure drop were not noticed during the 34 hours test. After 20 hours P1 and P2 augmented together because some condensed water accumulated in the gas exhaust. This determined also a slight change in the outlet gas composition. The alarm limit for the pressure was set just 25 mbar over P1 value, which was approximately 20 mbar. There were no particularly high pressure peaks during the test, except when the SC ratio was changed from 2 to 2.8.

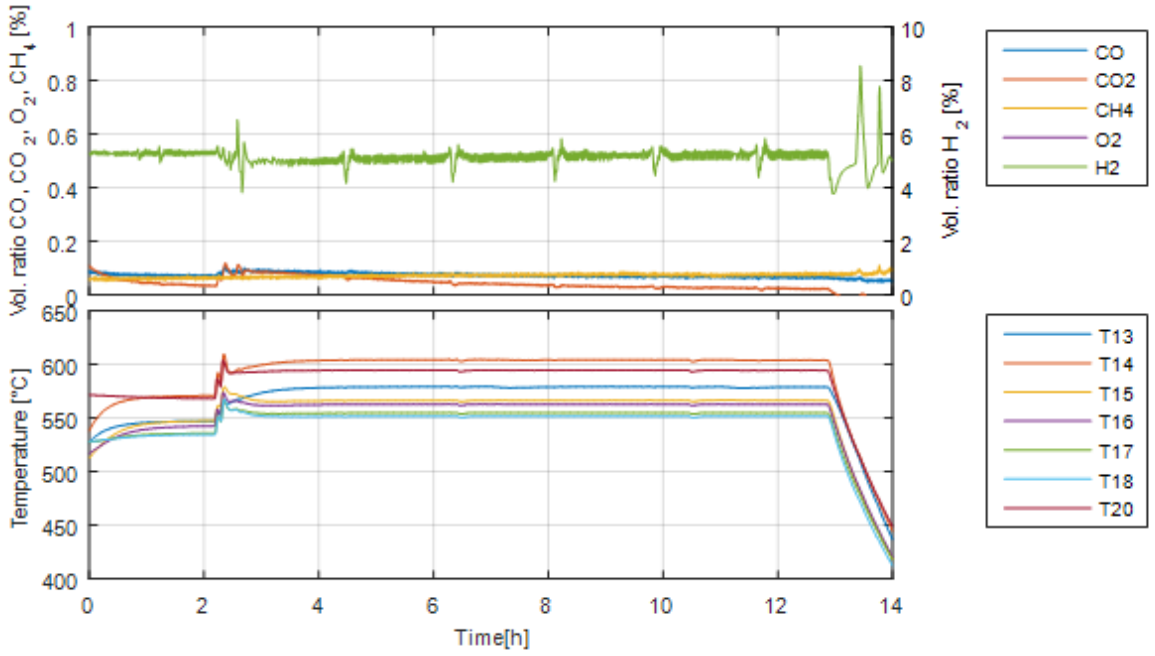

Figure 36 Carbon removal after the test on 16-09-2016

After the test, the catalyst has been washed with 400 Nl/h of forming gas and 18.6 Nl/h steam (Fig. 36). The temperature was increased to 580 °C at T12 and T19 after approximately 2 hours to ease the steam gasification process of carbon. The value of CO_2 concentration in the outlet gas was found much lower if compared with one of the other carbon removal procedures after diesel SR. However, the flow rate of steam was definitely lower than the one used in the other carbon removal procedures. After 13 hours the system was cooled down.

5.5.2. Test of 22-09-2016 / Catalyst 2

On 21-09-2016 two diesel tests with an SC ratio 4 and GHSV 600 h^{-1} were performed. However, due to some pressure peaks, which were not present in the test on 16-09-2016 with CH_4, the alarm deactivated the pumps and the tests were suspended. It was assumed that with GHSV 600 h^{-1}, the mass flow rate of diesel was too low for the diesel pump and that this could create some fluctuations in the pressures values. On 22-09-2016 the tests were carried out with GHSV 1200 h^{-1}.

Since on 21-09-2016 the tests were interrupted because of unexpected pressure peaks, the system operated without alarm for approximately 8 hours. After 8 hours, the pressure was checked and it was noticed that there were still 110 mbar peaks (Fig. 37). The pressure alarm was increased to 200 mbar.

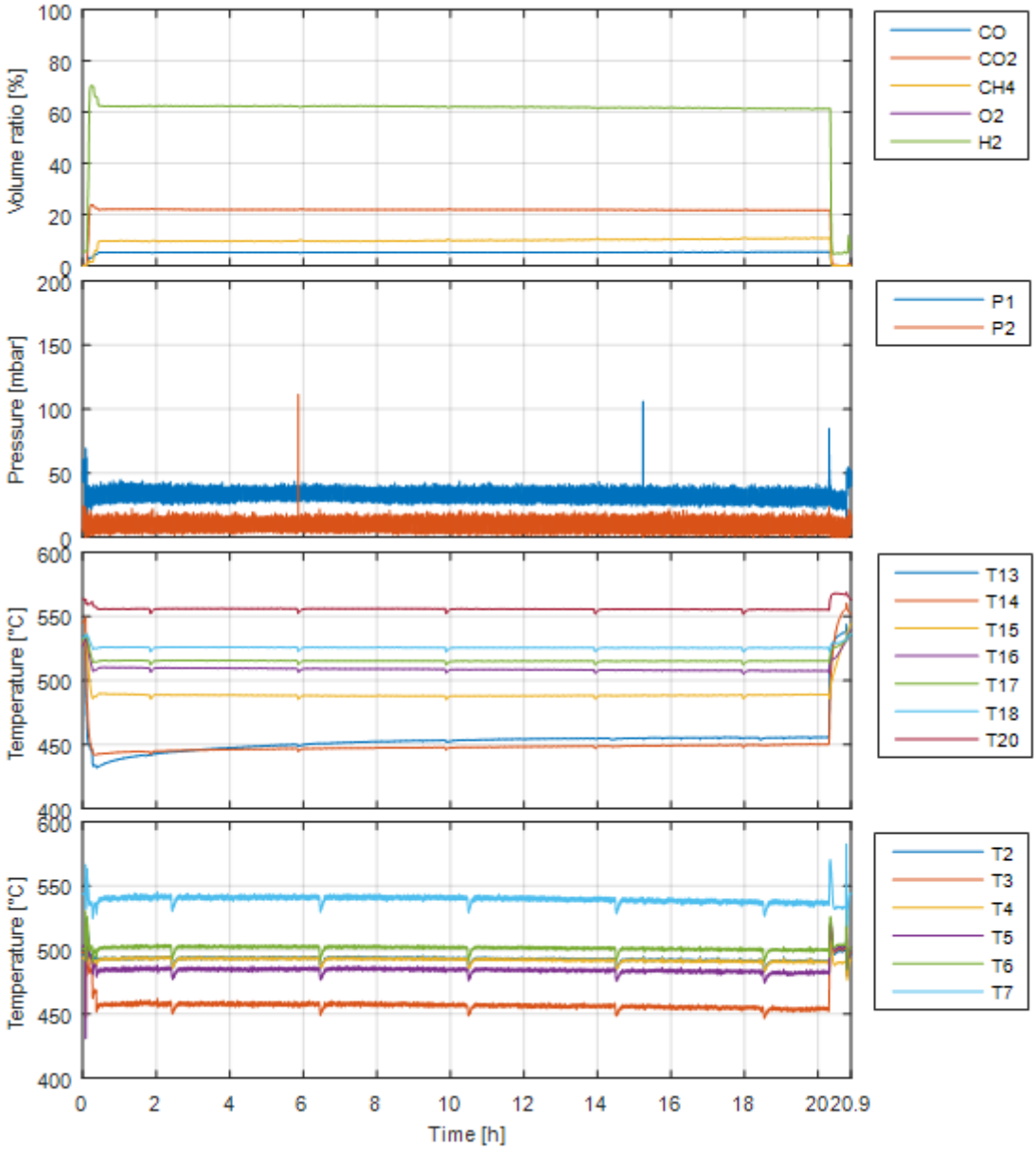

Figure 37 Volume ratio of the outlet gas, pressure at the inlet and outlet of the reactor, temperature distribution in the reactor and temperature distribution in the diesel evaporator on 22-09-2016 (SC=4, GHSV=1200h^{-1}, T12=545 °C, T19=545 °C and T1=510 °C).

At around 6:30 on the 23-09-2016, after approximately 20 hours of operation, the alarm limit was triggered. Surprisingly in the log file there is no evidence of a peak higher than 200 mbar.

Although the log file was updated every second the data were acquired every 200 ms. Some values of pressure could have exceeded the 200 mbar without being visible.

During the test the pressure difference between P1 and P2 remained quite stable, even though the outlet gas composition slightly changed. It was also noticed that some air was present in the piping circuit of the diesel pump. For this reason, the piping has been shortened for the following tests.

5.5.3. Test of 23-09-2016 / Catalyst 2

The test was carried out with SC ratio 3 and GHSV 1200 h^{-1} (Fig. 38). It was expected that, with a lower SC ratio and a consequent higher amount of diesel being pumped, the pressure peaks would have been reduced. After 8 hours of operation without any alarm limit, the pressure trend was checked and since no peaks were found the alarm was set to 75 mbar. Approximately 90 minutes after setting of the alarm, the two pumps were deactivated. It was still not possible to identify a pressure peak, which was exceeding the alarm limit. During the operation time the pressure difference and the activity of the catalyst remained stable.

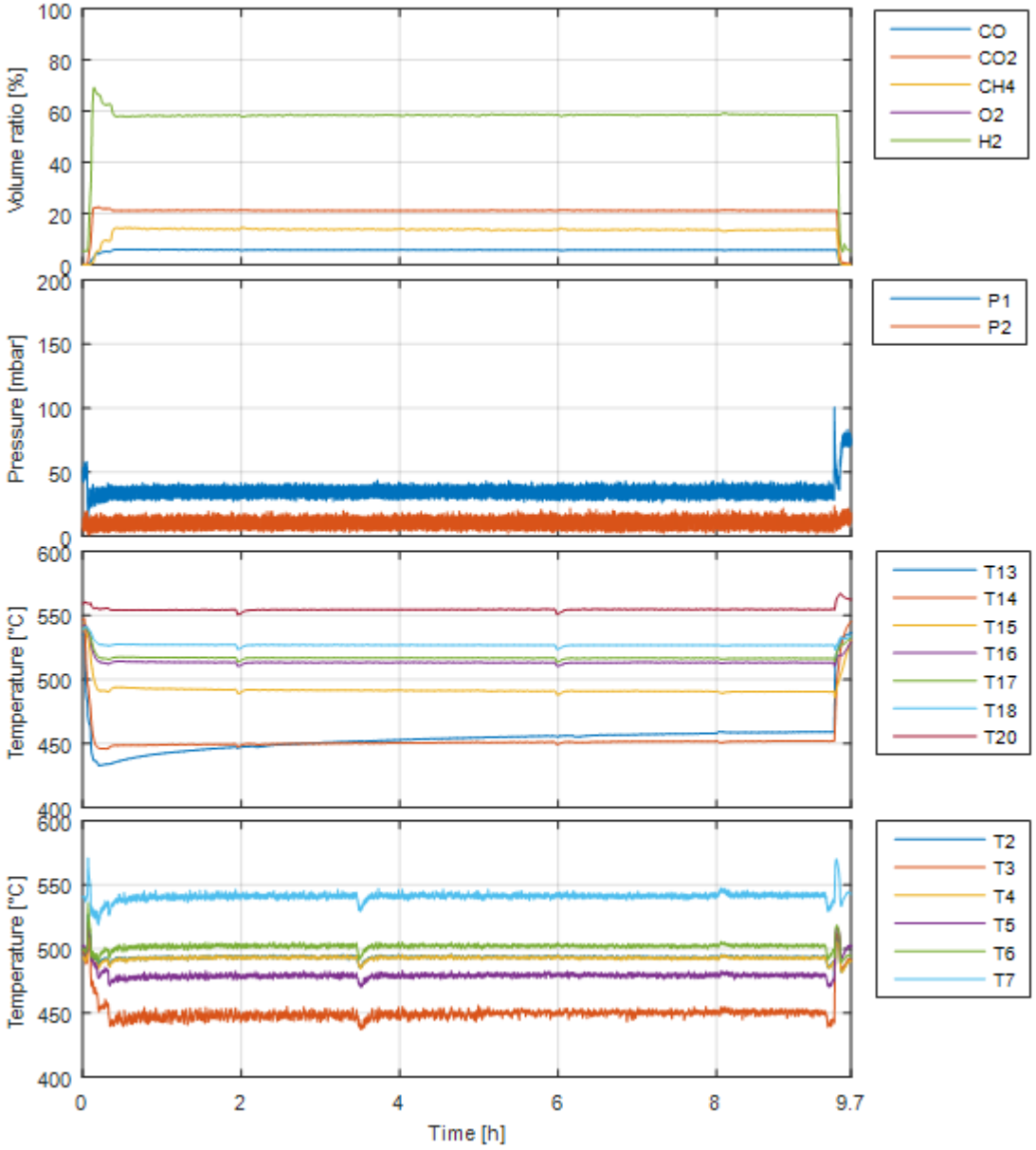

Figure 38 Volume ratio of the outlet gas, pressure at the inlet and outlet of the reactor, temperature distribution in the reactor and temperature distribution in the diesel evaporator on 23-09-2016 (SC=3, GHSV= 1200 h^{-1}, T12=545 °C, T19=545 °C and T1=510 °C).

After the test the system was washed with 400Nl/h of forming gas and 373 Nl/h of steam (Fig. 39). After approximately 3 hours the flow of steam was reduced to 18.6 Nl/h. With 373 Nl/h of steam, it was possible to observe in the outlet a gas a non-negligible concentration of CO_2. With 18.6 Nl/h of the steam the concentration of CO_2 was practically zero. The concentration peaks of CO, CO_2 and H_2 occurred after 4 hours and the corresponding temperature fluctuation cannot be explained by any specific event to my knowledge.

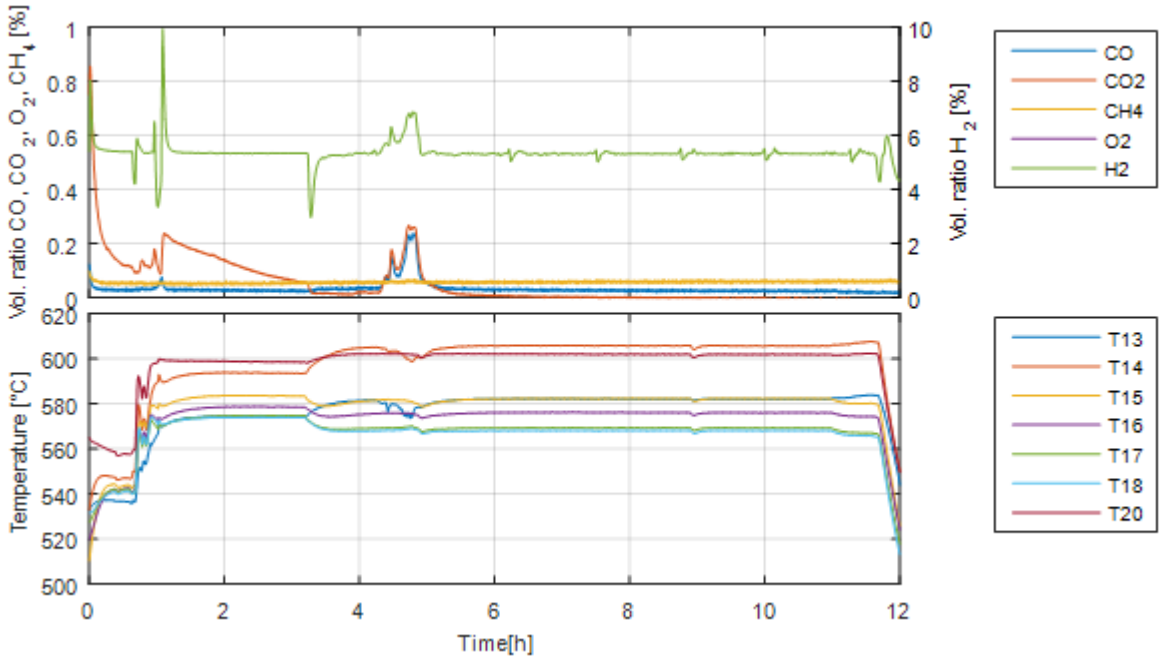

Figure 39 Carbon removal from the catalyst after the test of 23-09-2016 with400 Nl/h of forming gas and 373 Nl/h-18.6 Nl/h of steam (T12 and T19=580°C).

5.5.4. Test of 28-09-2016 / Catalyst 2

During the two tests on 22-09-2016 and 23-09-2016 a short-timed peak of pressure was sufficient to interrupt the reforming process. Therefore, it has been decided to use a time filter in the alarm to avoid interruptions of reforming process, every time a pressure peak was exceeding the alarm limit. In the new alarm design the pumps were stopped just when the pressure average was higher than the alarm limit for more than 3 seconds.

5.5.4.1. First day test

During the test carried out on 28-09-2016 the SC ratio and GHSV were respectively 3 and 1200 h^{-1}. The test started at 11:30, but after a couple of hours it was interrupted since the values of outlet gas concentration were slightly different from the ones measured on 23-09-2016. It was assumed that the pumps were not correctly calibrated. However, after the recalibration the value remained the same (Fig. 40).

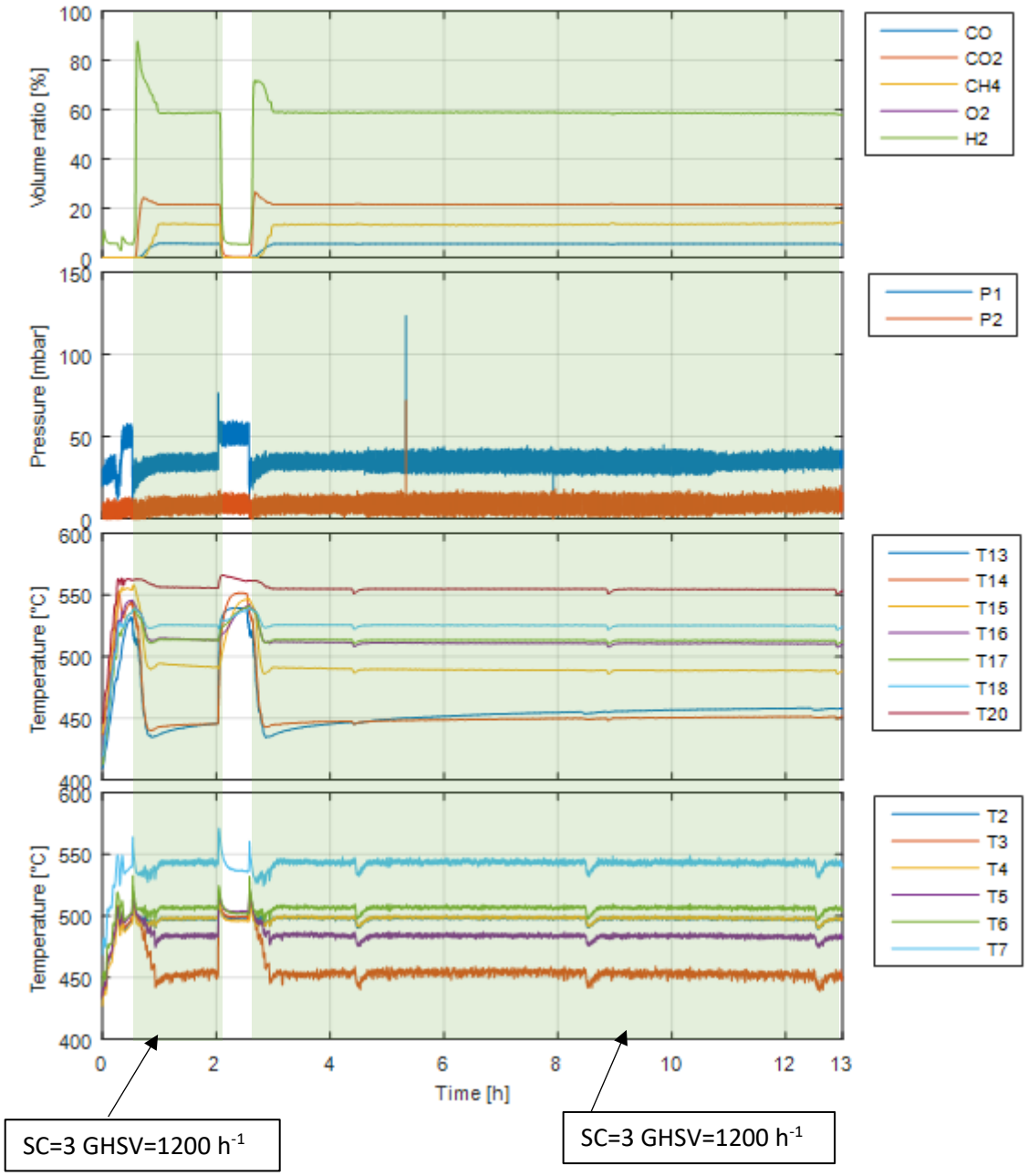

Figure 40 Volume ratio of the outlet gas, pressure at the inlet and outlet of the reactor, temperature distribution in the reactor and temperature distribution in the diesel evaporator on 28-09-2016 (SC=3, GHSV= 1200 h^{-1}, T12=545 °C, T19=545 °C and T1=510 °C).

The test was restarted at 14:00. The value of pressure difference and outlet gas composition remained stable for the rest of the day.

5.5.4.2. Second day test

During the second day test the values of outlet gas concentration and pressure difference were just the continuation of the previous day. There were just some peaks in the outlet pressure (Fig. 41).

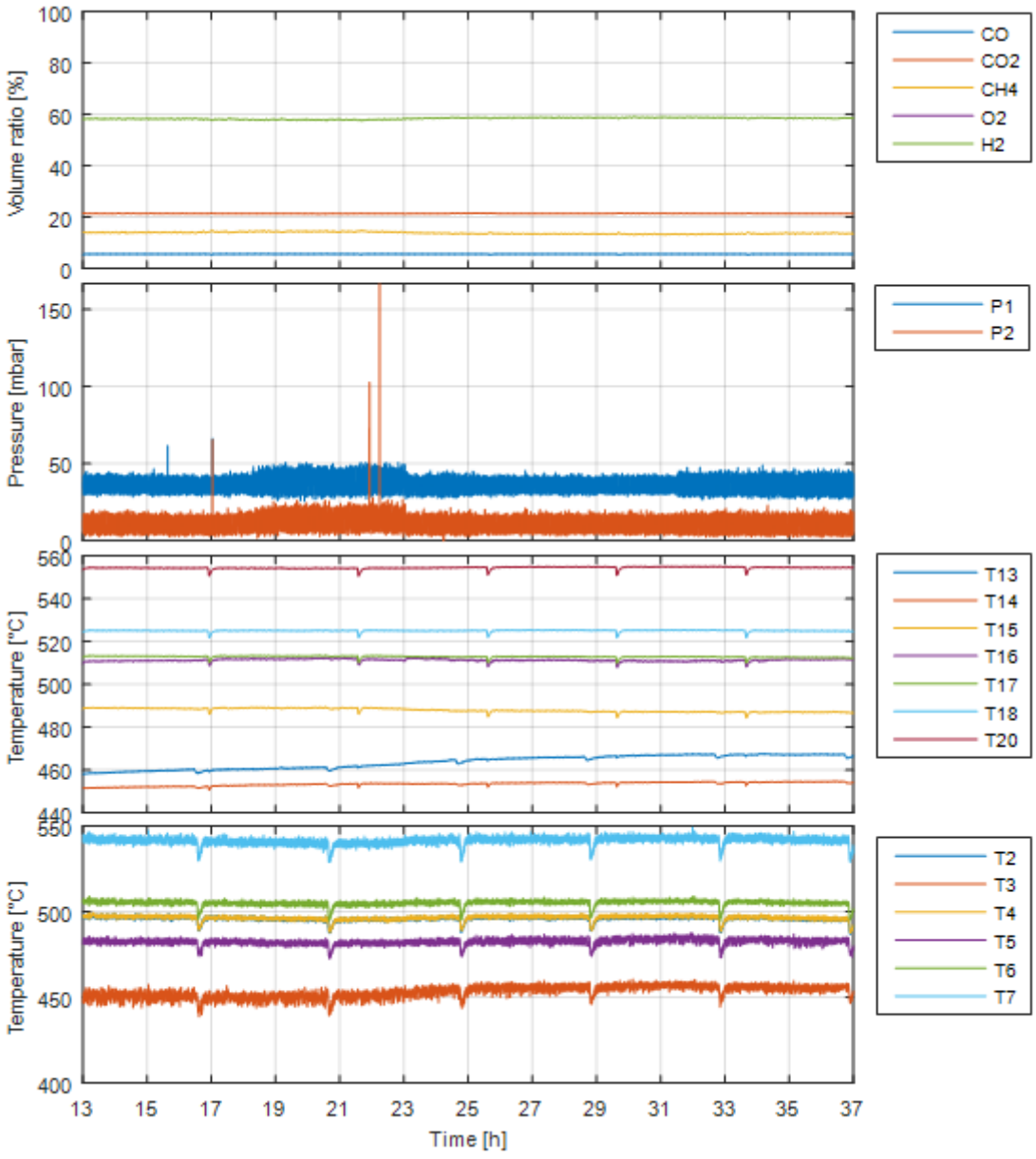

Figure 41 Volume ratio of the outlet gas, pressure at the inlet and outlet of the reactor, temperature distribution in the reactor and temperature distribution in the diesel evaporator on 30-09-2016 (SC=3, GHSV=1200 h^{-1}, T12=545 °C, T19=545 °C and T1=510 °C).

5.5.4.3. Third day test

On the third day, approximately after 46 hours, there was a sudden change in the concentrations of the outlet gas and a corresponding change in the values of pressures and temperatures in the reactor and in the values of temperatures in the diesel evaporator (Fig. 42).

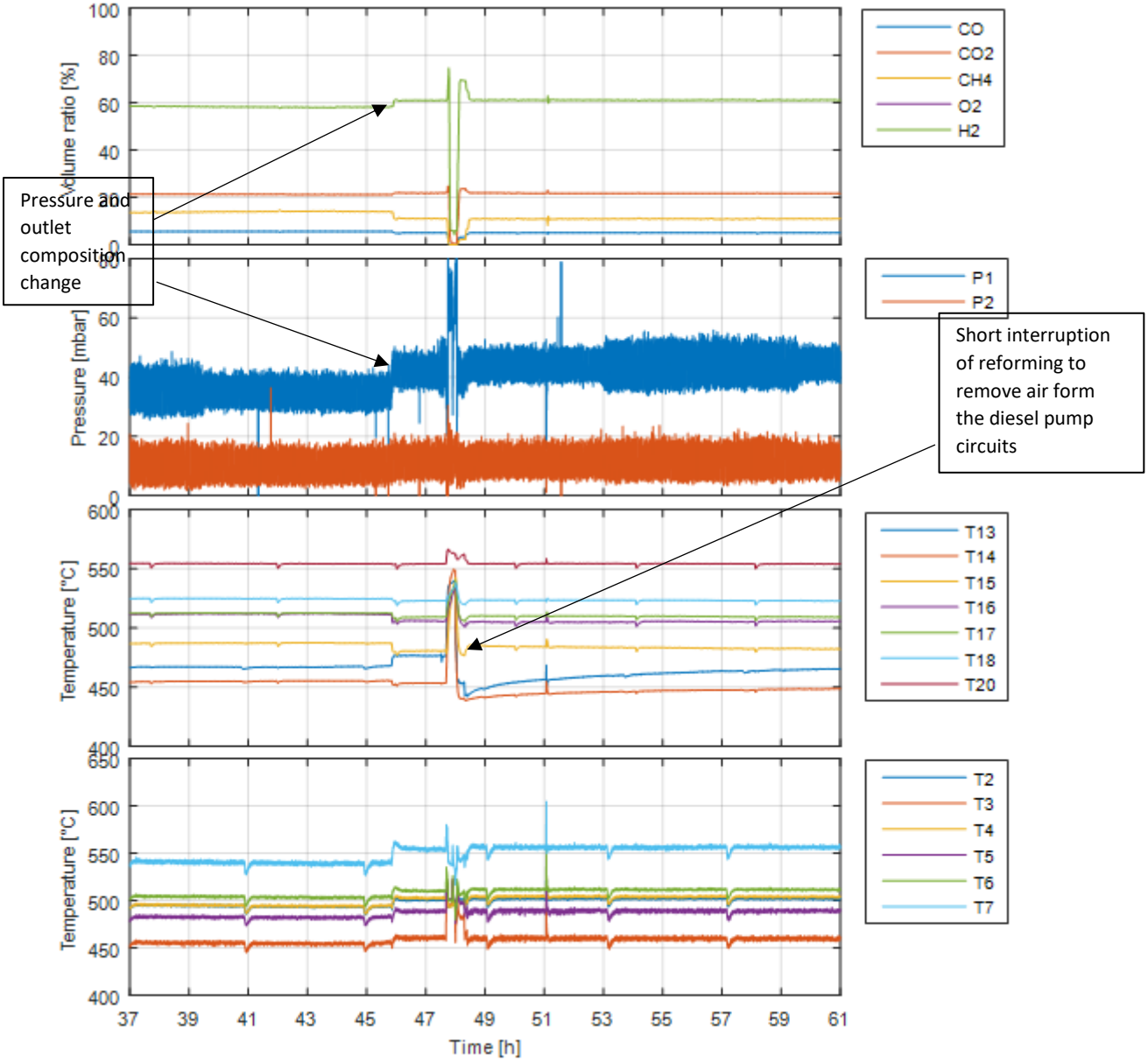

Figure 42 Volume ratio of the outlet gas, pressure at the inlet and outlet of the reactor, temperature distribution in the reactor and temperature distribution in the diesel evaporator on 31-09-2016 (SC=3, GHSV= 1200, T12=545°C, T19=545°C and T1=510 °C).

This change was hardly attributable to carbon formation since it occurred abruptly. A possible explanation to this could have been a sudden change in the flow rate. However, after the

fourth day test, the flow rate of the water pump has been controlled and no particular difference to nominal flow rate was found.

After 48 hours, some air was found upstream of the diesel pump and the operation has been suspended for some minutes to remove the air.

5.5.4.4. Fourth day test

On the fourth day, the values of pressures, temperatures and outlet gas concentration were quite similar to the ones on 30-09-2016 after the changes at 40th hour (Fig. 43).

After 82 hours, there was first a P1 pressure drop and then an abrupt increase of it. The pressure drop was probably caused by a problem with the water pump, which as in the test of 06-09-2016 stopped working. For a few seconds just the diesel pump was operating, which led to a sudden increase in P1 pressure up to approximately 350 mbar.

The reaction of the alarm instead of 3 seconds lasted 1.5 minutes. The problem was in the Labview application: the clock frequency 1 KHz was mistaken for the period, which was 200 ms.

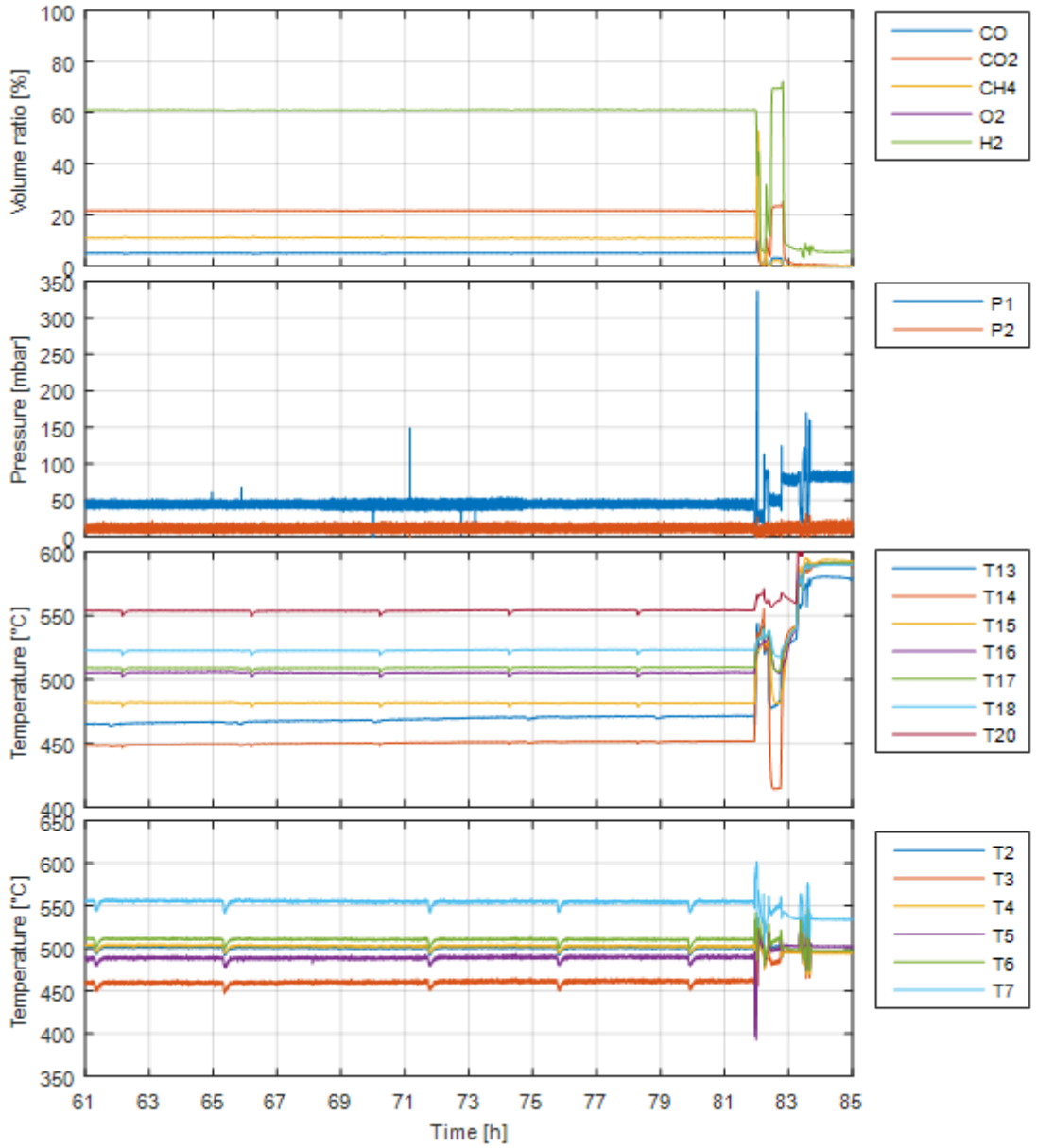

Figure 43 Volume ratio of the outlet gas, pressure at the inlet and outlet of the reactor, temperature distribution in the reactor and temperature distribution in the diesel evaporator on 01-10-2016 (SC=3, GHSV= 1200, T12=545°C, T19=545°C and T1=510 °C).

After the accident, the pressure difference at the catalyst exhibited a value 10-15 mbar higher. The catalysis was washed for approximately 14 hours with 400Nl/h of forming gas and steam (Fig. 44): initially the flow rate of steam was 746 Nl/h and, after 4 hours, 373 Nl/h During the carbon removal procedure the temperatures at T12 and T19 were set to 580 °C. The changes in the reactor temperatures after 4 hours corresponded to the change in steam flow rate from 746 Nl/h to 373 Nl/h.

Since the direct contact between the catalyst and vaporized diesel can seriously damage the catalyst, it has been decided to use more steam than in the previous carbon removal procedures.

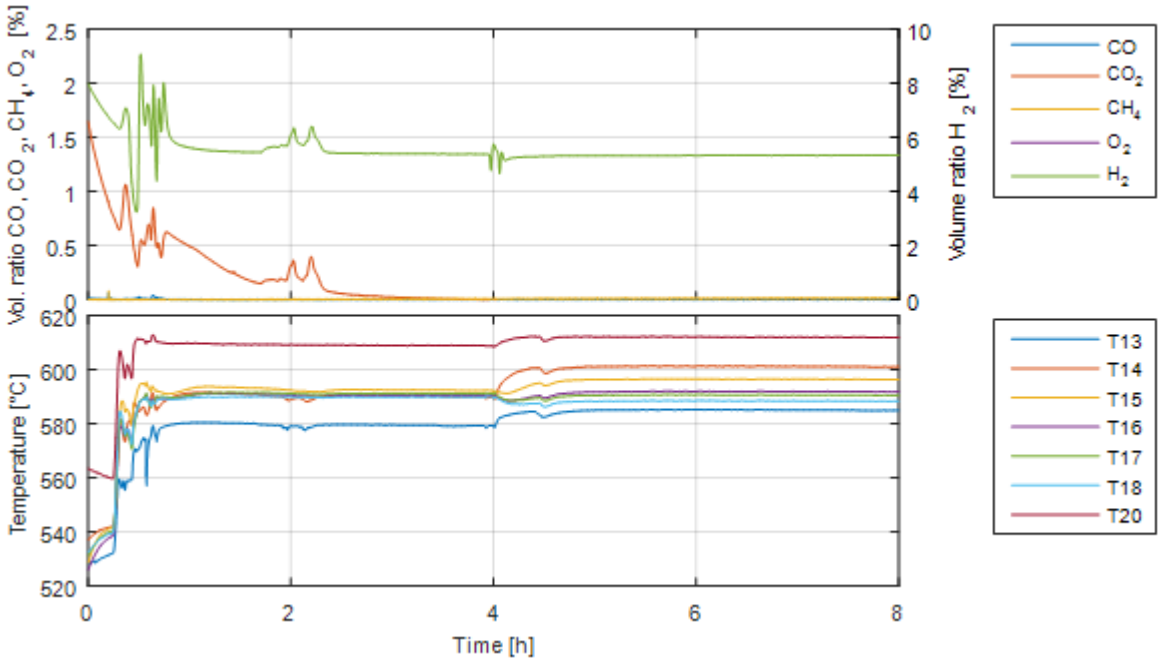

Figure 44 Carbon removal from the catalyst after the 4 days test (28-08-2016 01-10-2016) with 400 Nl/h of forming gas and 746 Nl/h-370 Nl/h of steam (T12=580°C and T19=580°C).

5.5.5. Test of 05-10-2016 / Catalyst 2

The issue with the alarm system was fixed. However, during the measurement on 01-10-2016, the alarm took more than a minute to deactivate the diesel pump. A prolonged direct contact between diesel and the catalyst determined probably a slight carbon formation: the value of pressures difference, P1-P2, was approximately 10 mbar higher than those on 28-09-2016 and 29-09-2016.

The alarm was set to 20 mbar over the value of pressure P1.

On 05-10-2016 a measurement with SC ratio 3 was conducted for approximately 1 hour (Fig. 45). The values of the outlet gas concentrations were found to be similar to those observed on 28-09-2016.

A measurement with SC 2.5 started approximately at 14:00, after some water had been be removed from the gas analyzer filters.

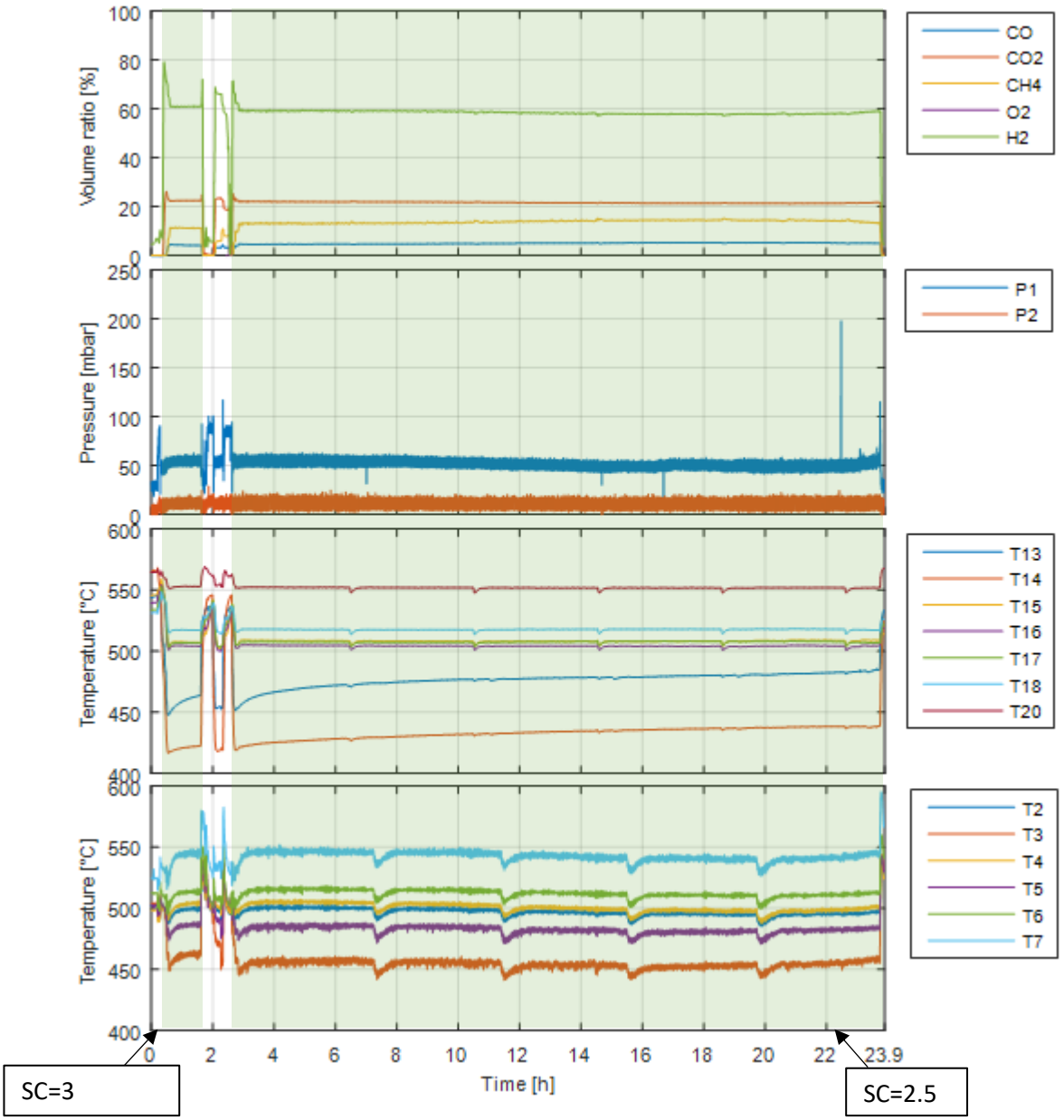

Figure 45 Concentration of the outlet gas, pressure at the inlet and outlet of the reactor, temperature distribution in the reactor and temperature distribution in the diesel evaporator on 05-10-2016 (SC=3 and SC=2.5, GHSV=1200 h^{-1}, T12=545°C, T19=545°C and T1=510 °C).

On 06-10-2016 at 07:30 the alarm was set 10 mbar over the average value of pressure P1. At 11:30 P1 exceeded for some seconds the alarm limit and in a few second the alarm interrupted the functioning of the two pumps.

The small fluctuations of P1 during the time seemed to corresponds to the small fluctuations in temperatures in the diesel evaporator.

The system was washed again with 373 Nl/h of steam and 400 Nl/h of forming gas till the next day in the morning.

5.5.6. Test of 07-10-2016 / Catalyst 2

One of the scope of the test was to assess whether the P1 pressure value increase on 06-10-2016 during the last minutes of the test corresponded also to a deterioration in the catalyst activity.

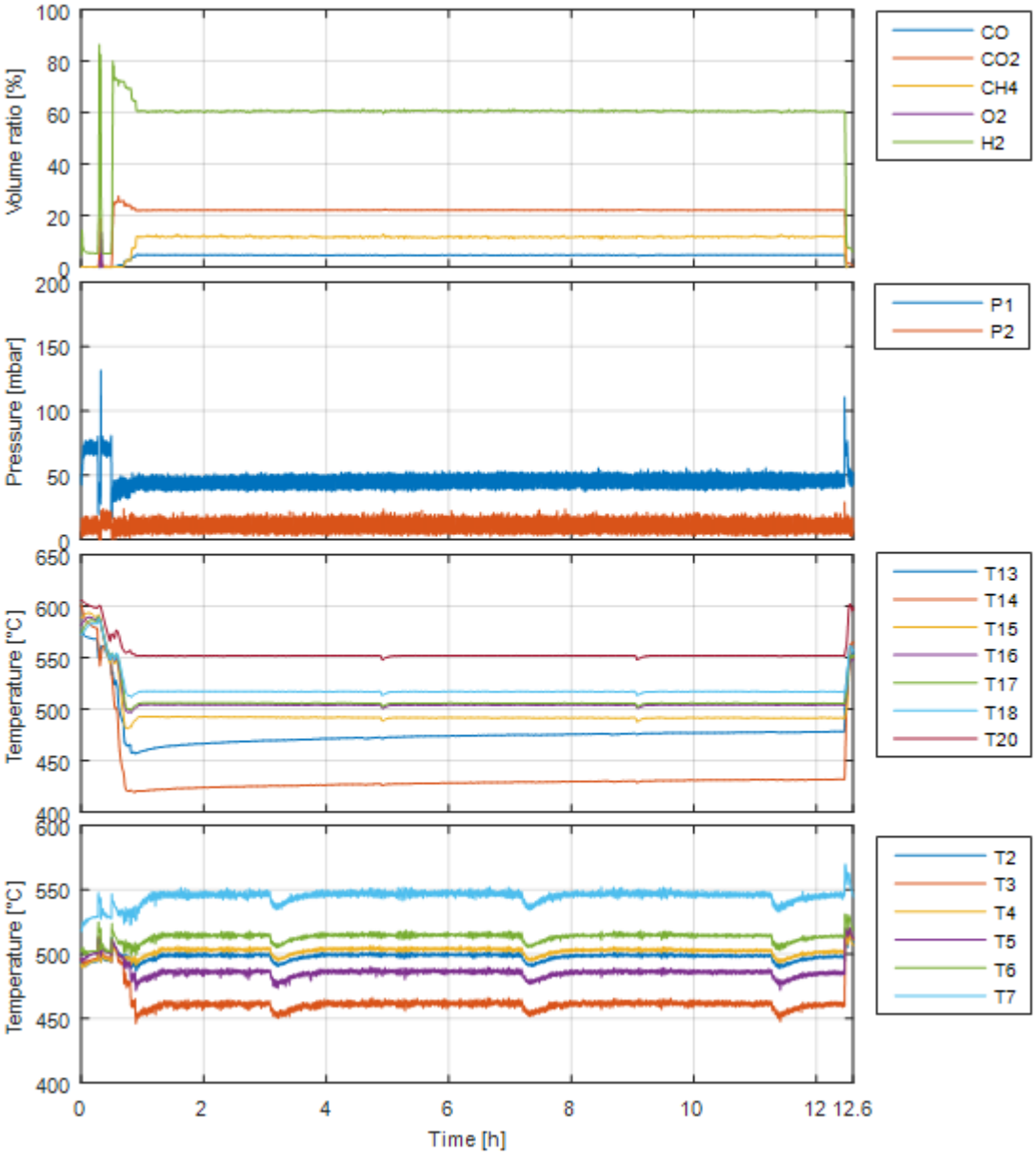

Figure 46 Volume ratio of the outlet gas, pressure at the inlet and outlet of the reactor, temperature distribution in the reactor and temperature distribution in the diesel evaporator on 07-10-2016 (SC=3, GHSV= 1200 h^{-1}, T12=545 °C, T19=545 °C and T1=510 °C).

This time the alarm limit was set 20 mbar over the pressure P1.

The comparison between this test and the initial short test on 05-10-2016 at SC ratio 3 did not evidence any significant deterioration. A decrease in pressure difference between the two tests should be emphasized.

During this test the temperatures in the diesel evaporator were quite stable and the value of P1 was not oscillating (Fig. 46).

The system was washed with 373 Nl/h water and 400 Nl/h of forming gas. In Fig. 47 is reported the carbon removal with steam and forming gas. After 2 hours, the concentration of CO_2 in the outlet gas was practically negligible.

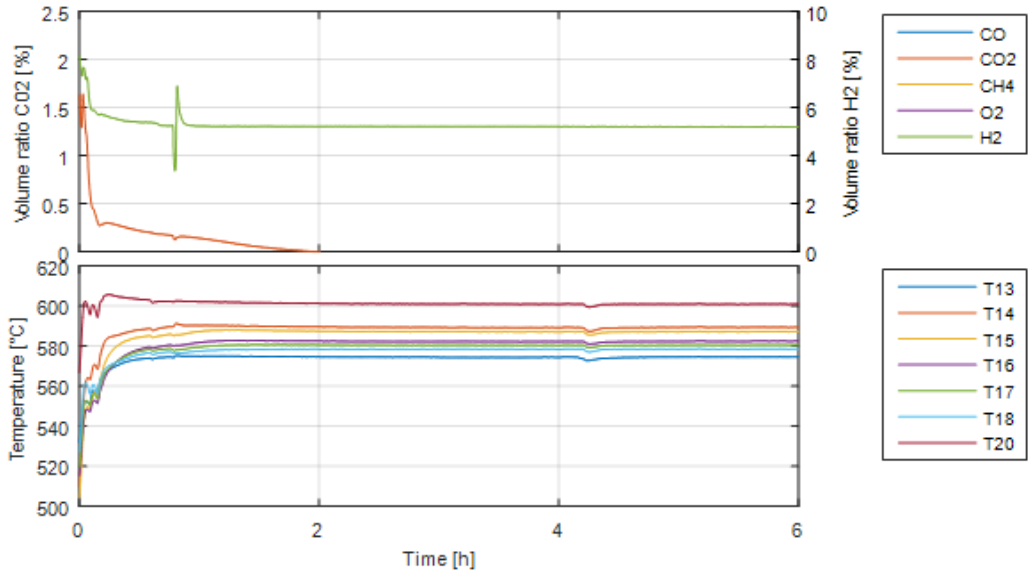

Figure 47 Carbon removal from the catalyst after the test of 07-10-2016 with 400 Nl/h of forming gas and 373 Nl/h of steam with T12 and T19 at 580 °C.

5.5.7. Test of 11-10-2016 / Catalyst 2

The test starting on 11-10-2016 was aimed at assessing the stability of diesel reforming during some days of operation with SC ratio 2.

5.5.7.1. First day test

As in the previous test several reference values were taken to see if there were possible changes in the catalyst activity: the values were comparable with the ones of previous tests (Fig. 48).

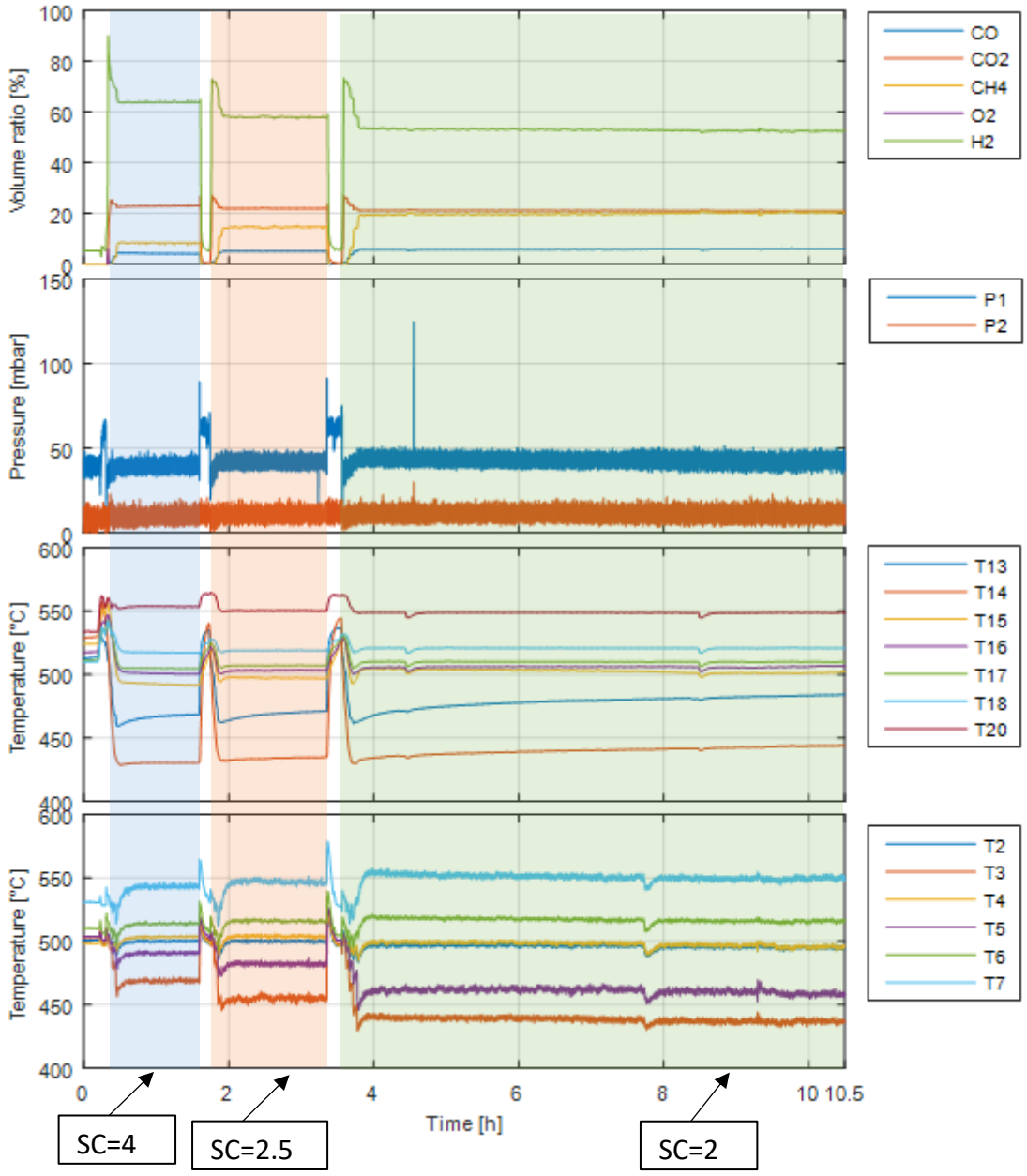

Figure 48 Volume ratio of the outlet gas, pressure at the inlet and outlet of the reactor, temperature distribution in the reactor and temperature distribution in the diesel evaporator on 11-10-2016 (SC=4, 2.5 and 2, GHSV= 1200 h^{-1}, T12=545 °C, T19=545 °C and T1=510 °C).

The test with SC ratio 2 started at 17:10. The pressure difference was stable for the rest of the day.

5.5.7.2. Second day test

On the second day (Fig. 49), after approximately 22 hours with SC ratio 2, there was a 5 mbar increase in ΔP with a slight rise of H2 concentration and a small reduction in CH4 concentration. At the same time, a rise of temperatures in the diesel evaporator occurred.

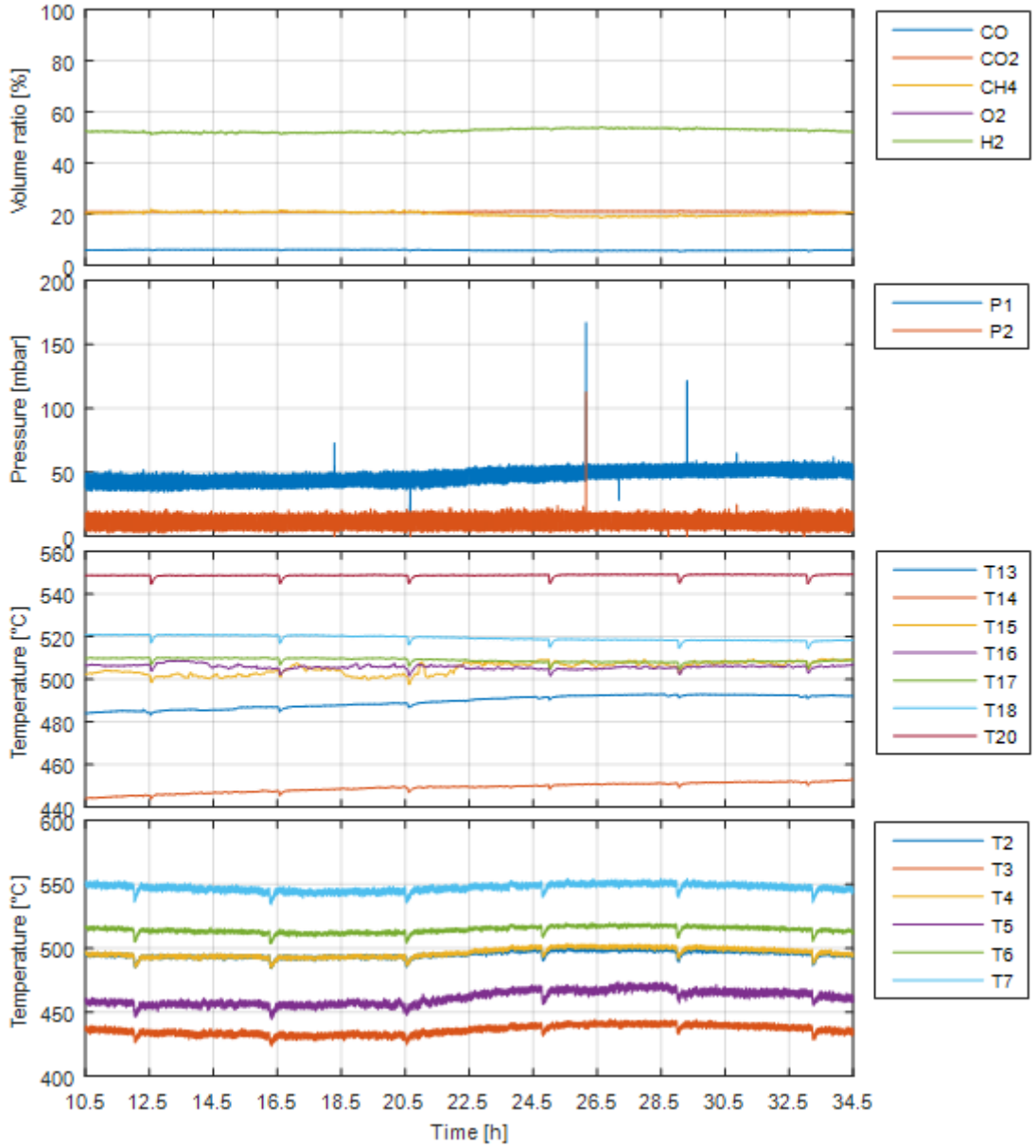

Figure 49 Volume ratio of the outlet gas, pressure at the inlet and outlet of the reactor, temperature distribution in the reactor and temperature distribution in the diesel evaporator on 12-10-2016 (SC=2, GHSV= 1200 h^{-1}, T12=545 °C, T19=545 °C and T1=510 °C).

After 32 hours, the temperatures in the diesel evaporator decreased again and so did also the concentration of H_2 in the exhaust gas. The pressure difference remained stable.

5.5.7.3. Third day test

After approximately 48 hours at SC ratio 2 there was a further augment in ΔP, approximately 10-15 mbar over values registered on 11-10-2016. The temperatures in the diesel evaporator continued fluctuating (Fig. 50).

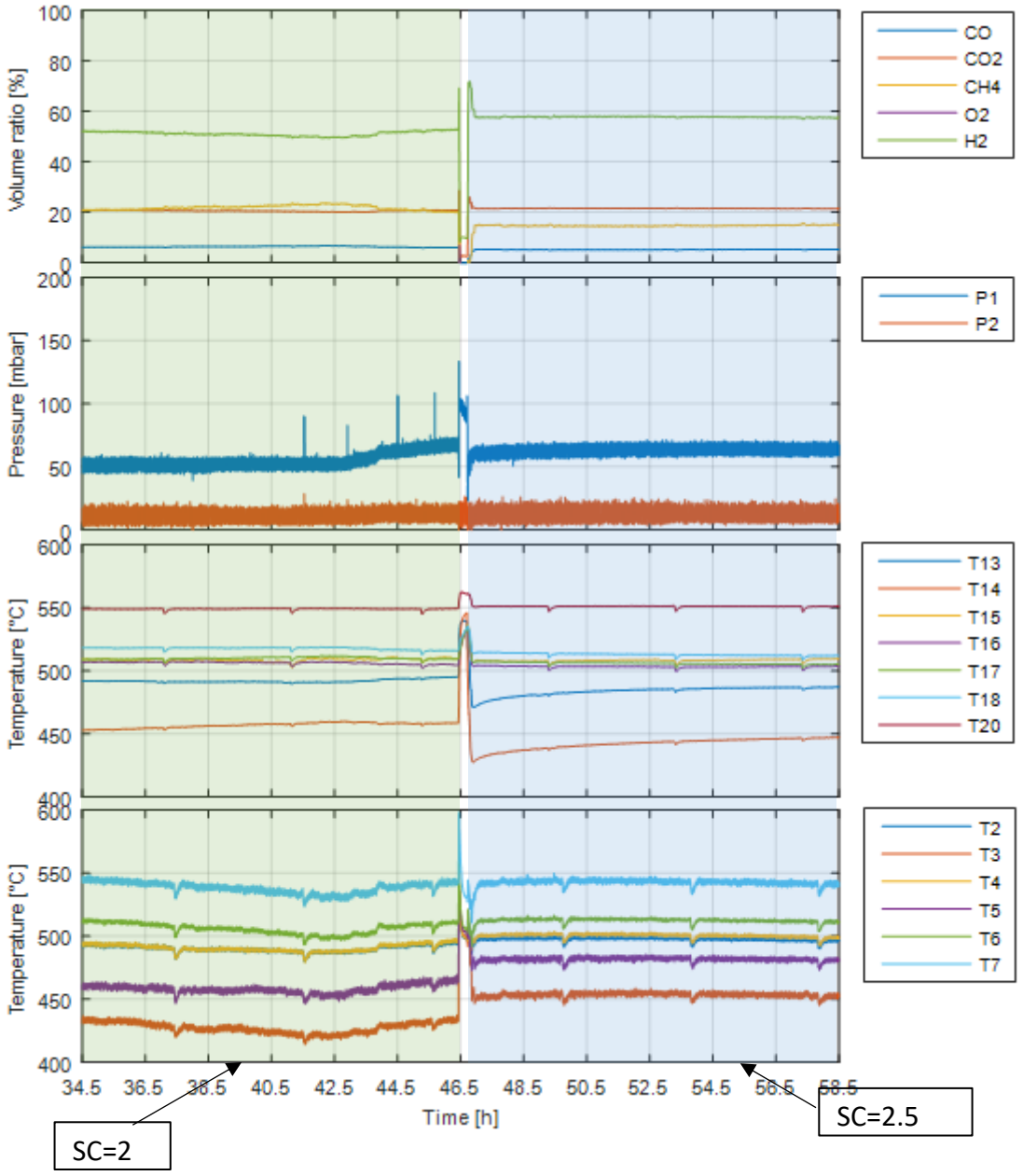

Figure 50 Volume ratio of the outlet gas, pressure at the inlet and outlet of the reactor, temperature distribution in the reactor and temperature distribution in the diesel evaporator on 13-10-2016 (SC=2 and 2.5, GHSV= 1200h^{-1}, T12=545°C, T19=545°C and T1=510 °C).

After 46.5 hours, it was decided to continue with SC ratio 2.5. The value of pressure and of temperatures in the diesel evaporator were more stable. However, pressure difference remained always 10-15 mbar higher if compared with the values registered on the first day of the test.

5.5.7.4. Fourth day test

After 72 hours the pressure difference, ΔP, increased 3 mbar over the initial pressure at SC ratio 2.5, if compared with the values registered on the previous day (Fig. 51).

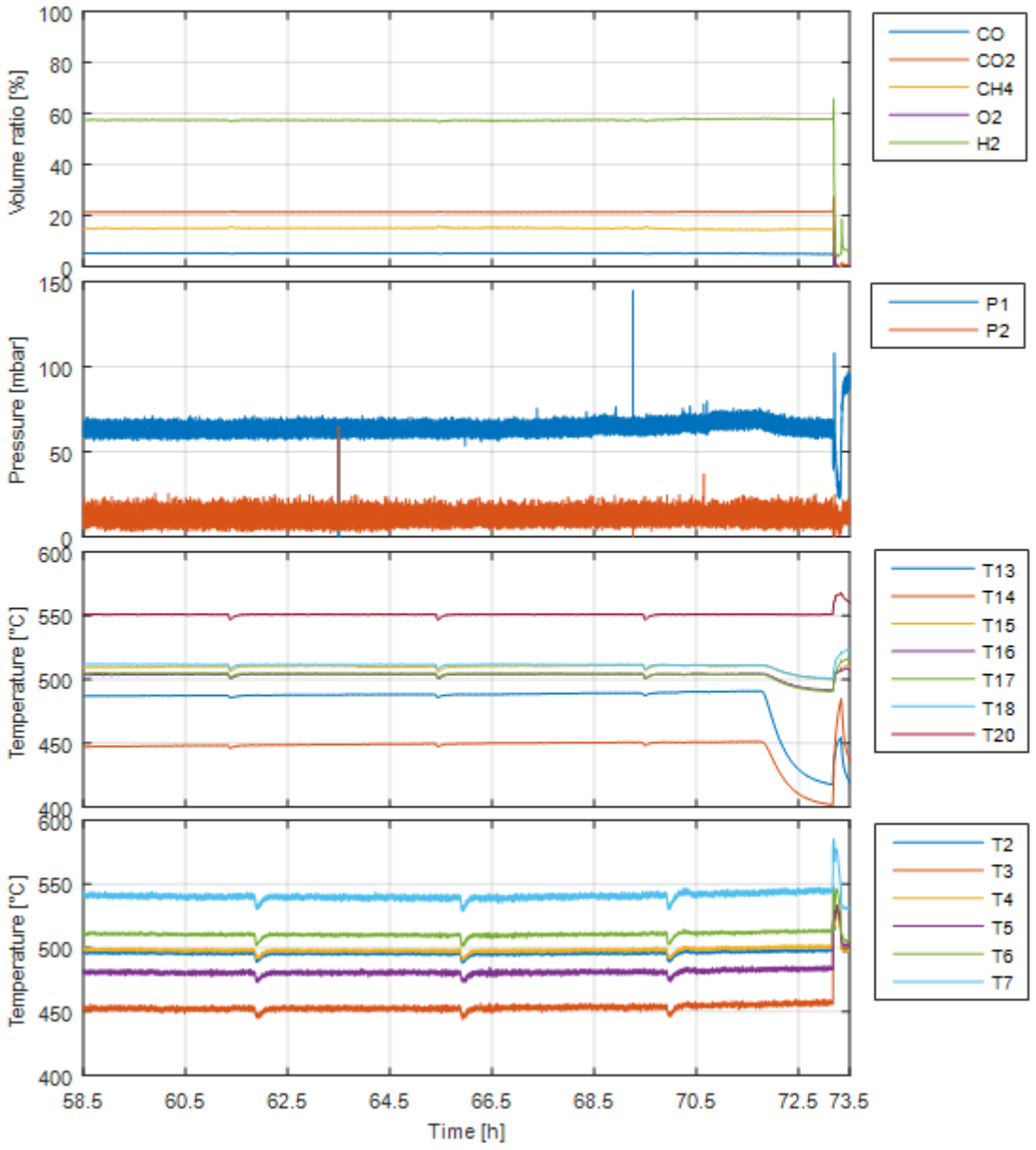

Figure 51 Volume ratio of the outlet gas, pressure at the inlet and outlet of the reactor , temperature distribution in the reactor and temperature distribution in the diesel evaporator on 14-10-2016 (SC=2.5, GHSV= 1200h^{-1}, T12=545°C, T19=545°C and T1=510 °C).

After approximately 71 hours, at 13:15 on 14-10-2016, the PID controller of the heating cable HB4 was not operating anymore. This resulted in a small decrease in ΔP and in a considerable decrease in temperatures at T13 and T14 in the reactor.

Even though the values of the outlet gas were stable the reaction was suspended approximately at 15:30 on 14-10-2016. The temperature at the inlet was too low.

After the test, the system has been washed with 373 Nl/h of steam and 400 Nl/h of forming gas (Fig. 52).

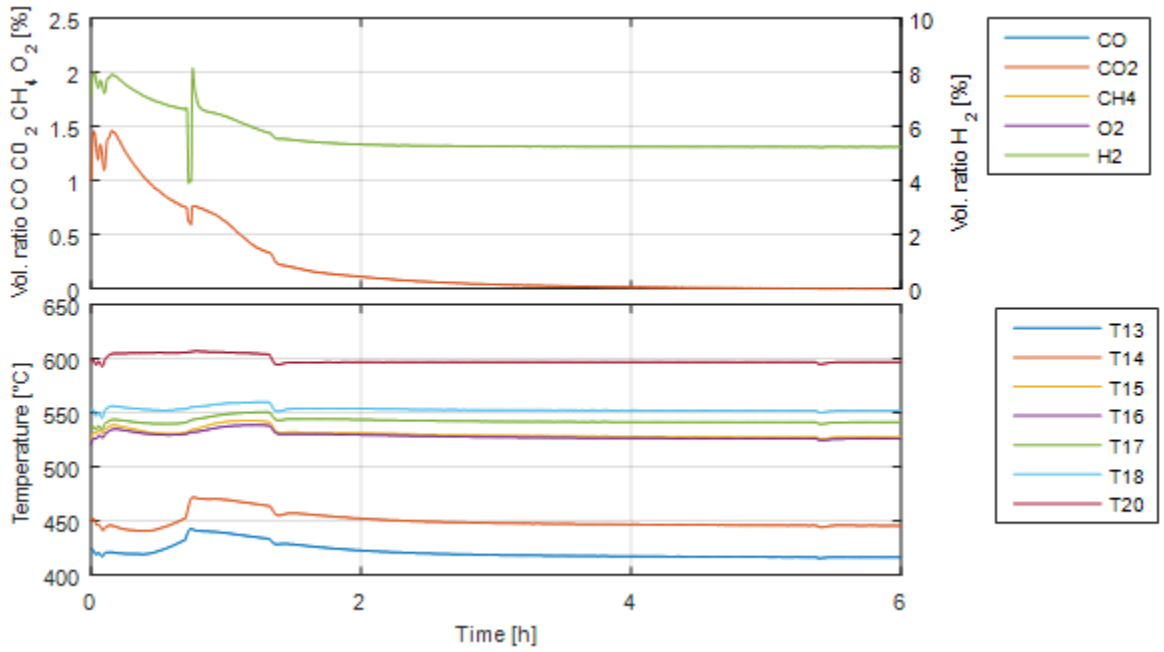

Figure 52 Carbon removal after the 4 days test (11-10-2016 14-10-2016) with 400 Nl/h of forming gas and 373 Nl/h of steam (T12=580 °C and T19=580 °C)

5.5.8. Test of 20-10-2016 / Catalyst 2

Starting from the 20-10-2016 the tests were carried out by my successor and I did just the data analysis contained in the present work.

On 19-10-2016 The PID controller was replaced.

Since the test with SC ratio 2.5 seemed to be more stable than the test with SC ratio 2, it was decided to continue with SC 2.5

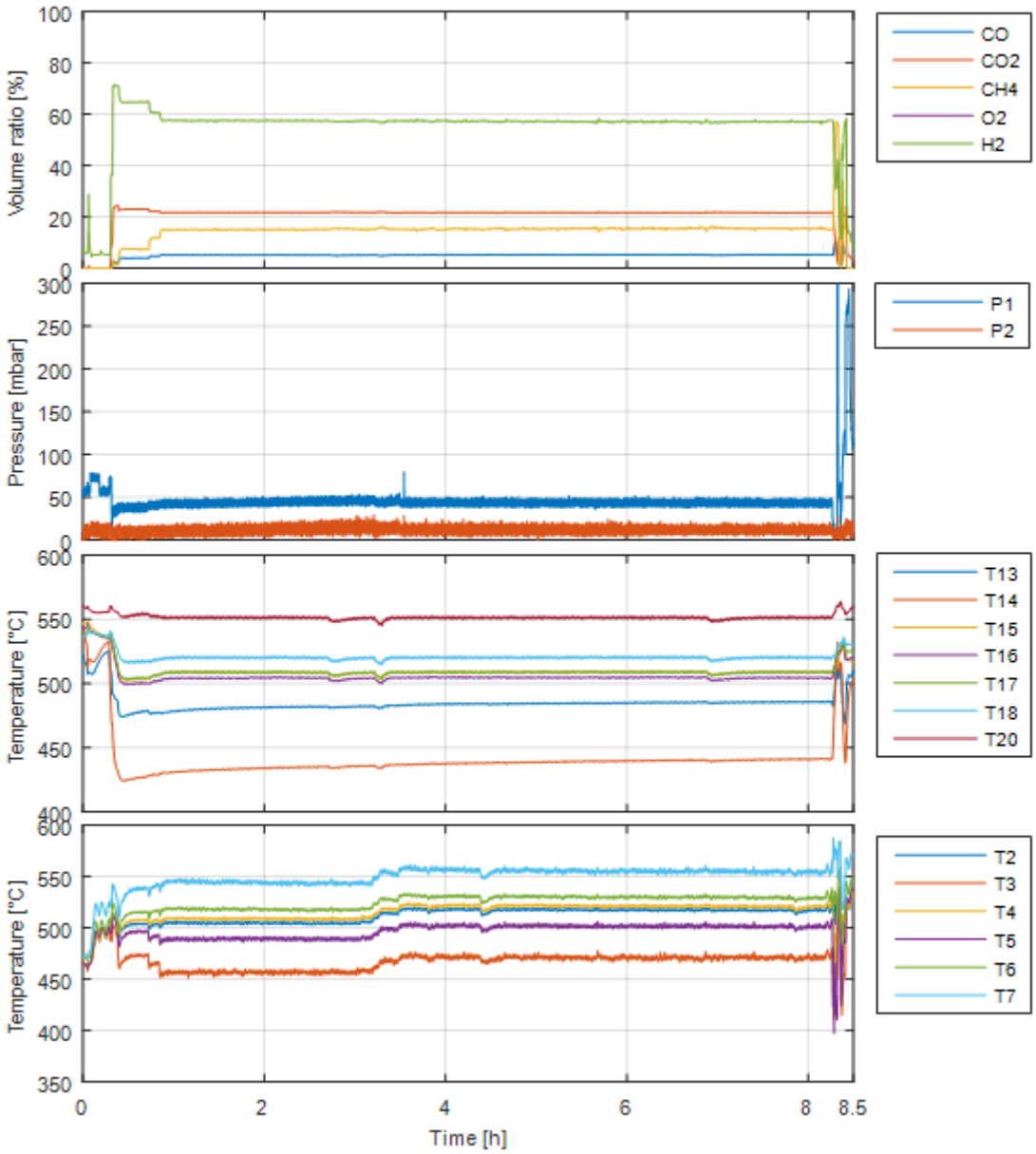

Figure 53 Volume ratio of the outlet gas, pressure at the inlet and outlet of the reactor, temperature distribution in the reactor and temperature distribution in the diesel evaporator on 20-10-2016 (SC=2.5 GHSV= 1200 h^{-1}, T12=545 °C, T19=545°C and T1=510 °C).

On the 20-10-2016 a further test with SC ratio 2.5 and GHSV 1200 h^{-1} was conducted (Fig. 53). The concentration values of outlet gas were comparable to those reported on 13-10-2016 and 14-10-2016. Instead, the difference between inlet and outlet pressure was lower.

The pressure limit of the alarm was set to 70 mbar. For unexplainable reasons at 18:16 the pressure decreased as on 01-10-2016 and then suddenly increased after few seconds. It seemed that again the water pump was not operating and just the diesel was supplied to the

system. After few seconds the diesel pump was automatically deactivated and forming gas was provided to the system.

The system has been washed for some hours with 373Nl/h of steam and 400 Nl/h of forming gas with T12 and T19 at 545 °C as depicted in Fig. 54.

Before the problem with the water pump, the values of outlet gas concentration and the pressure difference were stable. The value of CO_2 was zero after practically four hours.

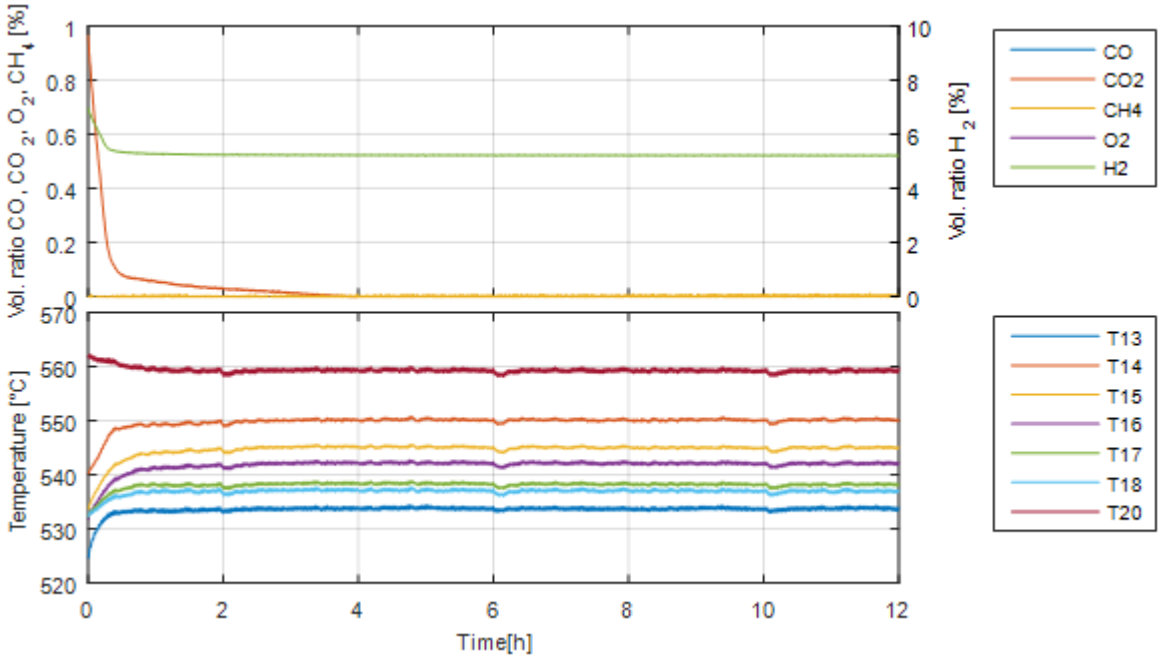

Figure 54 Carbon removal on 20-10-2016 with 373 Nl/h of steam and 400 Nl/h of forming gas. T12 and T19 were at 545 °C

5.5.9. Test of 24-10-2016 / Catalyst 2

The test with SC ratio 2.5 was repeated after the problem with the water pump (Fig. 55). Before the test was performed, it has been decided to substitute the 60-liter water container with a normal 20-liter container to have a shorter piping system.

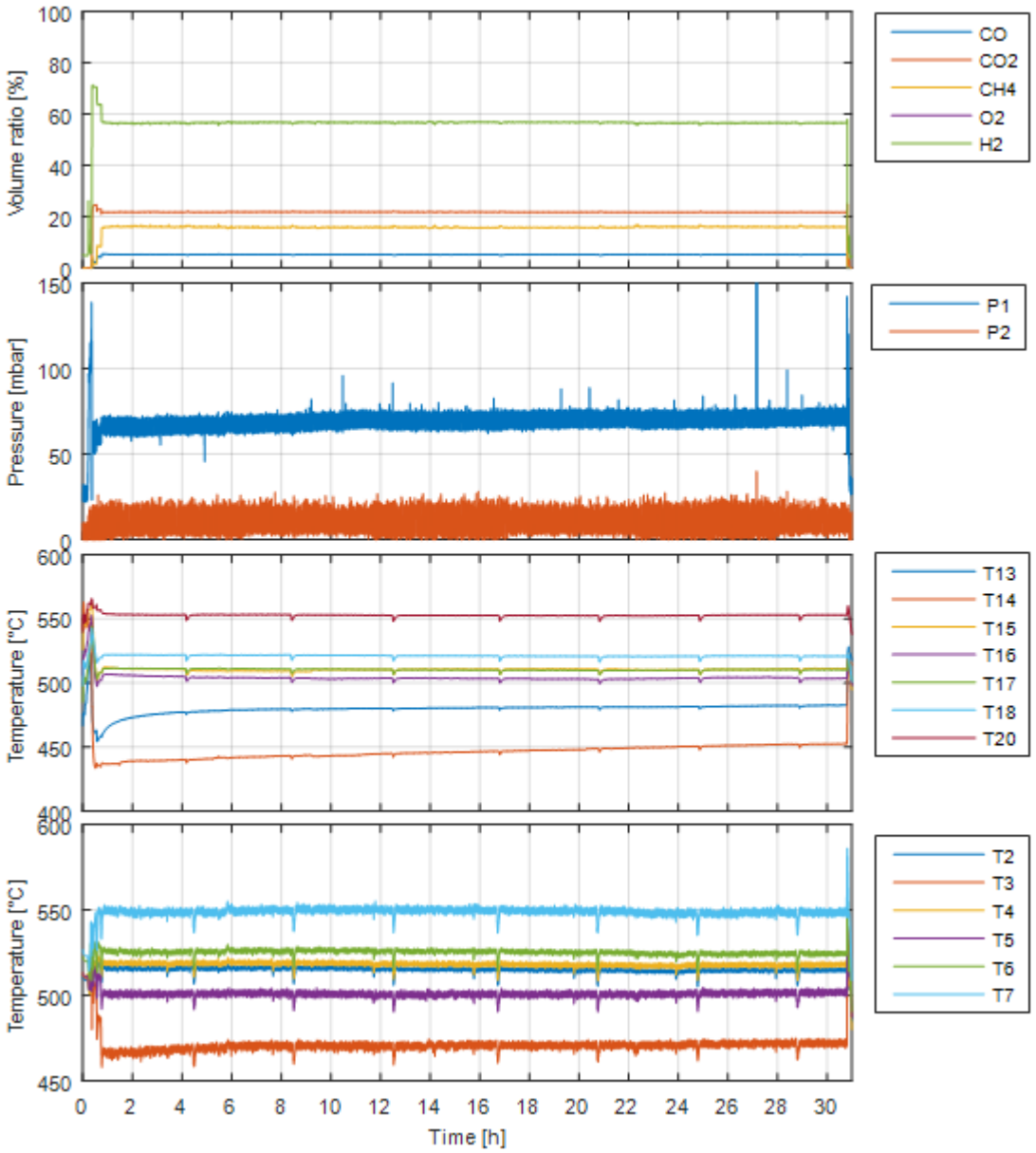

Figure 55 Volume ratio of the outlet gas, pressure at the inlet and outlet of the reactor, temperature distribution in the reactor and temperature distribution in the diesel evaporator on 24-10-2016. (SC=2.5, GHSV=1200 h^{-1}, T12=545°C, T19=545 °C and T1=510 °C.).

The test was carried out for approximately 31 hours and it had to be interrupted because the test rig could not be used on 26-10-2016 due to organizational issues at the University.

During the test the pressure difference had a small rise, approximately 5 mbar, and no substantial variations in the outlet gas composition were noticed. No carbon removal procedure has been performed after the test.

5.5.10. Test of 02-11-2016 / Catalyst 2

On 02-11-2016 a test with SC ratio 2.2 was conducted. The pressure difference, P1-P2, was slightly higher if compared with the previous test at SC ratio 2.5. The pressure alarm has been set to 90 mbar (Fig. 56). The test has been interrupted by the alarm after a rise in pressure P1.

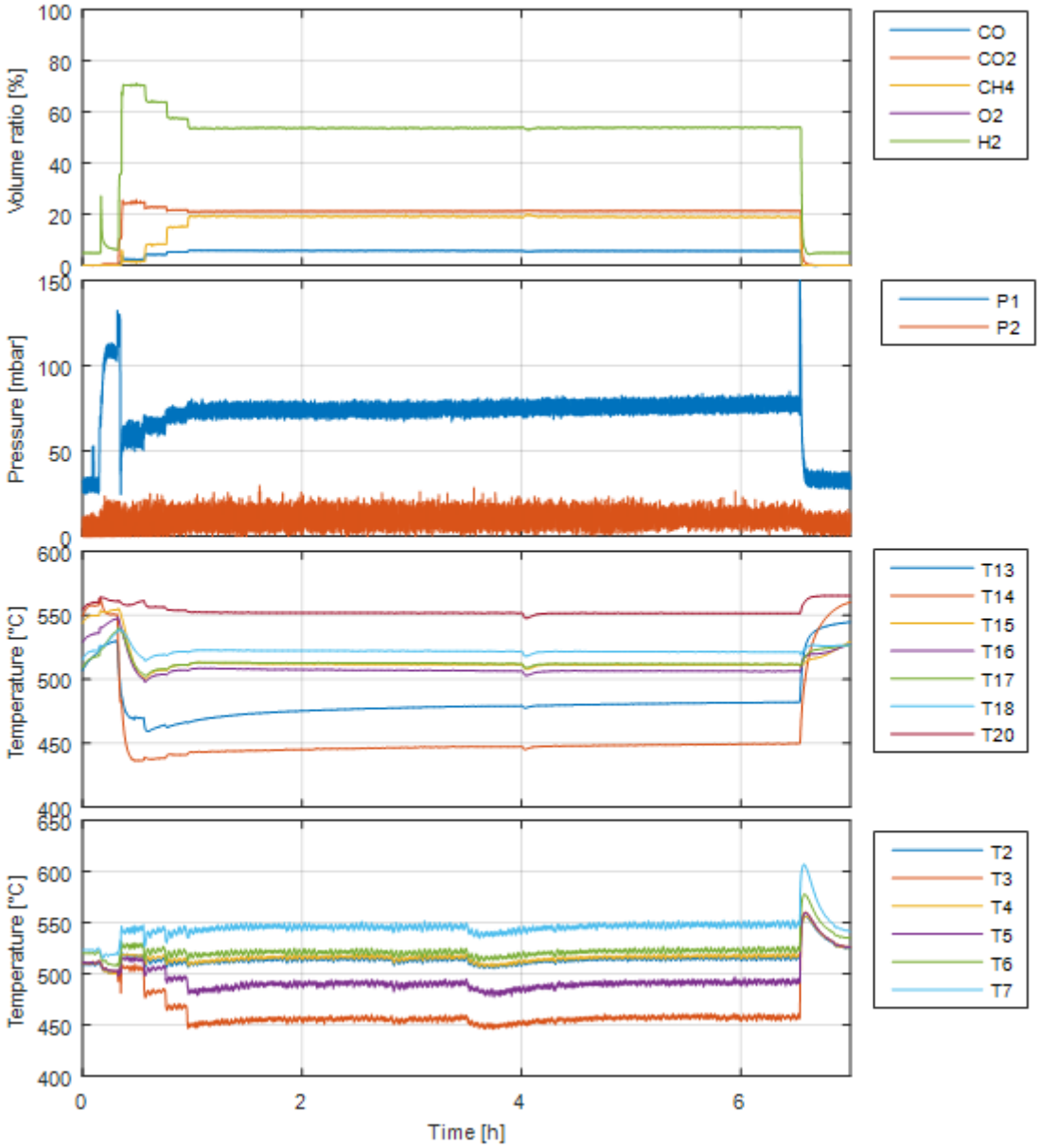

Figure 56 Volume ratio of the outlet gas, pressure at the inlet and outlet of the reactor, temperature distribution in the reactor and temperature distribution in the diesel evaporator on 02-11-2016 (SC=2.2 GHSV=1200 h^{-1}, T12=545 °C, T19=545 °C and T1=510 °C).

After the test the catalyst has been washed with 373 Nl/h of steam and 400 Nl/h of forming gas. There is no data concerning the carbon removal due to technical problems with the laptop connected with the gas analyzer.

5.5.11. Test of 10-11-2016 / Catalyst 2

It was the last test (Fig. 57). Since in the beginning the pressure difference was slightly higher if compared with the test carried out on 02-11-2016.

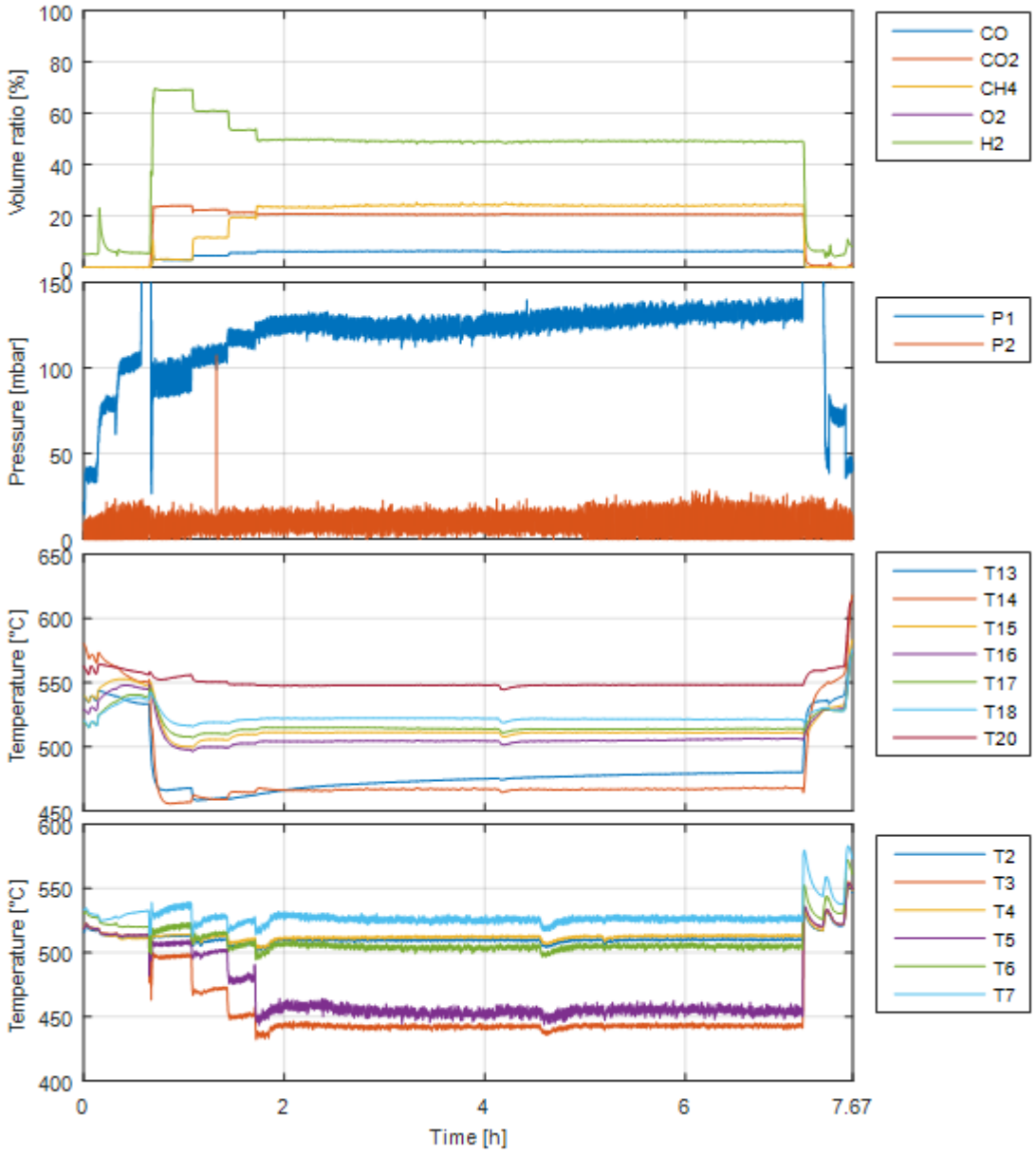

Figure 57 Volume ratio of the outlet gas, pressure at the inlet and outlet of the reactor, temperature distribution in the reactor and temperature distribution in the diesel evaporator on 10-11-2016 (SC=2.2, GHSV= 1200 h^{-1}, T12=545 °C, T19=545°C and T1=510 °C).

The activity of the catalyst was also deteriorated. The catalyst was changed due to the significant increase of pressure difference after few hours.

After a visual examination, several pellets were fragmented in smaller bits or even dust (right side of Fig. 28 in chapter 4).

6. Discussion of the results

As already mentioned in chapter 4, to determine the equilibrium conditions an internal application developed in Matlab/Simulink has been used. Due to the wide range of temperature distribution inside the diesel reactor, a direct comparison between the experimental results and the theoretical equilibrium was not feasible. Instead, it was attempted to find for H_2 and CH_4 a possible window of temperatures, within each reaction could occur. Since the temperatures at T12 and T19 were always kept constant, it was expected to have similar temperature windows for the different SC ratios and for the two different feedstocks used: methane and diesel. This analysis was carried out using the more comprehensive data of the second catalyst.

In Fig. 58 is depicted the determination of possible reaction temperatures windows in CH_4 reforming with data test performed on 16-09-2016. For the sake of completeness the comparison with the equilibrium was made also for CH_4 SR test performed on 02-09-2016 with SC 2.1. The difference of performance between the two catalysts could be attributed to the fact that, during the pre-testing and setting of the apparatus, due to problems with power supply the first catalyst was left at high temperature in air atmosphere. This could have led to possible oxidation. Another explanation could be also that the several heating and cooling processes during the setting and the pretesting determined a partial deterioration of the catalyst material.

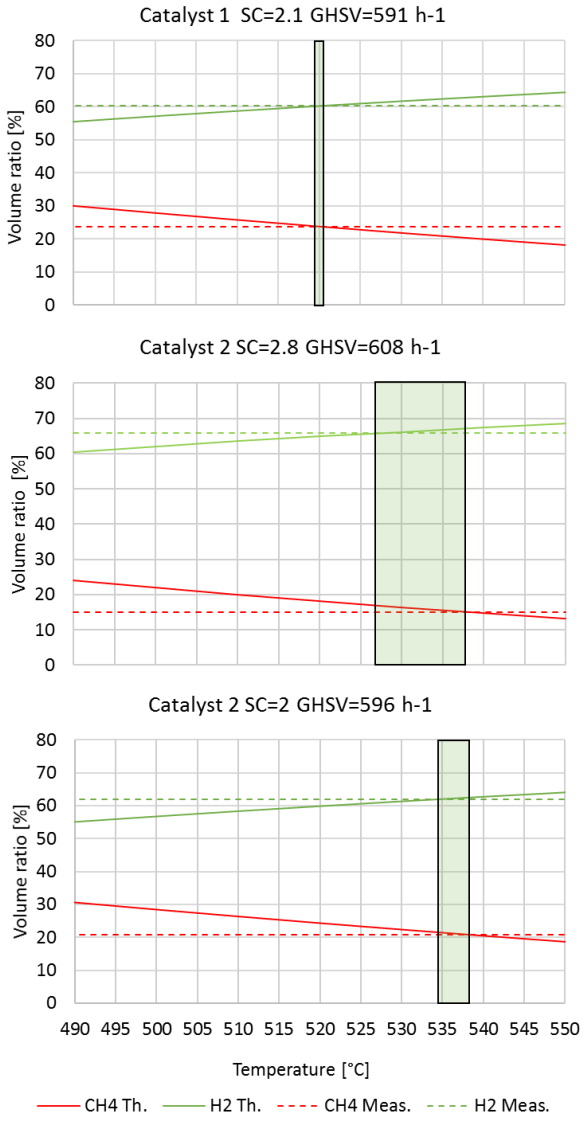

Figure 58 Determination of a possible temperature window for reforming activation with CH_4 on 02-09-2016 and 16-09-2016.

The same analysis was conducted with diesel (Fig. 59). The equilibrium was determined using the formula of dodecane, $C_{12}H_{26}$, which was the most suitable formula in the virtual reactor to approximate the diesel mixture. For the equilibrium determination the mass flows of diesel and water were obtained from the formula of $C_{16}H_{34}$ (hexadecane), which was used for the tests. The measured values were simply the average of the values of the tests with the same SC ratio. All the considered data were obtained from the measurements performed with the second catalyst.

The equilibrium was also calculated using the formula $C_{8.15}H_{18.3,}$ which was simply approximated by mixing $C_{12}H_{26}$ and CH_4 with mole fraction, respectively, of 0.65 and 0.35. Also in this case, the actual value of mass flows of the test has been used. The windows of temperatures are wider than in the case of dodecane, which could suggest a better approximation with dodecane. Unfortunately, since in the virtual reactor the heaviest hydrocarbon was dodecane, it was possible to obtain just hydrocarbons lighter than dodecane. The corresponding SC ratios and GHSV for $C_{12}H_{26}$ and $C_{8.15}H_{18.3}$ are reported in Table 2 and are very close to the SC and GHSV values for $C_{16}H_{34}$. The two comparisons with equilibrium are depicted in Fig. 59.

In the case of SC ratio 4, the comparison with equilibrium shows a window of temperatures lower than with the other SC ratios. This could be consistent with the higher SC ratio as suggested in [26]. Moreover, the tests with SC ratio 4 were not the principal focus of the present work and were basically performed just at the beginning of the measurements with the second catalyst and repeated on 11-10-2016. The measurements with the other SC ratios were repeated more often during the life of the catalyst and the statistic is more exhaustive.

It should be highlighted that, in respect to the deterioration analysis of the catalyst, a change in pressure difference between the inlet and the outlet pressure at the reactor cannot be associated only to a process involving carbon formation. For example, in the test conducted between the 28-09-2016 and the 01-10-2016, on the third day there was a sudden augment of pressure difference, which was too fast to be explained with carbon formation. Together with the increase in ΔP also a rise of temperature at T13 and of temperatures in the diesel evaporator occurred and an increase in H_2 concentration in the outlet gas.

On the other hand, there were some more evident signs which could be attributable to a process of carbon formation, as for example the gradual increase in pressure difference on 13-10-2016 with SC ratio 2. In this case the augment in pressure difference was also followed by a slight deterioration of the activity of the catalyst.

It should be considered also that, when the catalysts were replaced due to deterioration on 14-09-2016 and 15-11-2016, a process of fragmentation was found. This could be explained with presence of carbon wiskers, which can determine the breakdown of the pellets [13], but

also with the fact that the process of heating was generally quite fast: it lasted approximately 2-3 hours starting with room temperature and reaching 550 °C.

Table 2 SC ratios and GHSVs for the two formulas $C_{12}H_{26}$ and $C_{8.15}H_{18.3}$ obtained from mass flow values calculated for the formula $C_{16}H_{34}$ and used for the tests.

Mass Flow [g/h]		**SC ratio**			**GHSV [h-1]**		
Diesel	H_2O	$C_{16}H_{34}$	$C_{12}H_{26}$	$C_{8.15}H_{18.3}$	$C_{16}H_{34}$	$C_{12}H_{26}$	$C_{8.15}H_{18.3}$
125	638	4	4,02	4,04	1200	1207	1218
166	635	3	3,01	3,03	1200	1208	1223
198	632	2,5	2,51	2,53	1200	1209	1227
225	630	2,2	2,2	2,22	1200	1210	1231
246	629	2	2,01	2,02	1201	1213	1235

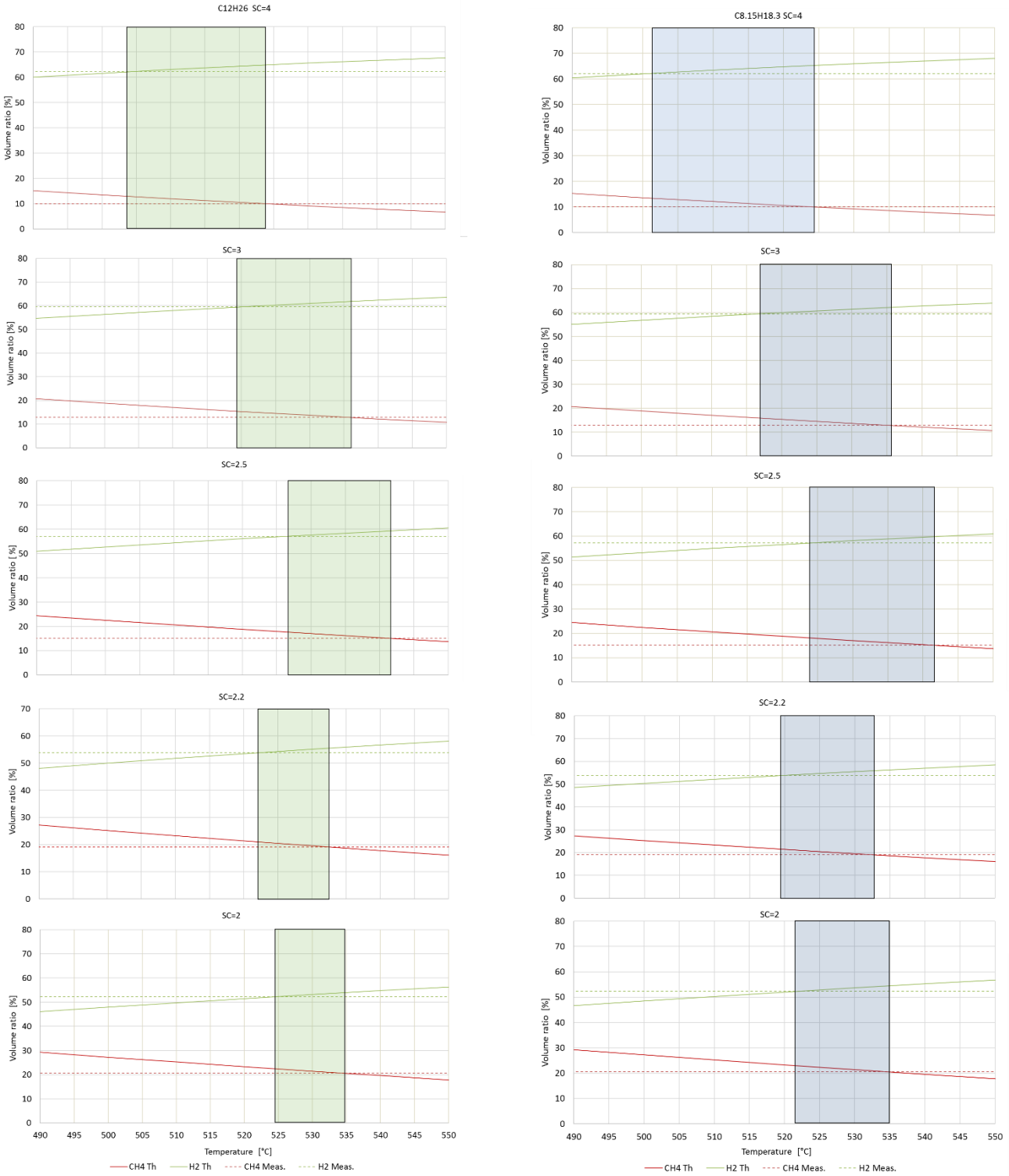

Figure 59 Determination of a possible temperature windows for the diesel reforming for different SC ratios Equilibrium was obtained for $C_{12}H_{26}$ and a mix $C_{8.15}H_{18.30}$

Initial and final values of the tests performed with diesel with the first and second catalysts are reported in the annex I (Tables 3 and 4).

Fig. 60 summarizes the trends of pressure difference and concentrations of CH_4 and H_2 in the outlet gas for the second catalyst. The concentrations and pressure difference values were taken at the same points. Changes in pressure drop within the mbar were not reported. Not just the initial and final values in pressure difference are considered, but also possible changes during the test as in the case of the 4 days' test started on 28-09-2016. The heating and cooling processes together with the carbon removal procedures are highlighted with transparent red lines but not displayed.

From Fig. 60, it is evident that the major variations in pressure drop occurred during the two direct contacts with diesel and before the last test. Other variations in pressure drop are attributable to GHSV and SC ratio changes, or changes during the operation with fixed GHSV and SC ratio. In the last case, it is not always evident if they correspond to carbon formation or other factors not related with catalyst degradation.

It seems also that, in some cases, the carbon removal procedure was effective in reducing the pressure drop. It is not clear what happened before the last test where the pressure drop changed dramatically. It could be that the fragmentation process finally determined the final deterioration of the catalyst with augment in pressure drop and changes in outlet gas composition.

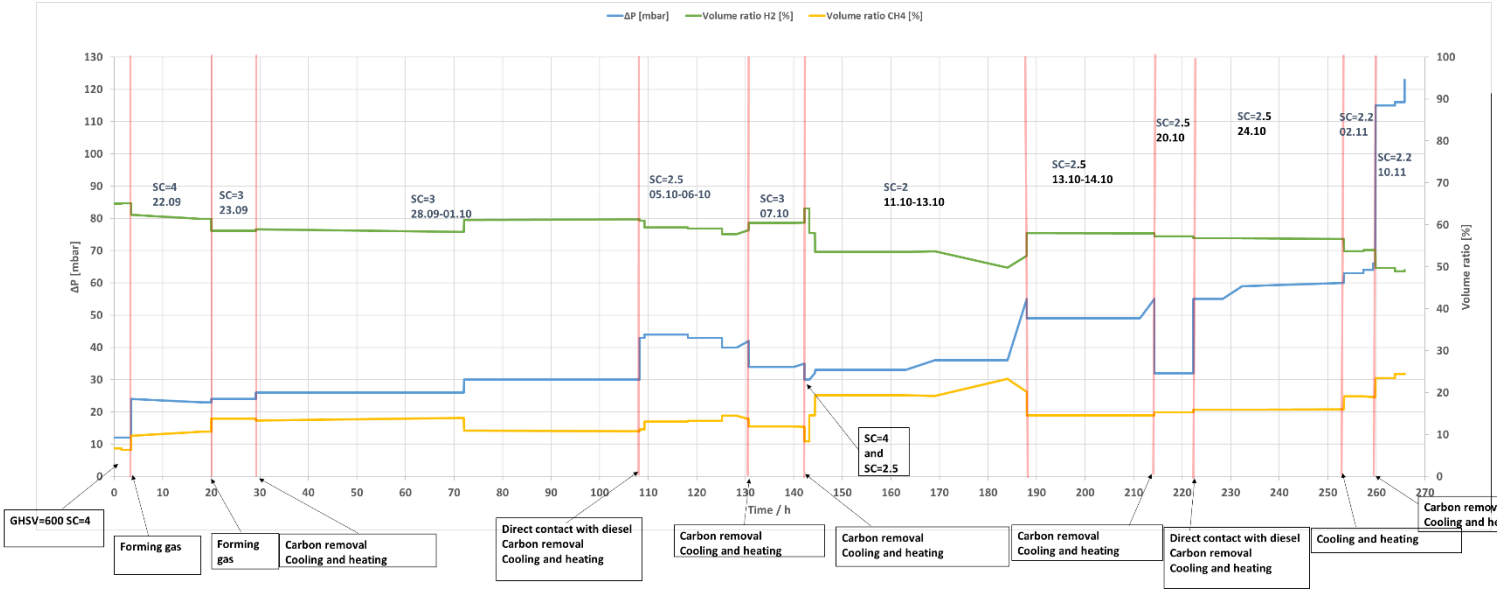

Figure 60 Summary of pressure trend together with changes in concentration for CH4 and H2. Except for the first hours the GHSV was always 1200 h^{-1}.

A further analysis concerning the temperatures distribution at the thermocouples T12-T20 is reported in Fig. 61. The approximation of equally spaced thermocouples was made for the purposes of graphical representation. In reality the distance between two consecutive thermocouples was not constant. In the legends of Figs. 61 and 62 each test is denoted by date and duration. Since in diesel SR the temperature distribution changed substantially over the first hours, in order to have a better comparison among the end values of different tests, just tests longer than 15 hours were considered. Shorter tests were considered just for SC ratio 2.2, since in this case we do not have tests longer than 6.5 hours. The temperatures together with the pressure difference were measured two hours after the beginning and 30 minutes before the end of each test.

Since the test with SC 3 lasted 79 hours and there was a sudden change in pressure and outlet gas composition after approximately 45 hours (Fig. 42), the temperatures and pressure difference were taken also 30 minutes before the changes occurred (160928_79h_mid in Fig. 61).

The tests with SC 4 and SC 3 considered in Fig. 61 were made before the catalyst was in direct contact with vaporized diesel on 01-10-2016. The value of temperature at the second point along the dimensionless length, which corresponds to the value of the temperature at thermocouple T13, was below 460 °C at the beginning and below 480 °C at the end of every test. The temperature at the third point, T14, was in the range of 440-460 °C. The temperature distribution patterns were similar for both SC ratios.

The catalyst during the tests with SC ratio 2.5, 2.2 and 2 was probably already lightly deteriorated and temperature distribution pattern exhibited a stronger marked minimum at the third point except for the last test of 10-11-2016. The temperature at T13 tended to be higher at the beginning and at the end of every test. During the test with SC ratio 2 the changes between the initial and final temperatures at the second and third point were more substantial than those during the tests with the other SC ratios.

In the last test of 10-11-2016 with SC ratio 2.2 the shape of the temperature distribution was different from that of the previous test of 02-11-2016. The initial and final temperatures at the third point were higher if compared with those at the same point registered on 02-11-

2016. Also the pressure difference was substantially higher on 10-11-2016 than that registered on 02-11-2016.

It can be inferred from the analysis that the major changes in temperature distribution shape occurred just after the four-day test started on the 28-09-2016 and in the last test on 10-11-2016. This is consistent with the direct contact between catalyst and vaporized diesel occurred on 01-10-2016 (Fig. 43) and with the considerably high pressure difference occurred on 10-11-2016 presumably due to a process of fragmentation of the catalyst.

The same graphical representation was produced for the methane SR tests performed on 02-09-2016 and on 16-09-2016 (Fig. 62). Also in this case the temperatures values were taken two hours after the beginning and 30 minutes before the end of each test. Since the values of temperatures were already stable at the beginning of every test, all the tests were considered. The temperatures distribution was quite constants over the duration of the tests. This is consistent with the better stability of methane SR. As a further remark, it is possible see that the temperature distribution pattern of the first catalyst was different from the one of the second. In the first catalyst the temperatures at the second and third points, T13 and T14, were higher, but at fourth point, T15, the temperature was lower. This resulted in a flatter and longer peak, which could suggest a possible partial deactivation, as already mentioned.

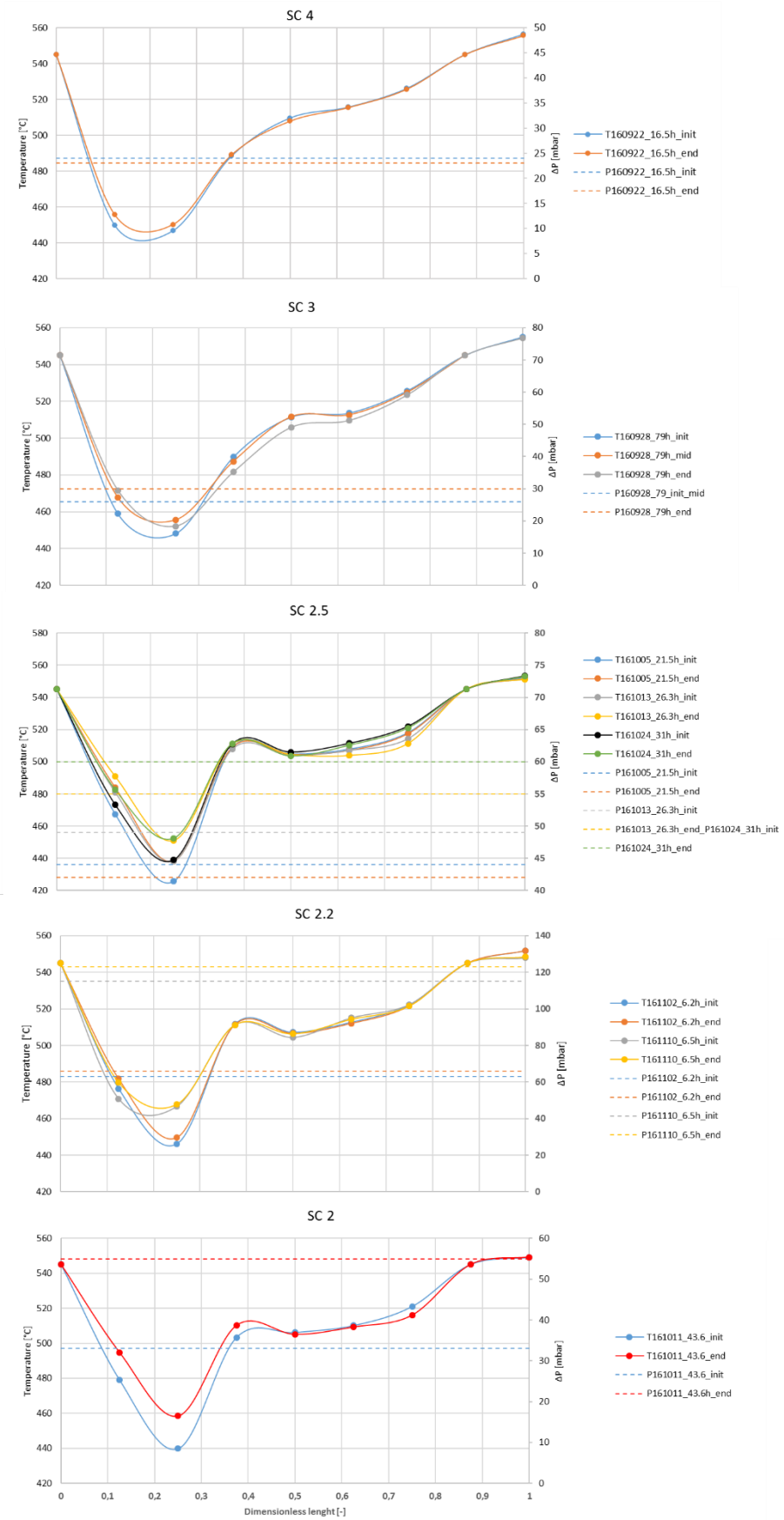

Figure 61 Temperatures distribution at the thermocouple T12-T20 and inlet outlet pressure difference by diesel SR (second catalyst, T12 and T13 at 545 °C, GHSV 1200h^{-1}).

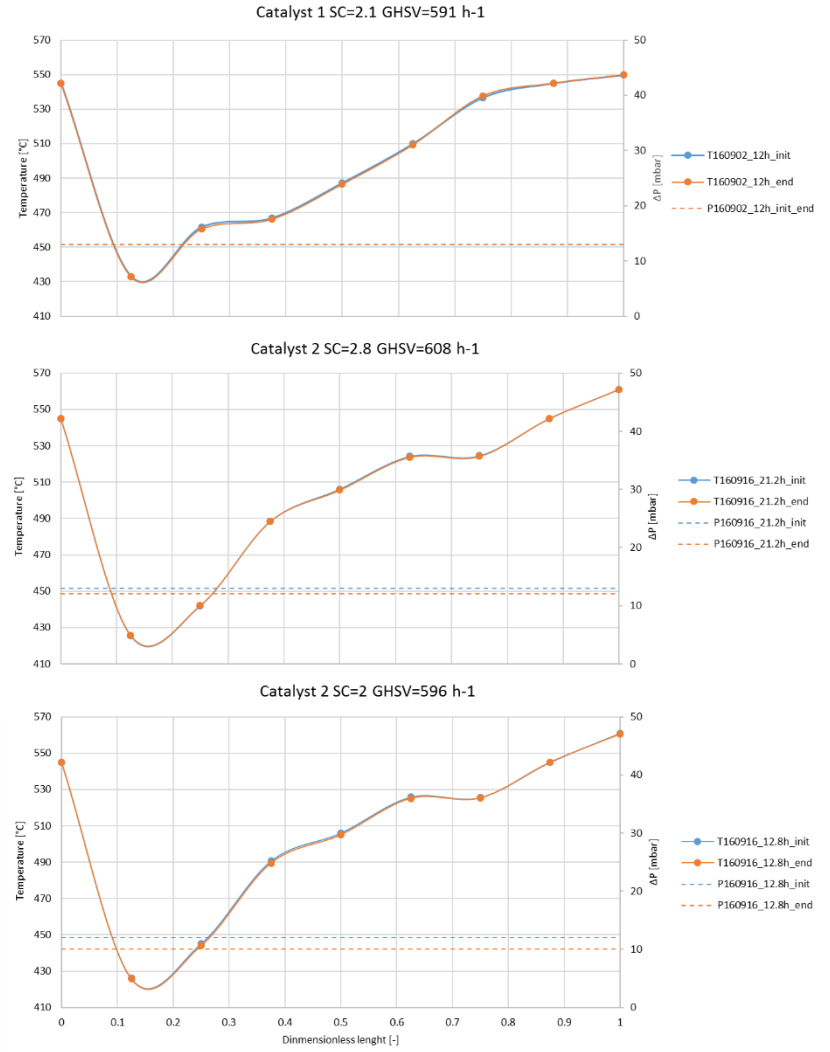

Figure 62 Temperatures distribution at the thermocouple T12-T20 and inlet outlet pressure difference by methane SR (first and second catalyst, T12 and T13 at 545 °C).

7. Summary and possible improvements

This work is based on the data gathered during the medium and long run diesel pre-reforming tests conducted at AVL and at the premises of TU Graz. Pre-reforming is generally used to convert higher hydrocarbons trough a catalytic steam reforming process into feedstocks that can be directly supplied to solid oxide fuel cell systems.

An important parameter to characterize the reforming process is the steam to carbon ratio[3]. The process of carbon formation at the catalyst is a typical side effect of diesel steam reforming and it can pose operational problems by progressive deactivation of catalyst. Carbon deposition can occur particularly at low SC ratios.

For the purposes of this thesis tests at SC ratio 4, 3, 2.5 and 2 have been performed. The results show a good stability of outlet gas composition values from SC ratio 4 to SC ratio 2.5 over several hours/days.

The comparisons of the results with the equilibrium of $C_{12}H_{26}$ suggest a satisfactory agreement with the temperatures applied to the reactor, 545°C at T12 and T19 (Fig. 59). A comparison also with the equilibrium conditions of a heavier hydrocarbon forming diesel or hexadecane would have been interesting.

Continuous tests longer than 80 hours could not be performed due to external events: failure of water pump, organizational limitations inside the university and rupture of part of heating systems. One possible solution, for the water pump failures, could be the use of a water pump controlled directly by the Crio system.

Fig. 36 depicts the concentrations of outlet gas during a carbon removal procedure after methane steam reforming. However, the steam mass flow was too low for a comparison with other values obtained from other carbon removal procedures performed in this work. A better comparison could clarify the mechanism of CO_2 production during the washing/carbon

[3] SC ratio = Moles of steam fed to the reactor / (Number of C atoms in hydrocarbon formula × Moles of hydrocarbon fed to the reactor)

removal procedure. Namely, to which extent the contribution to CO_2 production is due to a still running diesel steam reforming[4] or to the carbon steam gasification.

[4] Diesel steam reforming may run for some minutes or even hours after the diesel supply is interrupted.

Annex I

Tables 3 and 4 summarize the results of the tests performed with the two catalysts. The values of initial and final pressure are simply an average over half an hour at the beginning (when the values were stable) and at the end of the measurement. The same was done with the values of concentration in the outlet gas. When the tests were too short, 1 or 2 hours' test, the value were approximately averaged over 10 minutes. The lowest temperature in some cases corresponded to T13, or Tin, in other cases to T14.

Table 3 First catalyst tests summary

1st Catalyst	hours	Time[h]	S/C	GHSV[h-1]	Tin[°C] (T13)	Tout[°C] (T20)	Tlow	CO[%]	CO2[%]	CH4[%]	H2[%]	Pin[mbar]	Pout[mbar]	ΔP[mbar]
06.09.2016	13:30-14:30	1.0	2.0	600	455	549	453 (Tin)	6.520	21.256	19.444	53.627	25	5	20
06.09.2016	15:36-16:04	0.5	2.0	1000	445	549	442 (Tin)	6.993	20.705	20.560	52.766	40	7	33
06.09.2016	17:10-03:37	11.5	2.0	600	459	548	454 (Tin)	6.830	20.817	20.953	52.206	25	6	19
08.09.2016	18:20-19:00	0.3	2.0	600	455	548	409 (Tin)	8.219	19.470	30.602	43.114	119	4	115
09.09.2016	12:50-13:30	0.7	2.0	1000	469	548	425 (Tin)	8.459	18.933	32.837	41.458	181	6	175
09.09.2016	14:20-15:20	1.0	3.0	1000	455	549	422 (Tin)	6.837	20.551	24.589	48.879	182	6	176
09.09.2016	16:15-17:10	0.9	4.0	1000	451	548	435 (Tin)	5.541	21.783	18.675	54.345	174	5	169
09.09.2016	18:00-19:00	1.0	5.0	1000	447	548	431 (Tin)	4.955	22.225	15.189	57.688	181	6	175
13.09.2016	09:15-13:50	4.6	2.0	600	491	548	466 (T14)	8.592→10.263	18.775→14.634	34.995→46.693	39.194→31.549	153→193	6→4	147→189

Table 4 Second catalyst tests summary

2nd Catalyst	hours	Time[h]	S/C	GHSV[h-1]	Tin[°C] (T13)	Tout[°C] (T20)	Tlow	CO[%]	CO2[%]	CH4[%]	H2[%]	Pin[mbar]	Pout[mbar]	ΔP[mbar]
21.09.2016	12-13:30	1.5	4.0	600	443	548	443 Tin	5.318	22.234	6.657	65.043	20	8	12
21.09.2016	14:20-16:20	2.0	4.0	600	443	548	443 Tin	5.199	22.405	6.306	65.174	19	7	12
22.09.2016	14:00-6:30	16.5	4.0	1200	441→458	548	445→450 (T14)	5.154→5.421	22.013→21.781	8.995→10.788	63.419→61.285	34→32	10→9	24→23
23.09.2016	11:30-20:40	9.2	3.0	1200	438→458	549	448→452 (T14)	5.854	21.253	13.761	58.616	34	10	24
28.09.2016-01.10.2016	14:00-21:00	79.0	3.0	1200	445→472	554	447→452(T14)	5.631→5.037	21.622→21.72	13.359→10.802	58.913→61.297	35→45	9→15	26→30
05.10.2016	12:20-13:20	1.0	3.0	1200	463	552	422(T14)	4.203	22.590	11.191	60.986	55	12	43
05.10.2016	14:00-11:30	21.5	2.5	1200	461→484	552	422→438(T14)	4.575→5.068	22.073→21.589	13.066→13.666	59.405→58.721	55→53	11	44→42
07.10.2016	10:00-21:30	11.5	3.0	1200	466→478	552	422→432(T14)	4.672->4.705	22.133->22.116	11.92->11.842	60.471->60.540	44→46	10->11	34→35
11.10.2016	14:10-15:10	1.0	4.0	1200	466	552	430(T14)	4.091	23.004	8.35	63.938	40	10	30
11.10.2016	15:30-16:40	1.2	2.5	1200	468	550	433(T14)	5.078	22.002	14.556	58.034	42	10	32
11.10.2016-13.10.2016	17:10:-11:45	43.6	2.0	1200	471→494	549	435→459(T14)	5.907→6.039	21.172→20.872	19.37→20.212	53.489→52.649	44→67	11→12	33→55
13.10.2016-14.10.2016	12:20-14:40	26.3	2.5	1200	476→488	551	433→450(T14)	4.997→5.199	21.643→21.489	14.684→14.584	57.928→57.947	61→68	12→13	49→55
20.10.2016	10:30-18:30	8.0	2.5	1200	478→485	550	430→445(T14)	5.289	21.292	15.338	57.216	43	11	32
24.10.2016	10:50-17:50	31.0	2.5	1200	472→482	553	436→452(T14)	5.283→5.321	21.895→21.725	15.895→16.042	56.817→56.611	66→71	11	55→60
02.11.2016	13:10-19:20	6.2	2.2	1200	474→482	551	443→449(T14)	5.757→5.680	21.218→21.312	19.137→18.936	53.731→53.946	74→77	11	63→66
10.11.2016	09:00-15:30	6.5	2.2	1200	466→480	548	466→(T14)	6.138→6.277	20.806→20.382	23.477→24.539	49.765→49.146	125→133	10	115→123

Annex II

The calculation of the diesel and water quantities expressed in g/h and ml/min form desired SC ratio and GHSV was made on the basis of the system used in the previous AVL thesis [24]. The only change is the possibility to use different types of hydrocarbons simply by inserting the numbers of C and H atoms.

Table 5 Excel calculation to obtain diesel and water quantity given SC ratio and GHSV

C-Atoms	H-Atoms	Atomic Weight				
16	34	226				
SC	GHSV[h-1]	x mol $C_{16}H_{34}$	x $C_{16}H_{34}$	Total[Nm3/h]	Diesel[Nm3/h]	Diesel[g/h]
2,000	1200	0,031	0,03030	0,807	0,0245	246,528
Water[Nm3/h]	Water[Nl/h]	Water[g/h]	Water[ml/h]	Water[ml/min]		
0,783	783	628,319	630	10,49		

Bibliography

[1] G. Squadrito, L. Andaloro, M. Ferraro and V. Antonucci, "Hydrogen Fuel Cell Technology," in *Advances in Hydrogen Production, Storage and Distribution*, Oxford UK, Elsevier Ltd., 2014.

[2] L. Gandi´a, G. Arzamendi and P. M. Die´guez, "Renewable Hydrogen Energy: An Overview," in *Renewable Hydrogen Technologies*, Oxford UK, Elsevier B.V., 2013.

[3] D. Shekhawat, D. Berry and J. J. Spivey, "Introduction to Fuel Processing," in *Fuel Cells: Technology fo Fuel Processing*, Oxford, Elsevier B.V, 2011, pp. 1-8.

[4] M. O´Connell, Development and evaluation of a microreactor for the reforming of diesel fuel in the kW range, The Netherlands: Elsevier, 2009.

[5] D. Shekhawat, "Nonconventional Reforming Methods," in *Fuel Cells: Technology for Fuel Processing*, Elsevier B.V., 2011, pp. 161-279.

[6] J. Larminie, Fuel Cell Systems Explained, England: John Wiley & Sons Ltd, 2003.

[7] J. Fleig, Fuel Cells. Notes and slides of the course 2015, Wien Technische Universität, 2015.

[8] F. Barbir, PEM Fuel Cells: theory and Practice, UK: Elsevier Academic Press, 2005.

[9] I. EG&G Technical Services, Fuel Cell Handbook, West Virginia: National Energy Technology Laboratory, 2004.

[10] E. A. NRW. [Online]. Available: http://www.brennstoffzelle-nrw.de/brennstoffzellen/typen/. [Accessed 15 10 2016].

[11] S. Singhal and K.Kendall, Solid Oxide Fuel Cell: Fundamentals, Design and Applications, Elsevier, 2003.

[12] J. Boon and E. V. Dijk, "Adiabatic Diesel Pre-reforming," Energy research center of Nederland, Nederland.

[13] J. Rostrup-Nielsen and J. B. Hansen, "Steam Reforming For Fuel Cells," in *Fuel Cells: Technology for Fuel Processing*, Denmark, Elsevier B.V., 2011, pp. 49-71.

[14] J. Rostrup-Nielsen, T. Christensen and I. Dybkjaer, "Steam Reforming of Liquid Hydrocarbons," *Recent Advances in Basic and Applied Aspects of Industrial Catalysis,* vol. 113, no. Elsevier Science B.V., pp. 81-95, 1998.

[15] T. S. Christensen, "Adiabatic prereforming of hydrocarbons - an important step in syngas production," *Applied Catalyst A: General 138 ,* pp. 285-309, 1996.

[16] P. v. Beurden, "On the Catalityc Aspect of Steam Methane Reforming," ECN Energy Innnovation, 2004.

[17] J. R. Rostrup-Nielsen and T. Rostrup-Nielsen, "Large-scale Hydrogen Production," in *6th World Congr. of Chemical Engineering*, Melbourne Australia, 2001.

[18] J. Spivey, "Deactivation of Reforming Catalyst," in *Fuel Cells: Technologies for Fuel Processing*, Elsevier .

[19] A. Mitteregger, Regenerierung von deaktivierten Nickelkatalysatoren in der katalytischen Gasreinigung von Synthesegas aus der allothermen Biomassevergasung, TU Graz, 2016.

[20] M. Argyle and C. H. Bartholomew, "Heterogeneous Catalyst Deactivation and Regeneration: A Review," vol. 5, pp. 145-269, 2015.

[21] D. J. Haynes and D. Shekhawat, "Oxidative Steam Reforming," in *Fuel Cells: Thechnology for fuel processing*, Oxford UK, Elsevier B.V., 2011.

[22] D. Shekhawat, J. Spivey and D. Berry, Fuel Cell Technologies for Fuel Cell Processing, Oxford: Elsevier, 2011.

[23] M. R. Patel, C. N. Shah and N. Patel, "Pre-reformer,The Solution for Increasing Plant Throughput," *CEW, Chemical engineering world,* vol. 33, no. 2, pp. 69-73, 1998.

[24] K. Fasching, Untersuchungen zu Diesel-Steam-Reforming für SOFC-Systeme, Wien, 2015.

[25] S. Martin, G. Kraaij, T.Ascher, P. Baltzapoulou, G. Karagiannakis, D. Wails and A. Wörner, "Direct Steam Reforming of Diesel and Diesel-biodiesel Blends for Distributed Hydrogen Generation," *International Journal of Hydrogen Energy,* pp. 75-84, 2015.

[26] V. A. Kirillov, A. B. Shigarov, Y. I. Amosov, V. D. Belyaev and A. R. Urusov, "Diesel Fuel Pre-Reforming into Methane - Hydrogen Mixtures," *Theoretical Foundations of Chemical Engineering,* pp. 30-40, 2015.

[27] W. Georgi and P. Hohl, Einführung in LabView, München: Carl Hanser Verlag, 2015.

[28] S.Appari, V.M.Janardhanan, R.Bauri and S.Jayanti, "Deactivation and Regeneration of Ni Catalyst During Stream Reforming of Model Biogas: an Experimental Investigation," *International Journal of Hydrogen Energy,* 2013.

[29] J. Fleig, Physikalische Chemie für Physik und Materialwissenschaft, Wien Technische Universität, 2014.

[30] V. M. Janardhanan, V. Heuveline and O. Deutschmann, "Performance analysis of a SOFC under direct reforming conditions," *Journal of Power Sources,* vol. 172, p. 296–307, 2007.

[31] S. K. Masoudian, S. Sadighi and A. Abbasi, "Regeneration of a Commercial Catalyst for the Dehydrogenation of Isobutane to Isobutene," *Chem. Eng. Technol.,* vol. 36, 2013.

[32] "Hydrogen Analysis Resource Center," U.S: Department of Energy, January 2015. [Online]. Available: http://hydrogen.pnl.gov/hydrogen-data/lower-and-higher-heating-values-hydrogen-and-other-fuels.